

**THERMAL MODELLING & ANALYSIS OF ELECTRO  
DISCHARGE MACHINING PROCESS**

By

**ARKA MONDAL**

B.Tech (Mechanical Engineering), 2014

Kalyani Government Engineering College

Kalyani, Nadia- 741235

**EXAMINATION ROLL NO. - M4PRD1605**

THESIS

SUBMITTED IN PARTIAL FULFILLMENT OF THE REQUIREMENTS  
FOR THE AWARD OF THE DEGREE OF MASTER OF PRODUCTION  
ENGINEERING IN THE FACULTY OF ENGINEERING & TECHNOLOGY,

JADAVPUR UNIVERSITY

**2016**

**DEPARTMENT OF PRODUCTION ENGINEERING**

**JADAVPUR UNIVERSITY**

**KOLKATA-700032**

**INDIA**

**JADAVPUR UNIVERSITY**  
**FACULTY OF ENGINEERING AND TECHNOLOGY**

**CERTIFICATE OF RECOMMENDATION**

I/WE HEREBY RECOMMEND THAT THE THESIS ENTITLED “**THERMAL MODELLING & ANALYSIS OF ELECTRO DISCHARGE MACHINING PROCESS**” CARRIED OUT UNDER MY/OUR SUPERVISION AND GUIDANCE, BY **Mr. ARKA MONDAL**, MAY BE ACCEPTED IN THE PARTIAL FULFILLMENT OF THE REQUIREMENTS FOR THE DEGREE OF “**MASTER OF PRODUCTION ENGINEERING**”.

---

**(Prof. Souren Mitra)**

**Thesis Advisor**

**Dept. of Production Engineering**

**Jadavpur University**

**Kolkata-700032**

---

**(Prof. Arunanshu Shekhar Kuar)**

**Thesis Advisor**

**Dept. of Production Engineering**

**Jadavpur University**

**Kolkata- 700032**

---

**HEAD**

**Dept. of Production Engineering**

**JADAVPUR UNIVERSITY**

**KOLKATA- 700032**

---

**DEAN, F.E.T.**

**JADAVPUR UNIVERSITY**

**KOLKATA- 700032**

**JADAVPUR UNIVERSITY**  
**FACULTY OF ENGINEERING AND TECHNOLOGY**

**CERTIFICATE OF APPROVAL\***

The foregoing thesis is hereby approved as a creditable study of an engineering subject carried out and presented in a manner of satisfactory to warrant its acceptance as a pre-requisite to the degree for which it has been submitted. It is understood that by this approval, the undersigned do not necessarily endorse or approve any statement made, opinion expressed and conclusion drawn therein but approve the thesis only for the purpose for which it has been submitted.

COMMITTEE ON FINAL  
EXAMINATION FOR  
EVALUATION OF THE  
THESIS

---

---

---

\*Only in case the recommendation is concurred in

## ACKNOWLEDGEMENT

*It is my pleasure to record my appreciation to all who helped me either directly or indirectly, in initiating or completing the thesis. First and foremost, I am deeply grateful to **Dr. Souren Mitra**, Professor, Department of Production Engineering, Jadavpur University and **Dr. Arunanshu Shekhar Kuar**, Professor, Department of Production Engineering, Jadavpur University for supervising this thesis. Their constructive suggestion, guidance and support throughout my thesis work have thankfully acknowledged. I am also deeply indebted to **Shri Dipten Mishra**, Director of School Laser Science and Engineering, Jadavpur University and **Mr. K.Paramshivan** whose help, stimulating suggestion and encouragement helped me in all the time of my thesis work.*

*I would also like to express my gratitude to all the Faculty Members and Non-teaching staff of Production Engineering Department who directly or indirectly helped or encouraged me during thesis work.*

*I am ever indebted to my parents for their blessings in each synergy of my life.*

*Everything in this nature is time bounded, so, thanks to 'Almighty' for successful completion of this work.*

# TABLE OF CONTENTS

<b>CONTENTS</b>	<b>PAGE NO.</b>
<b>1. INTRODUCTION</b>	<b>1</b>
1.1. NEED OF ELECTRO DISCHARGE MACHINING	2
1.2. APPLICATIONS OF EDM	3
1.3. VARIOUS EDM PROCESSES	6
1.4. ADVANTAGES AND LIMITATIONS OF EDM	7
1.4.1. ADVANTAGES	7
1.4.2. LIMITATIONS	8
1.5. LITERATURE SURVEY	9
1.6. OBJECTIVE OF PRESENT RESEARCH	17
<b>2. FUNDAMENTAL FEATURES OF EDM</b>	<b>18</b>
2.1. BASIC EDM PROCESS	18
2.1.1. CHARACTERISTICS OF EDM	20
2.2. PROCESS PARAMETERS	21
2.2.1. ELECTRODE AND WORKPIECE	21
2.2.2. DIELECTRIC & FLUSHING	21
2.2.3. POWER GENERATOR	23
2.2.4. SPARK GAP	25
2.2.5. CONTROLLER SPECIFIC	25
2.3. PROCESS CRITERIA	26
2.4. STEPS OF EDM	29
2.5. MATERIAL REMOVAL AND SURFACE FINISH IN EDM	32
2.5.1. MATERIAL REMOVAL	32
2.5.2. SURFACE FINISH	33
<b>3. THERMAL MODELLING OF ELECTRO DISCHARGE MACHINING PROCESS</b>	<b>34</b>
3.1. NEED FOR THERMAL MODELLING	34
3.2. MODELLING TOOLS	34
3.3. FINITE ELEMENT ANALYSIS OF EDM	36
3.3.1. ASSUMPTIONS	36
3.3.2. WORKPIECE MATERIAL	37
3.3.3. GEOMETRY OF THE MATERIAL	38
3.3.4. MESHING	39
3.3.5. PARAMETER	40
3.3.6. HEAT FLUX	41

<b>4. RESULTS &amp; DISCUSSIONS</b>	<b>42</b>
4.1. ANALYSIS OF CHANGE OF TEMPERATURE DISTRIBUTION OVER SLICED PLANE	42
4.2. ANALYSIS OF CHANGE OF TEMPERATURE AT THE PLASMA ARC CENTRE	50
4.3. STUDY OF TEMPERATURE DISTRIBUTION ALONG RADIAL DIRECTION AND DEPTH FROM PLASMA ARC CENTRE	53
4.4. ANALYSIS OF TEMPERATURE DISTRIBUTION IN THE HEAT AFFECTED ZONE	73
4.5. STUDY OF CRATER SIZE	81
4.5.1. INFLUENCE OF PULSE-ON-TIME ON CRATER DIMENSION	82
4.5.2. INFLUENCE OF GAP CURRENT ON CRATER DIMENSION	86
<b>5. GENERAL CONCLUSION &amp; FUTURE SCOPE OF WORK</b>	<b>90</b>
5.1. GENERAL CONCLUSION	90
5.2. FUTURE SCOPE OF WORK	90
<b>6. REFERENCE</b>	<b>91</b>

## LIST OF FIGURES

1. Fig:1.1: Machining an impression with Die-sinking-EDM
2. Fig1.2: A turbine blade with internal cooling as applied in the high-pressure turbine.
3. Fig1.3: Small hole drilling EDM machines.
4. Fig.2.1: Schematic representation of the basic working principle of EDM process.
5. Fig.2.2: The basic circuit for different type of EDM generators
6. Fig2.3: Over cut due to drilling
7. Fig2.4: Surface texture
8. Fig2.6: A typical Electro Discharge Machine Set-up.
9. Fig2.5: Stages of EDM action
10. Fig2.7: Schematic representation of crater formation in EDM process.
11. Fig.2.8: Schematic representation of the sparks in EDM process.
12. Fig3.1: Isometric view of the Geometry taken for calculation
13. Fig3.2: Meshed Material
14. Fig3.3: The middle portion of extremely fine meshing
15. Fig4.1.Temp. Distribution over sliced plane 40V,2A,Ton=40microsecond

16. Fig4.2.Temp. Distribution over sliced plane 40V,2A,Ton=60microsecond
17. Fig4.3.Temp. Distribution over sliced plane 40V,2A,Ton=80microsecond
18. Fig4.4.Temp. Distribution over sliced plane 40V,3A,Ton=40microsecond
19. Fig4.5.Temp. Distribution over sliced plane 40V,3A,Ton=60microsecond
20. Fig4.6.Temp. Distribution over sliced plane 40V,3A,Ton=80microsecond
21. Fig4.7.Temp. Distribution over sliced plane 40V,4A,Ton=40microsecond
22. Fig4.8.Temp. Distribution over sliced plane 40V,4A,Ton=60microsecond
23. Fig4.9.Temp. Distribution over sliced plane 40V,4A,Ton=80microsecond
  
24. Fig4.10.Temp. Distribution over sliced plane 45V,2A,  
Ton=40microsecond
25. Fig4.11.Temp. Distribution over sliced plane 45V,2A,  
Ton=60microsecond
  
26. Fig4.12.Temp. Distribution over sliced plane 45V,2A,  
Ton=80microsecond
  
27. Fig4.13.Temp. Distribution over sliced plane 5V,3A,Ton=40microsecond
  
28. Fig4.14.Temp. Distribution over sliced plane 5V,3A,Ton=60microsecond
29. Fig4.15.Temp. Distribution over sliced plane 5V,3A,Ton=80microsecond
  
30. Fig4.16.Temp. Distribution over sliced plane 45V,4A,  
Ton=40microsecond

31. Fig4.17.Temp. Distribution over sliced plane 45V,4A,  
Ton=60microsecond
32. Fig4.18.Temp. Distribution over sliced plane 45V,4A,  
Ton=80microsecond
33. Fig.4.19. Change of Temperature at the Plasma Arc Centre Vgap=40V
34. Fig.4.20. Change of Temperature at the Plasma Arc Centre Vgap=45V
35. Fig4.21.: Temp. Distribution along radial direction  
40V,2A,Ton=40microsecond
36. Fig4.22.: Temp. Distribution along Depth 40V,2A,Ton=40microsecond
37. Fig4.23.: Temp. Distribution along radial direction 40V,  
2A,Ton=60microsecond
38. Fig4.24.: Temp. Distribution along Depth 40V, 2A, Ton=60microsecond
39. Fig4.25.: Temp. Distribution along radial direction 40V,  
2A,Ton=80microsecond
40. Fig4.26.: Temp. Distribution along Depth 40V, 2A, Ton=80microsecond
41. Fig4.27.: Temp. Distribution along radial direction 40V, 3A,  
Ton=40microsecond
42. Fig4.28.: Temp. Distribution along Depth 40V, 3A, Ton=40microsecond
43. Fig4.29.: Temp. Distribution along radial direction 40V, 3A,  
Ton=60microsecond
44. Fig4.30.: Temp. Distribution along Depth 40V, 3A, Ton=60microsecond

45. Fig4.31.: Temp. Distribution along radial direction 40V, 3A,  
Ton=80microsecond
46. Fig4.32.: Temp. Distribution along Depth 40V, 3A, Ton=80microsecond
47. Fig4.33.: Temp. Distribution along radial direction 40V, 4A,  
Ton=40microsecond
48. Fig4.34.: Temp. Distribution along Depth 40V, 4A, Ton=40microsecond
49. Fig4.35.: Temp. Distribution along radial direction 40V, 4A,  
Ton=60microsecond
50. Fig4.36.: Temp. Distribution along Depth 40V, 4A, Ton=60microsecond
51. Fig.4.37.: Temp. Distribution along radial direction 40V, 4A,  
Ton=80microsecond
52. Fig4.38.: Temp. Distribution along Depth 40V, 4A, Ton=80microsecond
53. Fig.4.39.: Temp. Distribution along radial direction 45V, 2A,  
Ton=40microsecond
54. Fig4.40.: Temp. Distribution along Depth 45V, 2A, Ton=40microsecond
55. Fig.4.41.: Temp. Distribution along radial direction 45V, 2A,  
Ton=60microsecond.
56. Fig4.42.:Temp. Distribution along Depth 45V, 2A, Ton=60microsecond
57. Fig.4.43.: Temp. Distribution along radial direction 45V, 2A,  
Ton=80microsecond
58. Fig4.44.: Temp. Distribution along Depth 45V, 2A, Ton=80microsecond

59. Fig.4.45.: Temp. Distribution along radial direction 45V, 3A,  
Ton=40microsecond
60. Fig4.46.: Temp. Distribution along Depth 45V, 3A, Ton=40microsecond
61. Fig.4.47: Temp. Distribution along radial direction 45V, 3A,  
Ton=60microsecond
62. Fig4.48.: Temp. Distribution along Depth 45V, 3A, Ton=60microsecond
63. Fig.4.49: Temp. Distribution along radial direction 45V, 3A,  
Ton=80microsecond
64. Fig4.50.: Temp. Distribution along Depth 45V, 3A, Ton=80microsecond
65. Fig.4.51: Temp. Distribution along radial direction 45V, 4A,  
Ton=40microsecond
66. Fig4.52. : Temp. Distribution along Depth 45V, 4A, Ton=40microsecond
67. Fig.4.53: Temp. Distribution along radial direction 45V, 4A,  
Ton=60microsecond
68. Fig4.54. : Temp. Distribution along Depth 45V, 4A, Ton=60microsecond
69. Fig.4.55: Temp. Distribution along radial direction 45V, 4A,  
Ton=80microsecond
70. Fig4.56. : Temp. Distribution along Depth 45V, 4A, Ton=80microsecond
71. Fig.4.57. Temp. Distribution at the Heat Affected Zone along Radial  
Direction 40V, 2A

72. Fig.4.58.Temp. Distribution at the Heat Affected Zone along Depth 40V, 2A
73. Fig.4.59.Temp. Distribution at the Heat Affected Zone along Radial Direction 40V, 3A
74. Fig.4. 60.Temp. Distribution at the Heat Affected Zone along Depth 40V, 3A
75. Fig.4.61.Temp. Distribution at the Heat Affected Zone along Radial Direction 40V, 4A
76. Fig.4.62.Temp. Distribution at the Heat Affected Zone along Depth 40V, 4A
77. Fig.4.63.Temp. Distribution at the Heat Affected Zone along Radial Direction 45V, 2A
78. Fig.4.64.Temp. Distribution at the Heat Affected Zone along Depth 45V, 2A
79. Fig.4.65.Temp. Distribution at the Heat Affected Zone along Radial Direction 45V, 3A
80. Fig.4.66.Temp. Distribution at the Heat Affected Zone along Depth45V, 3A
81. Fig.4.67.Temp. Distribution at the Heat Affected Zone along Radial Direction 45V, 4A
82. Fig.4.68.Temp. Distribution at the Heat Affected Zone along Depth45V, 4A
83. Fig.4.69. Crater Dimension.  $V_{gap}=40V$ ,  $I=2A$

84. Fig.4.70. Crater Dimension.  $V_{gap}=40V$ ,  $I=3A$
85. Fig.4.71. Crater Dimension.  $V_{gap}=40V$ ,  $I=4A$
86. Fig.4.72. Crater Dimension.  $V_{gap}=45V$ ,  $I=2A$
87. Fig.4.73. Crater Dimension.  $V_{gap}=45V$ ,  $I=3A$
88. Fig.4.74. Crater Dimension.  $V_{gap}=45V$ ,  $I=4A$
89. Fig.4.75. Crater Dimension.  $V_{gap}=40V$ ,  $T_{on}=40\text{microsecond}$
90. Fig.4.76. Crater Dimension.  $V_{gap}=40V$ ,  $T_{on}=60\text{microsecond}$
91. Fig.4.77. Crater Dimension.  $V_{gap}=40V$ ,  $T_{on}=80\text{microsecond}$
92. Fig.4.78. Crater Dimension.  $V_{gap}=45V$ ,  $T_{on}=40\text{ microsecond}$
93. Fig.4.79. Crater Dimension.  $V_{gap}=45V$ ,  $T_{on}=60\text{ microsecond}$
94. Fig.4.80. Crater Dimension.  $V_{gap}=45V$ ,  $T_{on}=80\text{ microsecond}$

## **LIST OF TABLES**

1. Table1.1. Various EDM processes & their Applications.
2. Table 3.1. Chemical composition of AISI 304 Stainless Steel.
3. Table3.2.Mechanical Properties of AISI 304 Stainless Steel.
4. Table.3.3. Physical & Thermal Properties of AISI 304 Stainless Steel.
5. Table.3.4. Parameter Setting.
6. Table.4.1. Temperature at Plasma Arc Centre.
7. Table.4.2. Crater Dimension

# **1. INTRODUCTION:**

Electro Discharge Machining (EDM) is an electro-thermal non-traditional machining process, where electrical energy is used to generate electrical spark and material removal mainly occurs due to thermal energy of the spark. EDM is mainly used to machine difficult-to-machine materials and high strength temperature resistant alloys. EDM can be used to machine difficult geometries in small batches or even on job-shop basis. Work material to be machined by EDM has to be electrically conductive.

Erosion of metals first by spark was first reported by Joseph Priestly in 1878 and electric-sparking has been utilized since long for its by-product, “colloidal metal powders”, but sparks were not used for machining as much until early thirties when the tap disintegrator was introduced. However controlled machining by electrical sparks was first introduced by Lazarenko in Russia in 1944. The first British patent was granted to Rudorffin 1950. USA Japan and Switzerland developed their machines around 1950. A machine for spark machining by “method x” was patented in USA in 1952. After pioneering the investigation of Lazarenko , the EDM has attracted worldwide attention as a technique for metal machining and since the considerable research and development have been carried out.

## **1.1. NEED OF ELECTRO DISCHARGE MACHINING:**

- i. The process can be applied, in general, to any electrically conductive material. Other properties like strength, brittleness, hardness etc. do not import ant restriction to the application of the process.
- ii. The process provides a simple and straightforward method of form producing drop forging, drawing and extruding dies and complex cavities in moulds and dies for plastics, die-casting, glass and ceramic manufacturing.
- iii. Though the process involves temperature rise at the local spot to a very high value, which can vaporise the localised material to machine, there is no heating of bulk materials. Though the heat affected zone (HAZ) surrounding the local points extends bulk to a depth of about few microns.
- iv. The high rate of heating and cooling at the treated surface renders some extra hardness (case-hardening) to the surface and this becomes a point of advantage in favour of the process.
- v. Simple geometrical shape configurations can easily be produced by piercing or die-sinking in hardened die plates with required surface finish and accuracy. The elimination of much complicated grinding and lapping is possible.
- vi. No mechanical stress is developed in the work material as there is no physical contact between tool and workpiece. This permits machining fragile and slender workpieces.
- vii. The process reduces time of machining in comparison with conventional grinding, honing or contour grinding etc.
- viii. The crater type non-directional (layless) surface pattern is said to retain lubricants, rendering the process particularly suitable for the finishing operations.
- ix. The surface finish produced by the EDM process can be controlled to the required extent, minimising the extra cost involved in additional operation for achieving improved surface finish.

## 1.2. APPLICATIONS OF EDM:

### i. PROTOTYPE PRODUCTION:

The EDM process is most widely used by the mould-making tool and die industries, but is becoming a common method of making prototype and production parts, especially in the aerospace, automobile and electronics industries in which production quantities are relatively low. In sinker EDM, a graphite, copper tungsten or pure copper electrode is machined into the desired (negative) shape and fed into the workpiece on the end of a vertical ram.

### ii. COINAGE DIE MAKING:

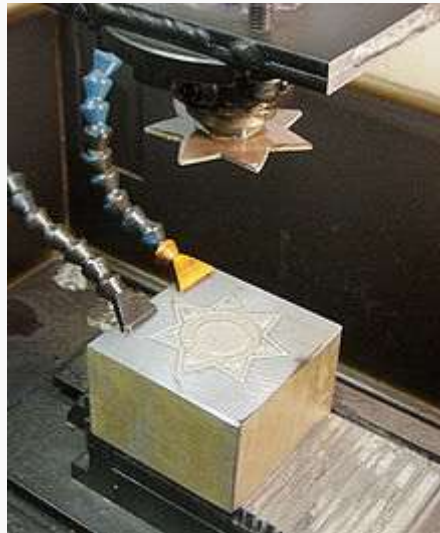


Fig:1.1: Machining an impression with Die-sinking-EDM [27]

For the creation of dies for producing jewelry and badges, or blanking and piercing (through use of a pancake die) by the coinage (stamping) process, the positive master may be made from sterling silver, since (with appropriate machine settings) the master is significantly eroded and is used only once. The resultant negative die is then hardened and used in a drop hammer to produce stamped flats from cutout sheet blanks of bronze, silver, or low proof gold alloy. For badges these flats may be further shaped to a curved surface by another die. This type of EDM is usually performed submerged in an oil-based dielectric. The finished object may be further refined by hard (glass) or soft (paint) enameling and/or electroplated with pure gold or nickel. Softer materials such as silver may be hand engraved as a refinement.

EDM control panel. Machine may be adjusted for a refined surface (electropolish) at end of process.

### iii. SMALL HOLE DRILLING:



Fig1.2: A turbine blade with internal cooling as applied in the high-pressure turbine.[27]



Fig1.3: Small hole drilling EDM machines.[27]

Small hole drilling EDM is used in a variety of applications. On wire-cut EDM machines, small hole drilling EDM is used to make a through hole in a workpiece in through which to thread the wire for the wire-cut EDM operation. A separate EDM head specifically for small hole drilling is mounted on a wire-cut machine and allows large hardened plates to have finished parts eroded from them as needed and without pre-drilling.

Small hole EDM is used to drill rows of holes into the leading and trailing edges of turbine blades used in jet engines. Gas flow through these small holes allows the engines to use higher temperatures than otherwise possible. The high-temperature, very hard, single crystal alloys employed in these blades makes conventional machining of these holes with high aspect ratio extremely difficult, if not impossible.

Small hole EDM is also used to create microscopic orifices for fuel system components, spinnerets for synthetic fibres such as rayon, and other applications.

There are also stand-alone small hole drilling EDM machines with an x–y axis also known as a super drill or hole popper that can machine blind or through holes. EDM drills bore holes with a long brass or copper tube electrode that rotates in a chuck with a constant flow of distilled or deionized water flowing through the electrode as a flushing agent and dielectric. The electrode tubes operate like the wire in wire-cut EDM machines, having a spark gap and wear rate. Some small-hole drilling EDMs are able to drill through 100 mm of soft or through hardened steel in less than 10 seconds, averaging 50% to 80% wear rate. Holes of 0.3 mm to 6.1 mm can be achieved in this drilling operation. Brass electrodes are easier to machine but are not recommended for wire-cut operations due to eroded brass particles causing "brass on brass" wire breakage, therefore copper is recommended.

#### **iv. METAL DISINTEGRATION MACHINING:**

Several manufacturers produce MDM machines for the specific purpose of removing broken tools (drill bits, taps, bolts and studs) from work pieces. In this application, the process is termed "metal disintegration machining" or MDM. The metal disintegration process removes only the centre out of the tap, bolt or stud leaving the hole intact and allowing a part to be reclaimed.[27]

### 1.3. VARIOUS EDM PROCESSES:

Table1.1. Various EDM processes & their Applications [1]

Variant	Application
Die sinking EDM	Replication moulds, embossing tools
EDM drilling	Injection nozzles
EDM milling	Micro injection moulds, embossing or coining tools
EDM grinding	Embossing or coining tools fluidic structures
EDM wire-EDM	Optoelectronic components, stamping tools
EDGrinding	Pin electrodes, rolling tools.

## 1.4. ADVANTAGES AND LIMITATIONS OF EDM:

### 1.4.1. ADVANTAGES:

EDM is a well known process for precision machining of difficult to cut materials. One of the main advantage of EDM is, it is thermal process. Here material is removed by melting and evaporation. So the hardness of the workpiece has no limitation for machining in Electro Discharge Machining. Even the hardest material can be machined here if it is a conductive material. Various advantage of this process is discussed here below.

- i. **Machining hard materials:** The capability of machining hard materials is a major benefit as most tools and moulds are made of hard materials to increase materials. The recent developments in cutting tools for turning and milling and the process of high speed machining allow to machine harder materials than before, but EDM still remains the only process to machine vary hard material.
- ii. **Absence of forces:** As the EDM process is based on a thermal principle, almost no mechanical forces are applied to workpice. A very minimal force is applied by the plasma arc in a very small area as the radius of the plasma arc is very small. This allows to machine very thin and fragile materials. Flushing and hydraulic forces may become large for some workpice geometry. The large cutting forces of mechanical materials removal process, however, remain absent.
- iii. **Machining of complex shapes:** Complex cavities can often be machined without difficulties by die-sinking EDM, provided an electrode is available, having the opposite shape of the cavity. In most cases , the soft electrode can be machined rather easily by conventional process as milling, turning, shaping etc. In this way complex cavities can be machined even on simple die –sinking EDM which can only erode material in downward direction. Due to modern NC control die sinking machine, even more complex shapes can be done by EDM-Milling. Modern multi axis NC controlled Wire cutting machine also allow to achieve more intricate shapes. Besides intricate shapes, conventional processes can be easily replaced by Electro Discharge Machining. EDM is also one of the only process capable of making 3 dimensional micro work pieces. A large growth of application for so called micro electro mechanical systems (MEMS) is predicted for the near future.
- iv. **The process provides a simple and straightforward method of form producing drop forging, drawing and extruding dies and complex cavities in moulds and dies for plastics, die-casting, glass and ceramic manufacturing.**
- v. **Though the process involves temperature rise at the local spot to a very high value, which can vaporise the localised material to machine, there is no heating of bulk materials. Though the heat affected zone (HAZ) surrounding the local points extends bulk to a depth of about few microns.**

- vi. The high rate of heating and cooling at the treated surface renders some extra hardness (case-hardening) to the surface and this becomes a point of advantage in favour of the process.
- vii. Simple geometrical shape configurations can easily be produced by piercing or die-sinking in hardened die plates with required surface finish and accuracy. The elimination of much complicated grinding and lapping is possible.
- viii. No mechanical stress is developed in the work material as there is no physical contact between tool and workpiece. This permits machining fragile and slender workpieces.
- ix. The process reduces time of machining in comparison with conventional grinding, honing or contour grinding etc.
- x. The crater type non-directional (layless) surface pattern is said to retain lubricants, rendering the process particularly suitable for the finishing operations.
- xi. The surface finish produced by the EDM process can be controlled to the required extent, minimising the extra cost involved in additional operation for achieving improved surface finish. [1]

#### **1.4.2. LIMITATIONS:**

Despite extensive research highlighting improved capabilities of the process, they are not still widely used. This is mainly due to the fact that available machine tools and process parameters are still not sufficiently reliable. The problematic areas of EDM are as follows.

- i) The slow rate of material removal.
- ii) Potential fire hazard associated with use of combustible oil based dielectrics.
- iii) The additional time and cost used for creating electrodes for ram/sinker EDM.
- iv) Reproducing sharp corners on the workpiece is difficult due to electrode wear.
- v) Specific power consumption is very high.
- vi) Power consumption is high.
- vii) "Overcut" is formed.
- viii) Excessive tool wear occurs during machining.
- ix) Electrically non-conductive materials can be machined only with specific set-up of the process.[2]

## 1.5. LITERATURE SURVEY:

Most of the published papers on EDM are mainly about the applications with EDM to meet the needs of industrial application. Many of them generally mention about the technology of EDM and its parametric studies and its effects on response parameters like MRR, Tool Wear Rate, Surface finish etc. Many have studied the different set-ups on EDM, like vibration set-up on work-piece, spiral tool, mixing abrasive slurry with dielectric etc., to get the better effects on response parameters with respect to process parameter. Many few works have been done on Thermal modelling which this research has focused. This thermal modelling papers have mainly studied the single spark with a point source. Here the earlier works related to basic EDM processes have been observed to take an idea about the basic physics in the stages of EDM and then the thermal modeling have been observed. .

**Yuan-Feng Chen , Yan-Cherng Lin et al.(2009) [3]**proposed a novel combined process that integrates electrical discharge machining (EDM) and ultrasonic machining (USM) to investigate the machining performance and surface modification on Al–Zn–Mg alloy. In the experiment, TiC particles were added into the dielectric to explore the influence of the combined process on the material removal rate (MRR), the relative electrode wear ratio (REWR), the surface roughness and the expansion of the machined hole. The elemental distributions of titanium and carbon on the cross-section were quantitatively determined using an electron probe micro-analyser (EPMA). The experimental results show that the combined process was associated with improved machining performance. The MRR and REWR of the combined process is higher than that of conventional processes and surface roughness becomes lower for combined process.

**M. P. Jahan & PegahKakavand& E. L. M. Kwang& M. Rahman & Y. S . Wong et al.(2015) [4]** identified influence of various operating parameters on the micro-EDM behaviour of an important Al alloy AA 2024, commonly known as ‘Duralumin’. The machining behaviour has been investigated by engraving micro grooves on the surface of the AA 2024 using different parameters settings from a resistance-capacitor (RC) type pulse generator. The operating parameters studied were capacitance, resistance, supply voltage, electrode rotational speed and gap control parameters. The micro-EDM machinability of the AA 2024 alloy was evaluated in terms of the material removal rate (MRR), tool wear ratio (TWR), surface roughness (SR) and machining depth of the micro grooves. It has been found that the increase of capacitance and voltage results in increase of discharge energy, causing higher MRR at the expense of higher tool wear and rougher machined surface. On the other hand, too low capacitance and gap voltage result in unstable machining by creating arcing and short-circuiting, which again makes the surface defective in addition to reducing the machining speed. The careful selection of gap control parameters improves the machining stability by reducing the arcing and short-circuiting as well as improves the overall machining performance.

**Balbir Singh, Jatinder Kumar, and Sudhir Kumar et al.(2015) [5]** showed that aluminium alloy 6061/10% SiC composite is machined using numerical controlled Z-axis (ZNC) electrical discharge machining (EDM) process. Improvement in material removal rate (MRR) is explored using tungsten powder suspended dielectric fluid in EDM process (powder-mixed electrical discharge machining (PMEDM)). Peak current, pulse on time, pulse off time, and gap voltage are studied as process parameters. Mathematical relation between process parameters and MRR is established on basis of response surface methodology. The results obtained are further compared with MRR achieved from machining using simple EDM. The existence of tungsten particles in kerosene resulted in 48.43% improvement in MRR. The influence of tungsten powder-mixed dielectric fluid on machined surface is analyzed using scanning electron microscope and energy dispersive spectroscopy (EDS). The results revealed improvement in surface finish and reduction in recast layer thickness with PMEDM. EDS analysis reported presence of tungsten and carbon in recast layer deposited on machined surface.

**G. D'Urso, C. Merla et al.(2014) [6]** investigated -influence of four different workpiece materials (stainless steel, titanium, magnesium and brass), three electrode materials (copper, brass and tungsten carbide) and two different electrode shapes (cylindrical and tubular). Moreover, an analysis of the geometrical characteristics of the micro holes in terms of conicity and diametrical overcut was carried out. An influence of electrode geometries, electrode material and workpiece material on the final output was found.

The electrode material shows a relevant influence on the final value of the TWR indicator: the tungsten carbide electrode can be considered as the best in terms of tool wear; on the contrary, the brass electrode shows the worst performance. , the copper based electrode has demonstrated to have a “damping effect” on the diametrical overcut: this electrode material should be chosen to ensure a better repeatability of the experiments. The influence of TC electrode geometry (tubular and cylindrical) on the final results was then evaluated. In this case, on the TWR indicator, no relevant influence of the process parameters can be found. On the contrary, the electrode shape seems to have the most relevant effect, even though a monotone trend cannot be found. As regards steel and brass workpiece, the most effective electrode shape is the cylindrical one, ensuring the lower TWR value while for titanium and magnesium workpiece materials the tubular electrode ensures the lowest value of the TWR. Moreover, for magnesium and brass, the TWR absolute value is lower if compared with the other workpiece materials, for each machining condition and for each electrode geometry. For this reason, these two materials can be considered easily machinable with microEDM technology. Differently, both the electrode geometry and the physical properties of the material show a relevant effect on the DOC.

**Soraya Plaza, Jose A. Sanchez, Endika Perez, Ruben Gil, Borja Izquierdo, Naiara Ortega, Inigo Pombo et al. (2014) [7]** observed that there is a growing interest in the machining of micro-holes with high aspect-ratio in difficult-to-machine alloys for the aerospace industry. Processes based on electro discharge machining (EDM) and developed for the manufacture of both micro-electrode and micro-hole are actually used, but most of them involve micro-EDM machines. In this work, the influence of EDM parameters on material removal rate, electrode wear, machining time and micro-hole quality when machining Ti6Al4V is studied. Due to an inefficient removal of debris when increasing hole depth, a new strategy based on the use of helical shaped electrodes has been proposed. The influence of helix angle and flute depth with respect to process performance has been addressed. Main results include 37% reduction in machining times (hole diameter 800  $\mu$ m) when using electrode helix angle of 45° and flute-depth of 50  $\mu$ m, and an additional 19% with flute-depth of 150  $\mu$ m. Holes of 661  $\mu$ m diameter and as much as 6.81 mm depth, which yields in aspect ratio of 10:1, have successfully been machined in Ti6Al4V. Increasing helix angle to higher values (75°) results in more instabilities during the process and a longer machining time. This is probably due to the fact that in this case, debris must travel a longer way, and as a consequence, flushing is poorer. On the other hand, further reductions in helix angle do not introduce any improvement in the results.

**M.P. Jahan, Y.S. Wong, M. Rahman et al. (2012) [11]** introduced a simplistic analytical model to evaluate the effectiveness of low frequency workpiece vibration during the micro-EDM drilling of deep micro-holes. In addition, experimental investigation has been conducted to validate the model by studying the effects of workpiece vibration on machining performance, surface quality and dimensional accuracy of the micro-holes. The effect of vibration frequency and amplitude for three different settings of aspect ratios has been studied experimentally. Moreover, the vibration experiments have been conducted at different levels of gap voltages and capacitances in order to understand the effect of electrical parameters and effectiveness of low-frequency workpiece-vibration at different levels of discharge energies. It has been shown analytically that the effectiveness of low frequency workpiece vibration during micro-EDM drilling can be evaluated by a parameter ' $K_v$ ' (ratio of maximum acceleration of the vibrating plate in gravitational direction to gravitational acceleration ' $g$ '), which can be determined from the vibration frequency, amplitude and phase angle of the vibrating workpiece. The theoretical model reveals that for  $K_v > 1$ , the position of debris particles will be above the workpiece; thus can be flushed away from machined zone effectively. The experimental reasons for improved micro-EDM drilling performance at the setting of  $K_v > 1$  are found to be the increased effective discharge ratio, reduced short circuits and improved dielectric flushing. The experimental results also reveal that the low frequency vibration is more effective at the low discharge energy level, thus making it more suitable for micro-EDM. Considering the effect on both the machining characteristics and micro-hole accuracy parameters, vibration frequency of 750 Hz and amplitude of 1.5  $\mu$ m was found to provide improved performance for the developed vibration device.

**Lin Li , C. Diver, J. Atkinson R. Giedl-Wagner, H. J. Helml et al. [10]**proposed high quality holes of diameters less than 145  $\mu\text{m}$  are required for the manufacture of next generation diesel fuel injection nozzles for improved combustion efficiency and reduction of emission to the environment. The current practice of using electro-discharge machining (EDM) drilling of fuel injection nozzles is limited in terms of the hole size it can produce effectively and the length of time needed to drill. In addition, the tooling cost is high. This paper reports on an investigation into a sequential laser and EDM micro-drilling technique for the manufacture of next generation fuel injection nozzles. A laser-drilled pilot hole is rimmed out by EDM drilling. It was found that this hybrid process has eliminated the problems of recast and heat affected zones typically associated with the laser drilling process. The new process has enabled a 70% reduction in total drilling time compared to standard EDM drilling as less material is removed by the EDM. The quality of the holes is as good as direct EDM drilling, thus eliminating the need for re-certification of the drilling process. Various combinations of laser/EDM drilling conditions have been examined. Optimum diameters for the pilot hole and the EDM electrode have been identified for a particular diameter of fuel injection nozzle, giving the minimum total drilling time and the best quality holes. A special system was designed to enable the alignment of nozzles to be controlled to within  $\pm 20 \mu\text{m}$ . The technique has enabled valuable cost savings and increase in production capacity for next generation fuel injection nozzle manufacture.

**Cheol-Soo Lee , Eun-Young Heo , Jong-Min Kim , In-Hugh Choi , Dong-Won Kim et al.(2015) [9]**said electrode wear of EDM-drilling is rapid compared to that of die-sinking EDM and makes it difficult to control the electrode feed and machine precisely. Thus, this paper presents an effective model to estimate the electrode wear of EDM-drilling. To validate the proposed method, a commercial EDM drilling machine was used. Experimental results show that electrode wear amount can be predicted acceptably. This study proposes an electrode wear estimation model and compensation method through pass through-hole EDM drilling experiments. First, exponential wear curves are fitted by the machining hole count based model, as well as by the machining time based model. After then, frequency and time domain models are compensated in accordance with the EDM environment including discharge conditions, where a memory less property is adopted. The experiments show that the machining time based model more rapidly converges.

**D. Gurgu, E. Vazquez, I. Ferrer et al.(2013) [8]**introduced application of the conventional EDM process to manufacture micro cavities with the objective to obtain how the process parameters could effects on the result. As a result the dimensions and shape of the micro-

cavities are analyzed. In this research the conventional EDM process has been experimented to manufacture products on the micro scale. The results provide recommendations of operating conditions for better micro-cavities manufacturing in stainless steel 316L. The dimensions of the cavities obtained were close to the desired values achieving percentage of error below 5% however the roughness also should be measured.

**Hao Tong, Yong Li, Yang Wang et al.(2008) [12]**suggested improvement of the machining efficiency and accuracy, the method of assisting workpiece vibration was introduced into such micro-EDM process using the tool electrodes with non-circular cross-section or array structures. The micro-amplitude vibration of workpiece was realized by applying high-frequency sine-wave voltage to drive a piezoelectric (PZT) actuator. A number of machining experiments were designed and carried out by changing the frequency and the amplitude of vibration at different discharge parameters. The experimental results showed that the effective discharge ratio increased obviously due to the assisting high-frequency vibration. Moreover, the increase of the effective discharge ratio also increased the spark explosive force, which could accelerate the dielectric liquid circulation and debris removal during the EDM process assisted with workpiece vibration. Therefore the machining stability, the machining accuracy and efficiency of the micro-EDM process are improved. The machining efficiency increased 18 times and the dimension accuracy improved by 10.5  $\mu\text{m}$  when using a tungsten electrode of  $\varnothing 175\mu\text{m}$  at the vibration frequency of 6 kHz and the amplitude of 3  $\mu\text{m}$ . In this study, the emphasis is laid on the effects of assisting workpiece vibration with gap servo control on the EDM performance of micro-structures. Furthermore, the process principle of the effects is analyzed to explain our experimental results. The experimental data and the process analysis suggest that higher frequency vibration helps to acquire higher machining efficiency, and good machining effects can be obtained when the vibration amplitude is set nearly equal to the discharge gap.

**Prof.Dr. Ir. J.-P. Kruth” (I), Ir. L. Stevens, Prof.Dr. Ir. L. Froyen, Dr. Ir. B. Lauwers et al.[14]**studied white layer at the surface of a workpiece. The research work, described in this paper, aims to acquire a profound knowledge of this layer. The influence of workpiece material, electrode material and type of dielectric on the composition and the metallographic phases of the white layer is discussed. The measurements yield that the use of an oil dielectric increases the carbon content in the white layer. A water dielectric on the other hand, causes a decarbonisation. The carbon in the white layer machined in an oil dielectric appears as iron carbides ( $\text{Fe}_3\text{C}$ ) in columnar, dendritic structures. This is a result of the very rapid re-solidification of the molten material. In between the carbide dendrites, rest austenite and also some ferrite can be found.

**D.D.DiBitonto et al.(1989) [15]**observed that a variable mass cylindrical plasma model (VMCPM) which is developed for sparks created by electrical discharge in a liquid media. The model consist of three differential equations-one each from fluid dynamics, an energy

balance, and the radiation equation-combined with a plasma equation of state. A thermo-physical property subroutine allows realistic estimation of plasma enthalpy, mass density, and particle fractions by inclusion of the heats of dissociation and ionization for a plasma created from de-ionized water. Problems with the zero-time boundary conditions are overcome by an electron balance procedure. Numerical solution of the model provides plasma radius which is function of time, temperature, pressure, and mass as a function of pulse time for fixed current, electrode gap, and power fraction remaining in the plasma. Moderately high temperatures ( $>5000$  K) and pressure ( $>4$  bar) persist in the sparks even after long pulse times (to  $\sim 500$  micros). Quantitative proof that superheating is the dominant mechanism for electrical discharge machining (EDM) erosion is thus provided for the first time. Some quantitative inconsistencies developed between our (1)cathode, (2)anode, and (3) plasma models (this series) are discussed with indication as to how they will be rectified in a fourth article to follow shortly in this journal. While containing oversimplifications, these three models are believed to contain the respective dominant physics of the EDM process but need be brought into numerical consistency for each time increment of the numerical solution.

**S.Hinduja, M.Kunieda et al. [18]** reviewed models that have been developed to simulate the thermal models for the spark in EDM. This paper has detected that it is necessary to obtain correct boundary condition, especially the energy distribution and arc plasma diameter. This paper has identified some specific areas which should be kept in mind to do thermal simulation of Electro Discharge machining. In addition to describe the relative merits of the techniques developed in thermal models, the paper describes some salient application and conclude with desirable future enhancement of these models.

**Fritz Klocke, Sebastian Schneider, Simon Harst, David Welling, Andreas Klink et al. [19]** observed that during Electric Discharge Machining process several material loadings take place on the workpiece surface within the processing zone. To model the comprehensive material removal and its effects on the resulting material properties especially in the rim zone and on surface integrity it is necessary to describe these loadings on several length scales in detail. In this paper the different main material loadings occurring during the EDM process are theoretically determined and analyzed with regard to their importance and impact on different scales. Based on this, existing modelling and simulation approaches for the EDM process are critically evaluated and extended regarding a comprehensive description of energy dissipation.

**Y.B. Guo, A. Klink, F. Klocke et al.(2013)[20]**observed that EDM gap phenomena in the micro-scale time and space domains are very complex and challenging to analyze experimentally. However, the gap phenomena are critical to produce optimal surface integrity for superior performance of EDMed components. Nevertheless, the highly nonlinear transient dynamic process involving time/space-dependent plasma and heat flux has not been well understood. This work presents a multiscale finite element modelling for single discharging of ASP2023 tool steel to incorporate the plasma-induced time/space-dependent Gaussian heat flux via a user subroutine. The long-standing numerical singularity of heat flux in EDM modelling is solved using the innovative functions of discharge current. The effects of discharge duration and current on temperature profiles, crater formation, and dimensions are investigated. The basic mechanisms of superheating and melting can be successfully predicted. In addition, melting front recedes at long discharge duration, while melting front advances at high discharge current. Here the temperature has reached almost  $8 \times 10^5 \text{C}$  only at 2.5% of total pulse on-time. There after the temperature has fallen to  $3.423 \times 10^4 \text{C}$  . They have plotted the temperature distribution radially and along subsurface. The paper has described the change of material properties with temperature distribution.

**C. Mascaraque-Ramirez, P. Franco et al.(2015) [21]**proposed a simplified numerical model to analyse the surface finish in penetration EDM with minimized time for numerical computation. This model is focused on prediction of the material removal and surface irregularities on the workpiece material, from the heat transfer and cutting temperatures provoked by the successive sparks. The changes originated on the topography of machined surface can be properly predicted as a function of cutting time by the proposed model. They have eliminated the material, which is in above melting point temperature after sparks.From this they have predicted the surface texture and from this they have taken the surface roughness value.

**J.F. Liu, Y.B. Guo et al.(2016) [20]**said that the, rapid heating and cooling process in EDM may result in poor surface integrity such as white layer on the component surface. Complex phase transformations occur in both white layer and heat affected zone (HAZ) which are detrimental to product performance. This paper presents a numerical approach to predict and analyze the formation mechanisms of WL and HAZ and corresponding phase transformation in EDM of ASP 2023 tool steel. Massive random discharges on the machined surface are successfully simulated. The predicted transformed martensite in WL and HAZ matches the experimental data in reasonable accuracy. Also, the effects of EDM conditions on the thickness of WL and HAZ are investigated. By increasing the discharge duration and voltage, more thermal damage can be found in EDMed surface including thick WL and HAZ and thick martensite zone in particular.

**Jiajing Tang, Xiaodong Yang et al.(2016) [23]**observed in EDM, the extremely high thermal power density results in melting and evaporating followed by removal electrode material, forming a discharge crater on electrode surfaces. Thus, during the formation process of discharge crater, there are the three physical forms (including solid, liquid and vapour) of electrode material and the different phase transformation between them simultaneously. In order to clarify the processes of discharge crater formation and material removal in electrical discharge machining (EDM), in this paper, the thermo-hydraulic coupling numerical model of discharge crater formation was established and analysed with finite element method (FEM). The model is based on the theory of Multi-physics coupling related to the electrode material removal process, and the equations of heat conduction and fluid flow were coupled. In addition, the level set method was used to track the variation of the discharge crater surface. The simulation of the processes of discharge crater formation and material removal in EDM were realized. The temperature distribution, the velocity distribution and the acceleration distribution of heated zone were analysed. It can be found that after discharge is ignited, material removal began to occur. It was also found that the metal removal efficiency was 0.04, leaving most of the molten zone re-solidified. It can be considered that the flow flied formed in the heated zone is one of mechanisms of the material removal and the forming of the discharge crater.

**Y. Zhang, Y. Liu, Y. Shen, Z. Li, R. Ji, F. Wang et al.(2016) [24]**proposed a new method of investigation the characteristic of EDM plasma. The heat flux of the plasma was investigated by comparing the boundary of the melted material in the crater which was obtained by metallographic method and the isothermal surface of the thermal-physical model calculated by finite element method (FEM). The results indicated that the Gauss heat source was much more consistent with the actual EDM process compared with the other heat source type, such as point heat source, circular heat source. The data proposed in this paper can be further used in the existing thermo physical models, expecting to bring the models preciously more close to the actual case.

## **1.6. OBJECTIVE OF PRESENT RESEARCH:**

Electro Discharge Machining is a widely used non-conventional machining process to machine difficult to machine materials. EDM gap phenomenon is a very complex and challenging to analyse. It is a highly nonlinear dynamic transient process where plasma arc is function of both space and time. Also heat flux on the surface yet has not been well understood. Therefore of EDM is in its development stage. In this research step has been taken to reach closer. The objective of this project is,

- i. to study the physical phenomenon happening in the intermediate stages of the Electro Discharge Machining.
- ii. to carry out thermal modelling of the process using suitable FEM.
- iii. to simulate the temperature distribution of the material after applying the heat source on the surface.
- iv. to predict the crater size due to single spark on the surface.
- v. to analyse the temperature distribution in the heat affected zone.
- vi. to predict and analyse the influence of different parameters like pulse-on-time gap current on crater size.

## **2. FUNDAMENTAL FEATURES OF EDM**

### **2.1. BASIC EDM PROCESS:**

Fig.2.1 shows schematically the basic working principle of EDM process. In EDM, a potential difference is applied between the tool and workpiece. Both the tool and the work material are to be conductors of electricity. The tool and the work material are immersed in a dielectric medium. Generally kerosene or deionised water is used as the dielectric medium. A gap is maintained between the tool and the workpiece. Depending upon the applied potential difference and the gap between the tool and workpiece, an electric field would be established. Generally the tool is connected to the negative terminal of the generator and the workpiece is connected to positive terminal.

As the electric field is established between the tool and the job, the free electrons on the tool are subjected to electrostatic forces. If the work function or the bonding energy of the electrons is less, electrons would be emitted from the tool (assuming it to be connected to the negative terminal). Such emission of electrons are called or termed as cold emission. The “cold emitted” electrons are then accelerated towards the job through the dielectric medium. As they gain velocity and energy, and start moving towards the job, there would be collisions between the electrons and dielectric molecules. Such collision may result in ionisation of the dielectric molecule depending upon the work function or ionisation energy of the dielectric molecule and the energy of the electron. Thus, as the electrons get accelerated, more positive ions and electrons would get generated due to collisions. This cyclic process would increase the concentration of electrons and ions in the dielectric medium between the tool and the job at the spark gap. The concentration would be so high that the matter existing in that channel could be characterised as “plasma”. The electrical resistance of such plasma channel would be very less. Thus all of a sudden, a large number of electrons will flow from the tool to the job and ions from the job to the tool. This is called avalanche motion of electrons. Such movement of electrons and ions can be visually seen as a spark. Thus the electrical energy is dissipated as the thermal energy of the spark.

The high speed electrons then impinge on the job and ions on the tool. The kinetic energy of the electrons and ions on impact with the surface of the job and tool respectively would be converted into thermal energy or heat flux. Such intense localised heat flux leads to extreme instantaneous confined rise in temperature which would be in excess of 10,000°C.

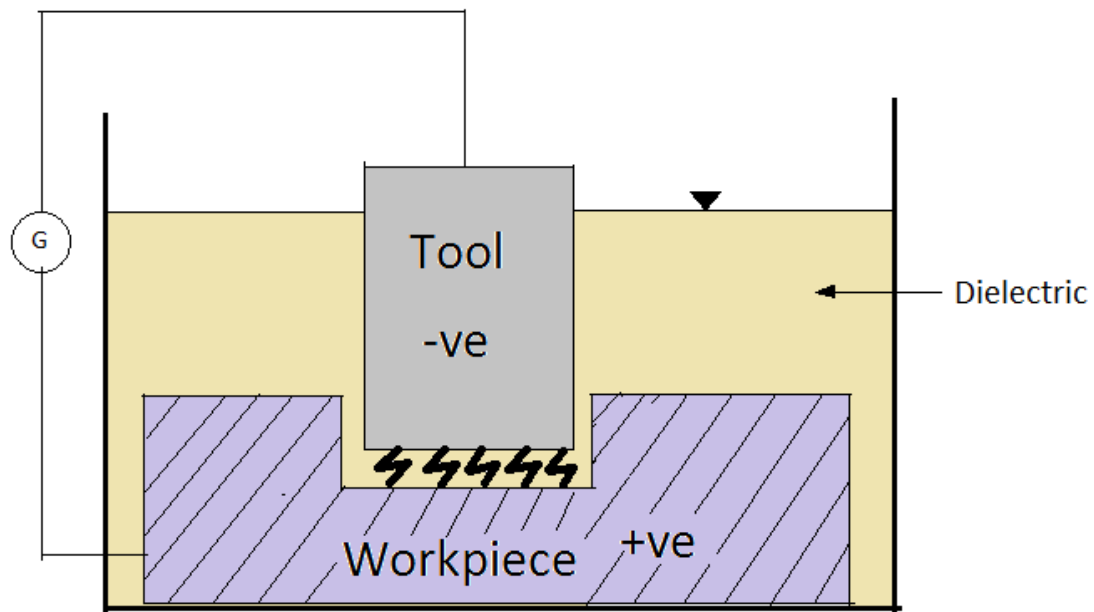


Fig.2.1:Schematic representation of the basic working principle of EDM process.

Such localised extreme rise in temperature leads to material removal. Material removal occurs due to instant vaporisation of the material as well as due to melting. The molten metal is not removed completely but only partially. As the potential difference is withdrawn as shown in Fig. 1, the plasma channel is no longer sustained. As the plasma channel collapse, it generates pressure or shock waves, which evacuates the molten material forming a crater of removed material around the site of the spark. Thus to summarise, the material removal in EDM mainly occurs due to formation of shock waves as the plasma channel collapse owing to discontinuation of applied potential difference. Generally the workpiece is made positive and the tool negative. Hence, the electrons strike the job leading to crater formation due to high temperature and melting and material removal. Similarly, the positive ions impinge on the tool leading to tool wear. In EDM, the generator is used to apply voltage pulses between the tool and the job. A constant voltage is not applied. Only sparking is desired in EDM rather than arcing. Arcing leads to localised material removal at a particular point whereas sparks get distributed all over the tool surface leading to uniformly distributed material removal under the tool.[2]

### **2.1.1. CHARACTERISTICS OF EDM:**

- i. The process can be used to machine any work material if it is electrically conductive.
- ii. Material removal depends on mainly thermal properties of the work material rather than its strength, hardness etc.
- iii. In EDM there is a physical tool and geometry of the tool is the positive impression of the hole or geometric feature machined.
- iv. The tool has to be electrically conductive as well. The tool wear once again depends on the thermal properties of the tool material.
- v. Though the local temperature rise is rather high, still due to very small pulse on time, there is not enough time for the heat to diffuse and thus almost no increase in bulk temperature takes place. Thus the heat affected zone is limited to 2 – 4  $\mu\text{m}$  of the spark crater.
- vi. However rapid heating and cooling and local high temperature leads to surface hardening which may be desirable in some applications.
- vii. Though there is a possibility of taper cut and overcut in EDM, they can be controlled and compensated. [25]

## 2.2. PROCESS PARAMETERS:

Parameters that influence the EDM process can be classified into the following groups:

### 2.2.1. ELECTRODE AND WORKPIECE:

As already discussed, the electrode in EDM process is the means of providing electrical energy to work-material, as well as the necessary form to the latter. The work surface sometimes being the inverse profile of the tool, its accuracy depends upon the form stability of the tool under the severe electrical and flushing stress conditions. Moreover the share of heat that the tool receives from the plasma channel, is to be dissipated away faster unlike work-material in order to reduce surface temperature. Theoretically, any material that is a good electrical conductor can be used as a tool with more or less advantages. In general, tool or electrode materials can be classified into four groups:

- (i) Metallic electrodes : Electrolytic copper, Tellurium or Chromium Copper, Copper Tungsten, Brass, Aluminium, Aluminium Alloy, Silver Tungsten, Steel
- (ii) Non-metallic : Graphite
- (iii) Combined metallic and non-metallic : Copper-Graphite
- (iv) Metallic coating as Insulators : Copper on moulded Plastic, and copper on ceramics.[1]

The properties of the work-piece material and electrode material that affects the machining process-

- a) Diameter
- b) Materials
- c) Thermal Properties

### 2.2.2. DIELECTRIC & FLUSHING:

Since the process of removal of materials (both from work and tool) mainly depends on thermal evaporation and melting, the presence oxygen in the atmosphere surrounding the spark would lead to formation of metal oxides which adversely affect the continuation or generation of repetitive sparks (most of metal oxides are bad conductor). Hence it is pertinent to use dielectric fluid which contain no oxygen for liberation during the process to help ionization, without disturbing the process. But the performance (mainly the failure) of the dielectric to suit the purpose is extremely important.

The failure of dielectrics under the dielectric stress, termed as dielectric breakdown, is found to spread over the wide range of applied stresses, depending upon of environment and mode of use.

In general, the main basic mechanism of dielectric breakdown in the three states of matter are : 1)intrinsic, 2)thermal 3) discharge or avalanche.

#### Breakdown Mechanism:

The earlier theory of breakdown in liquids have assumed that it occurs by avalanche ionization of the atoms included by conduction electrons accelerated in the applied field. The cathode electrode is assumed to be source of this electrons which are emitted either by field effect or by the schottky-effect.

The electron liberated from the cathode gain from the applied field more energy than it lose in vibrational collision with the molecules of the liquid dielectric. These electrons are accelerated until they gain sufficient energy to ionize the liquid molecules and initiate an electron avalanche. Considering this mechanism, Lawis analytically showed that the vibrational collision account for the major energy loss in the hydrocarbons where bond vibration is the main absorbent. The applied field E, at which an avalanche can be initiated and is given as

$$eE\lambda = ch\gamma \text{-----} 2.1$$

Where  $\lambda$  is mean free path of electron of charge e, c is the velocity of light and  $h\gamma$  ionization quantum for the electrode molecule.

The theory satisfactorily predicts the order to magnitude of the breakdown strength of the dielectrics. But it does not account for the ignition-delay between the application of a pulse of voltage greater than the breakdown voltage and the actual onset of breakdown.

The dielectric generally used in EDM are Deionized water, EDM oil, Kerosene etc.

The properties of the material and characteristics that influences the machining:

- a) Sp. Resistance
- b) Pressure
- c) Contamination
- d) Flow rate
- e) Supply method

### 2.2.3. POWER GENERATOR:

The process parameters in EDM are mainly related to the waveform characteristics Gap Voltage-

- a) Polarity
- b)  $T_{on}$  and  $T_{off}$
- c) Resistance
- d) Capacitance
- e) Discharge Current
- f) Gap Voltage

Fig. x depicted general nature of voltage pulses used in electro-discharge machining. Different power generators are used in EDM and some are listed below:

**I. Resistance-capacitance type (RC type) Relaxation generator :**

It is normal charging and discharging circuit. Here as the resistance increases the energy per pulse drops and vice versa. And as the capacitance increases the energy per pulse increases.

**II. Rotary impulse type generator:**

It supplies the voltage waveform based on the principles as in the case of DC generators. This type of generator supplies very high voltage in excess of 110V. Arcing is frequent since the waveform is uncontrollable, so the TWR is very high, more than 100% of MRR. The use is being restricted since uneconomical, high inaccuracy in machining process and high surface damage.

**III. Electronic pulse generator**

It has been observed that the Relaxation generator with its simplicity could not meet the demand for higher production which reflected in high amount of tool wear. So, only restricted to low MRR machining system.

To search for higher production with lower MRR there were innumerable circuit modification of relaxation circuit but these are of no use. Only electronic pulse generator is suitable for the use.

**IV. Hybrid EDM generator:**

The hypothetical waveforms for this for this type of generators are shown in figure 2.2.4. This type of generator uses trapezoidal waveform instead of square waveform. Instead of sudden rise of voltage a slope has been maintained to match with the ionisation characteristics of dielectric. [1]

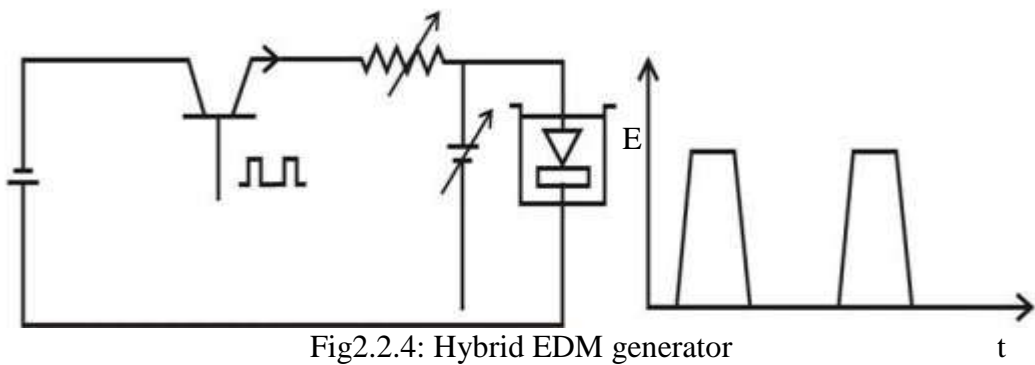
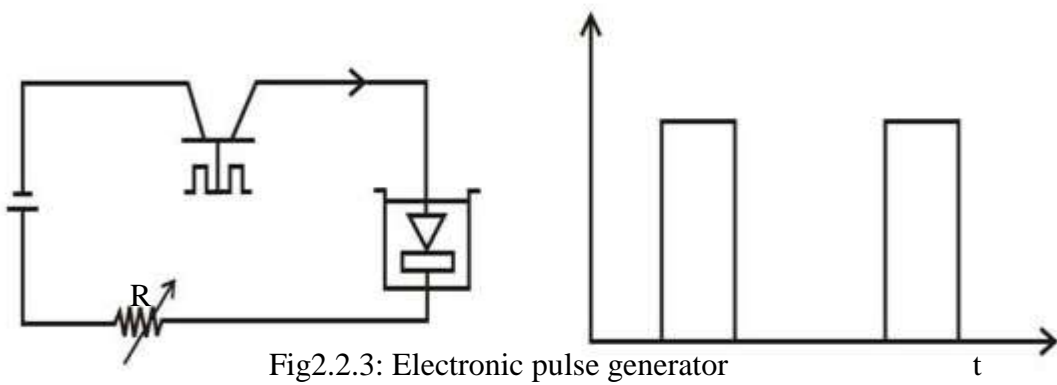
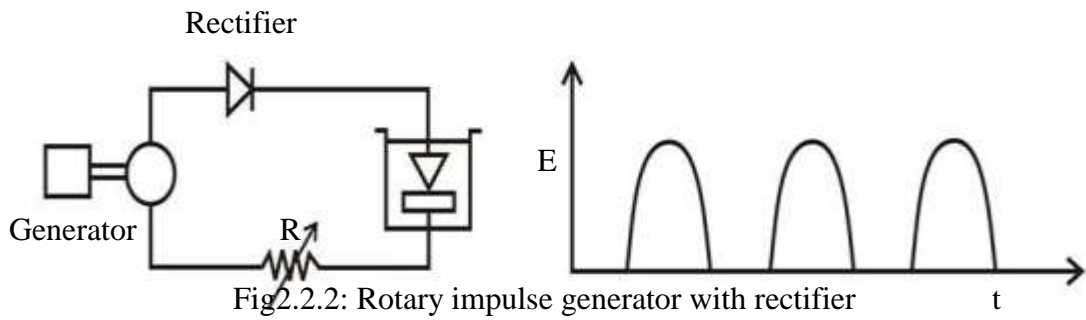
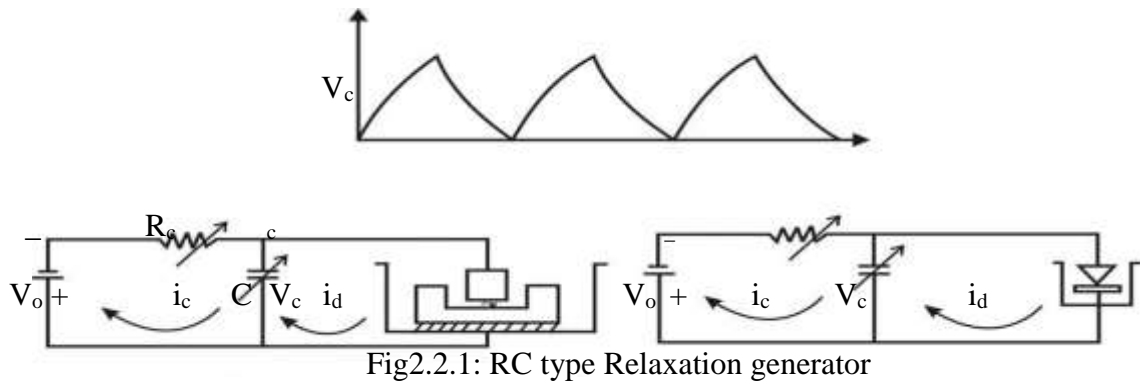


Fig.2.2: The basic circuit for different type of EDM generators [25]

#### **2.2.4. SPARK GAP:**

It is the gap between the electrode and workpiece material is known as spark gap.  
It is typically maintained by the servo motor.

#### **2.2.5. CONTROLLER SPECIFIC:**

- a) Control Strategy
- b) Discharge control circuit

### 2.3. PROCESS CRITERIA:

Various response parameters can be obtained during machining by EDM by varying different process parameters as discussed below:

i. **Material Removal Rate (MRR):**

Material removal rate in EDM is defined as the amount of material removed from workpiece in unit time and usually expressed in mg/min. In EDM the MRR generally calculated by weight reduction taking weight of it before and after the machining per unit time. Volumetric MRR is the volume of material removal per unit time, expressed as

$$\text{Vol. MRR(mm}^3\text{/min)} = \frac{[\text{workpiece weight loss(gm)}] * 1000}{[\text{Density(gm/cc)}] * [\text{Machining time(min)}]} \quad \text{-----} \quad 2.2$$

ii. **Tool Wear Rate (TWR):**

Tool wear rate (TWR) is the amount of the weight of the loss of the tool per unit time when the machining is carried out. It is expressed as mg/min. Tool wear should be low as machined cavity should be low, as machined cavity is the mirror image of the tool shape.

Relative Tool Wear Rate (RTW) is also a important response parameter which is a unit less term expressed as [(TWR)/(MRR)].

iii. **Diametric Overcut:**

When the electro discharge machining is done, the diameter of the machined area diameter will be greater than the diameter of the tool due to sidewise spark and also due to the distribution of the temperature due to spark. Diametric overcut is the difference of the diameter of the machined area and the diameter of tool. This overcut should be minimized to get accurate geometry.

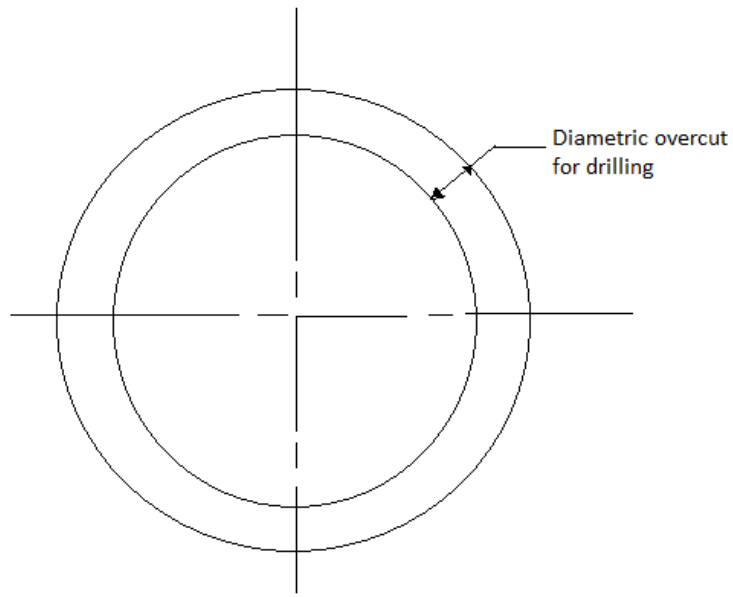


Fig2.3: Over cut due to drilling

iv. Hole Taper:

For a through hole, taper can be measured. The top and bottom diameter of a hole is not same in case of EDM. Taper hole can be measured as:

$$\text{Taper Rate} = \frac{(D-d)}{2H} \quad \text{-----} \quad 2.3$$

Where D=diameter of the machined area, d= diameter of the tool, H= Hole depth.

v. Heat Affected Zone:

The HAZ is the area of base metal, which is not melted and has its microstructure and properties affected by machining. The heating and re-cooling causes the change of the material properties.

vi. Surface Finish:

The surface roughness here is measured by  $R_z$ ,  $R_a$ ,  $R_{max}$  measurement.

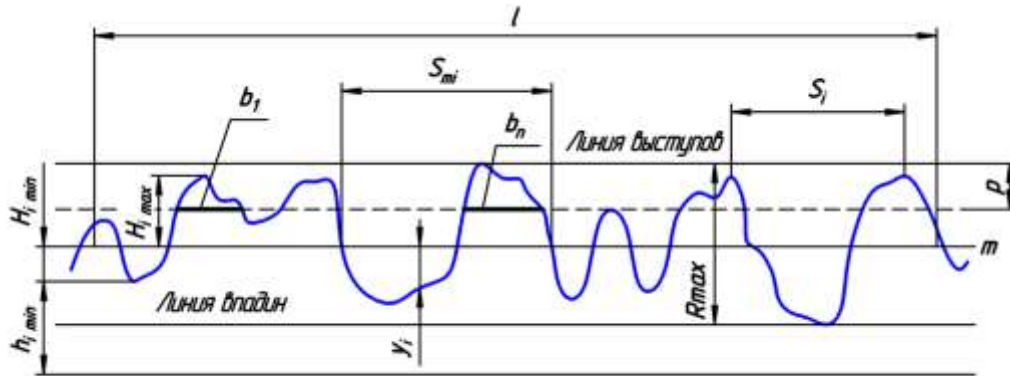


Fig2.4: Surface texture[28]

Where,  $R_a = (1/n) \sum (y_i)$  ----- 2.5

$R_z = \sqrt{[(1/n) \sum (y_i^2)]}$  [n is the sample size] [28] ----- 2.6

vii. Recast Layer:

The EDMed surface tolerates the solidification behaviour of the molten metal after the discharge cessation and subsequent phase transformation. So, the surface roughness value gets hampered and the value should be as low as possible. The surface is made up of three layers: white layer/ recast layer, Heat Affected Zone, Unaffected layer.

A layer created by the re-solidification of the molten metal of the workpeice surface after it has been melted by the EDM process. This layer thickness should be minimum to get high quality products.

viii. Surface Cracks:

There may be surface cracks due to EDM, due to high temperature rise and thermal stress development due to it. It can be seen by a Non Destructive Test (NDT), seeing it in microscope after etching the surface. [2]

## 2.4. STEPS OF EDM:

EDM is generally used for producing blind cavities; here the electrode and a work piece are submerged in an insulating liquid, known as dielectric fluid. So, principally this is similar to that of common EDM process. The die sinker EDM is also known by different names such as ram EDM, sinker EDM, vertical EDM and plunge EDM. The process has the following characteristics –

- i. Non-contact machining: Machining can be done without applying pressure on the material. Therefore high precision machining of curved surface, inclined surfaces and thin sheet materials that are difficult to machine is possible.
- ii. 3D Machining: It facilitates generation of 3dimensional features with the help of a solid tool and its associated motions. Further complex shapes can be machined by combining the process with other micro machining techniques like ultrasonic machining, laser radiation, LIGA technology, chemical etching processes etc.
- iii. Micro-EDM can machine any material by irrespective of their hardness provided they are electrically conductive

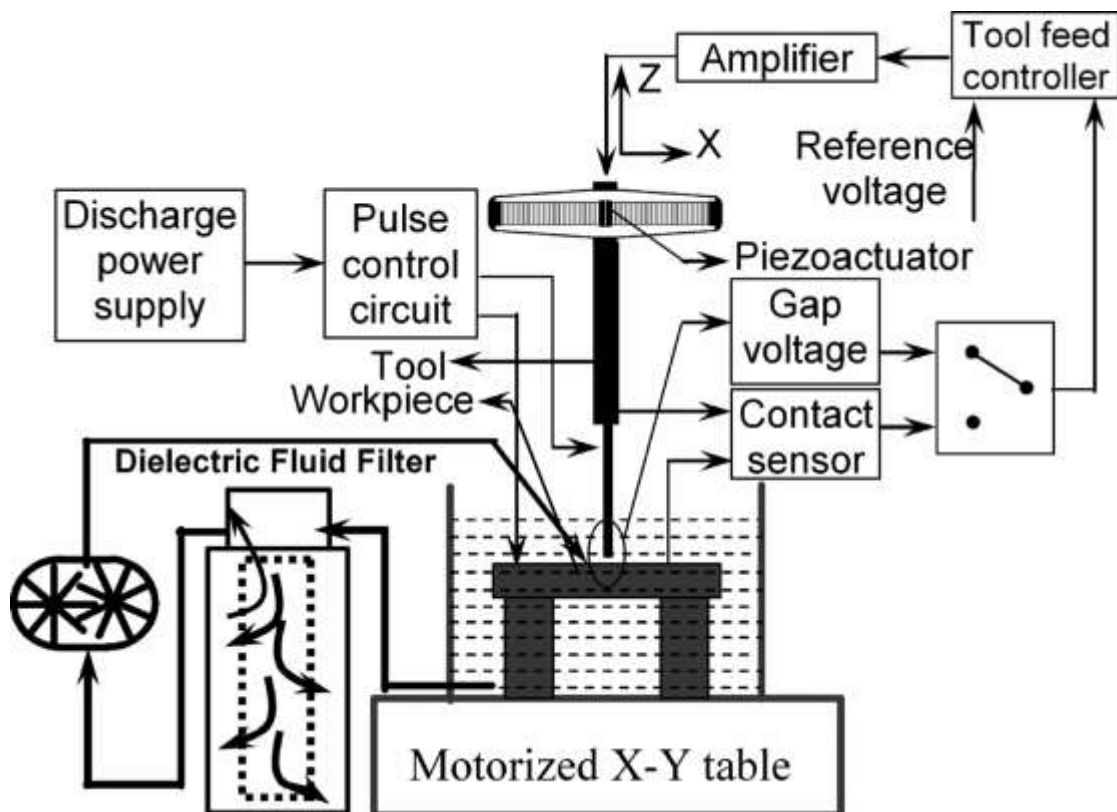


Fig2.5: A typical Electro Discharge Machining Set-up[25]

The steps of EDM are shown in figure2.6:

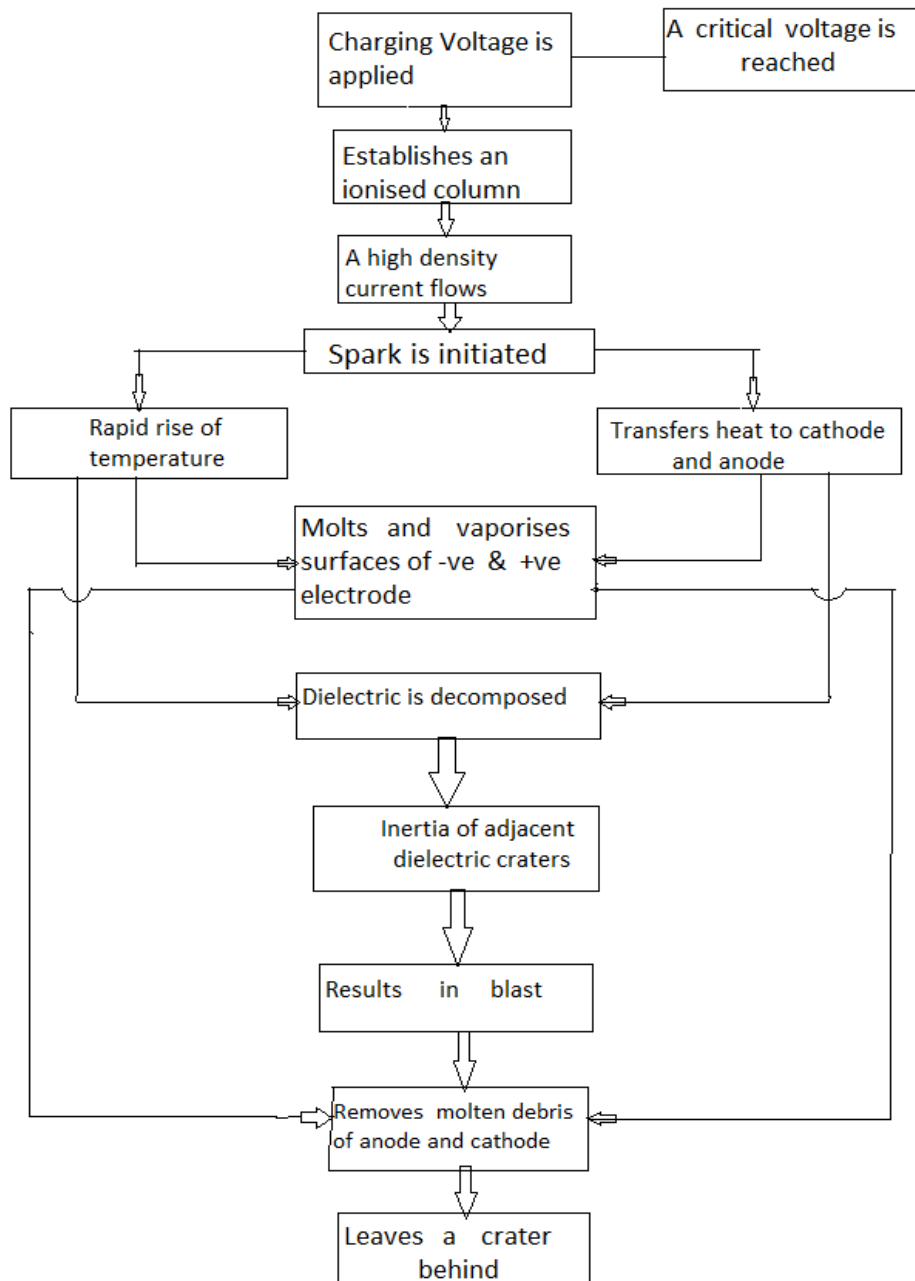


Fig2.6: Stages of EDM action

After applying the voltage between workpiece and tool a critical voltage is reached when the ionisation starts. The ions are accelerated towards the workpieces. During this the ions collide with dielectric material and ionize the dielectric. Thus the count of electron increases and dielectric breaks down and avalanche of electrons strikes the material and erodes the material by melting and vaporization.

## 2.5. MATERIAL REMOVAL AND SURFACE FINISH IN EDM:

### 2.5.1. MATERIAL REMOVAL:

Material removal in EDM mainly occurs due to intense localised heating almost by point heat source for a rather small time frame. Such heating leads to melting and crater formation as shown in Fig.

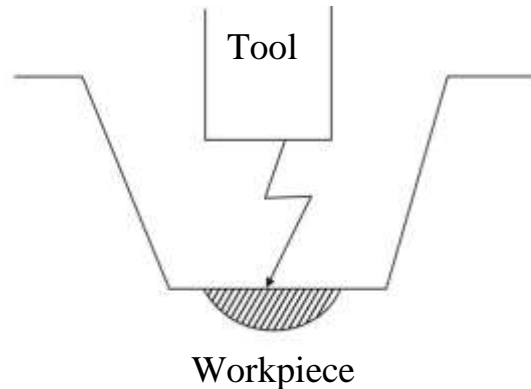


Fig2.7: Schematic representation of crater formation in EDM process.[25]

The molten crater can be assumed to be hemispherical in nature with a radius  $r$  which forms due to a single pulse or spark. Hence material removal in a single spark can be expressed as

$$\Gamma_s = \frac{2}{3}\pi r^3 \quad \text{-----} \quad 2.1$$

Now as per Fig. 2, the energy content of a single spark is given as

$$E_s = VIt_{on} \quad \text{-----} \quad 2.2$$

A part of this spark energy gets lost in heating the dielectric, and rest is distributed between the impinging electrons and ions. Thus the energy available as heat at the workpiece is given by

$$E_w \propto E_s$$

$$E_w = kE_s \quad \text{-----} \quad 2.3$$

Now it can be logically assumed that material removal in a single spark would be proportional to the spark energy. Thus

$$\Gamma_s \propto E_s \propto E_w$$

$$\therefore \Gamma_s = gE_s$$

Now material removal rate is the ratio of material removed in a single spark to cycle time. Thus

$$MRR = \frac{I_s}{t_c} = \frac{\Gamma_s}{t_{on} + t_{off}}$$

$$MRR = g \frac{VIt_{on}}{t_{on} + t_{off}}$$

$$\text{-----} \quad 2.4$$

The model presented above is a very simplified one and linear relationship is not observed

in practice. But even then such simplified model captures the complexity of EDM in a very efficient manner. MRR in practice does increase with increase in working voltage, current, pulse on time and decreases with increase in pulse off time. Product quality is a very important characteristic of a manufacturing process along with MRR. The followings are the product quality issues in EDM

- i. Surface Finish
- ii. Over Cut
- iii. Taper Cut

**2.5.2. SURFACE FINISH:**

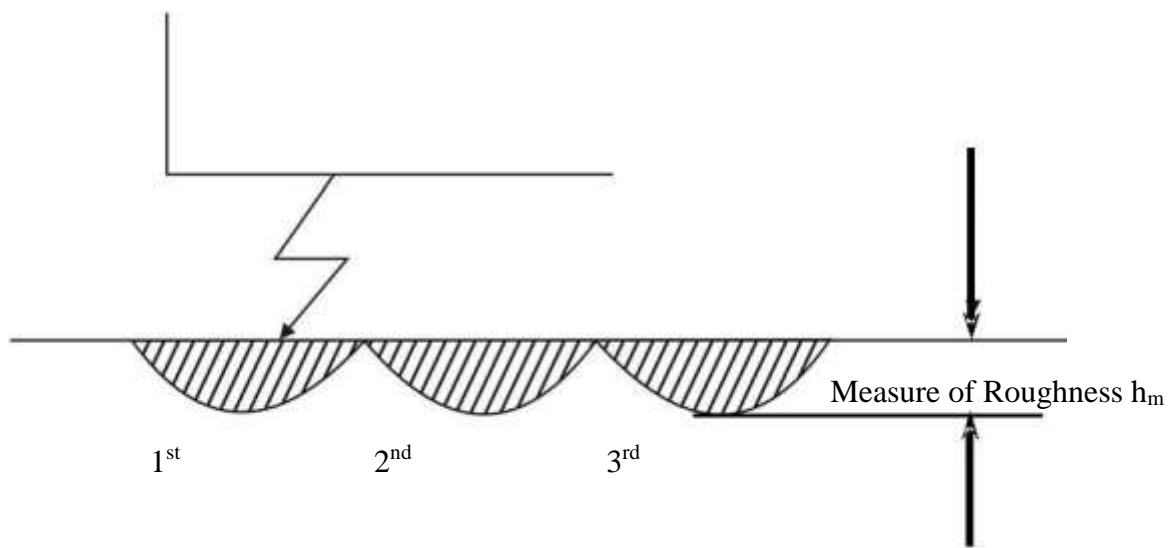


Fig.2.8: Schematic representation of the sparks in EDM process.[25]

Thus

$$h_m = r \text{ and } \Gamma_s = \frac{2\pi r^3}{3} \tag{2.5}$$

$$\therefore r = h_m = \left[ \frac{3}{2} \cdot \frac{1}{\pi} \cdot \Gamma_s \right]^{1/3} \tag{2.5}$$

Now  $\Gamma_s = gE_s = gVIt_{on}$

$$\therefore h_m \propto (\Gamma_s)^{1/3} \propto \{VIt_{on}\}^{1/3} \tag{2.6}$$

Thus it may be noted that surface roughness in EDM would increase with increase in spark energy and surface finish can be improved by decreasing working voltage, working current and pulse on time.

In EDM, the spark occurs between the two nearest point on the tool and workpiece. Thus machining may occur on the side surface as well leading to overcut and tapercut. Taper cut can be prevented by suitable insulation of the tool. Overcut cannot be prevented as it is inherent to the EDM process. But the tool design can be done in such a way so that same gets compensated. [25]

### **3. THERMAL MODELLING OF ELECTRO DISCHARGE MACHINING:**

#### **3.1. NEED FOR THERMAL MODELLING:**

In modern days thermal modelling is becoming a very useful tool to analyse any thermal machining processes. The need of thermal modelling is as follows:

- i. The physical phenomenon happening in between the steps of the thermal process can be easily by thermal modelling.
- ii. It is hard to determine the temperature distribution in the material due to thermal loading given in a time span of microsecond range. It can be easily done by thermal modelling.
- iii. The melted and vaporized part can be predicted by thermal modelling before doing the experiment. Also the Heat Affected Zone can be observed.
- iv. The effects of process parameters on response parameters can be predicted.
- v. The feasibility of machining any material by any thermal process can be checked by thermal modelling

#### **3.2. MODELLING TOOLS:**

Various Finite Element Analysis softwares are available for solving the complex calculations and analyse the modelling. Some of this softwares are mentioned below:

##### **i. COMSOL MULTIPHYSICS:**

COMSOL Multiphysics is a finite element analysis, solver and simulation software / FEA software package for various physics and engineering applications, especially coupled phenomena, or multiphysics. The package is cross-platform (Windows, Mac, Linux). In addition to conventional physics-based user interfaces, COMSOL Multiphysics also allows entering coupled systems of partial differential equations (PDEs). The PDEs can be entered directly or using the so-called weak form. Since version 5.0 (2014), COMSOL Multiphysics is also used for creating physics-based apps. These apps can be run with a regular COMSOL Multiphysics license but also with a COMSOL Server license. An early version (before 2005) of COMSOL Multiphysics was called FEMLAB.

## **ii. ABAQUS:**

Abaqus FEA(formerly ABAQUS) is a software suite for finite element analysis and computer-aided engineering, originally released in 1978. The name and logo of this software are based on the abacus calculation tool. The Abaqus product suite consists of five core software products:

- Abaqus/CAE, or "Complete Abaqus Environment" (a backronym with an obvious root in Computer-AidedEngineering). It is a software application used for both the modeling and analysis of mechanical components and assemblies (pre-processing) and visualizing the finite element analysis result. A subset of Abaqus/CAE including only the post-processing module can be launched independently in the Abaqus/Viewer product.
- Abaqus/Standard, a general-purpose Finite-Element analyser that employs implicit integration scheme (traditional).
- Abaqus/Explicit, a special-purpose Finite-Element analyser that employs explicit integration scheme to solve highly nonlinear systems with many complex contacts under transient loads.
- Abaqus/CFD, a Computational Fluid Dynamics software application which provides advanced computational fluid dynamics capabilities with extensive support for preprocessing and postprocessing provided in Abaqus/CAE.
- Abaqus/Electromagnetic, a Computational electromagnetics software application which solves advanced computational electromagnetic problems.

The Abaqus products use the open-source scripting language Python for scripting and customization. Abaqus/CAE uses thefox-toolkit for GUI development.

## **iii. ANSYS:**

ANSYS, Inc. is an American Computer-aided engineering software developer headquartered south of Pittsburgh in Cecil Township, Pennsylvania, United States. Ansys publishes engineering analysis software across a range of disciplines including finite element analysis, structural analysis, computational fluid dynamics, explicit and implicit methods, and heat transfer.

There are many other software like DEFLUX, Altair Engineering Acusolve, Pumplinx, AVL FIRE etc.

### **3.3. FINITE ELEMENT ANALYSIS OF EDM:**

The modelling of Electro Discharge Machining here done by considering only single spark. The heat input here by the spark has a Gaussian distribution on the surface of its application. Based on this heat source differential equations are solved by taking some initial boundary condition and also materials properties like thermal conductivity, specific heat, density and emissivity.

In this modelling the finite element analysis software COMSOL is used. The differential equations are solved by this software. The material geometry has been divided into very small elements by COMSOL and solutions have been made for this small elements and it has given some favourable results.

#### **3.3.1. ASSUMPTIONS:**

The assumptions in making the present model are as follows:

- a) The material is isotropic.
- b) Initially the material is flat.
- c) As the melted and vaporized portion is very small, the material killing is not considered here.
- d) Here the single spark is considered only in a single stage.
- e) Effect of debris and bubbles coming out of the machining zone has been considered as minimum and has not taken into account.
- f) Convection of heat from the surface is not considered here.
- g) The thermal expansion and contraction is not considered.
- h) As there point source has been considered as stated before, there the heat emission from the tool is not considered.
- i) There the pressure created by the plasma arc is not considered.
- j) The flow of the dielectric in the machining zone is not considered here.
- k) There the effect of spark gap on the power distribution is not considered.

### 3.3.2. WORKPIECE MATERIAL:

In this simulation AISI 304 stainless steel has been considered. Type 304 is the most versatile and widely used of all the stainless steels. Their chemical composition, mechanical properties, weldability and corrosion/oxidation resistance provides the best all-round performance at relatively lower cost. These have excellent low-temperature properties and respond well to hardening by cold working. The carefully controlled chemical compositions of various sub-grades provide a large range of cold work hardenability, enabling them to suit for various applications by direct drawing without intermediate annealing.

#### Chemical composition:

Table 3.1. Chemical composition of AISI 304 Stainless Steel

Material	Fe	C	Mn	P	S	Si
AISI 304 Stainless Steel	96.845%	.08%	2%	.045%	.030%	1%

#### Mechanical Properties:

Table3.2.Mechanical Properties of AISI 304 Stainless Steel

Tensile Strength [Mpa]	Yield Strength[Mpa]	Hardness[HB]
585	240	150

#### Physical & Thermal Properties:

Table.3.3. Physical & Thermal Properties of AISI 304 Stainless Steel

Density	Thermal Conductivity	Specific Heat	Melting Point Temp.	Emissivity
Varying from <b>7854Kg/m<sup>3</sup></b> to <b>7501.68 Kg/m<sup>3</sup></b> over the range of temp. 200K to 1728K	Varying from <b>12.60 W/mK</b> to <b>35.62W/mK</b> over the range of temp. 200K to 1728K	Varying from <b>402 J/KgK</b> to <b>4490.90J/KgK</b> over the range of temp. 200K to 1728K	1673 K	0.6

Here the properties like Density, Thermal Conductivity and Specific Heat are given in 120 steps. They are varied with temperature and maximum steps are attached around the region of the material's melting point temperature which is 1673K to include the latent heat of melting of the material.

### **3.3.3. GEOMETRY:**

As the calculation is done by considering only one spark. So, here a small part of material is taken, where the temperature distribution and melted portion can be detected easily. Here the total geometry is of  $100\mu\text{m}$ (length)  $\times$   $100\mu\text{m}$  (width)  $\times$   $40\mu\text{m}$  (depth). The geometry has been constructed in 5 parts as shown in figure. The middle portion which is our main part of interest is of  $10\mu\text{m} \times 10\mu\text{m} \times 40\mu\text{m}$ .

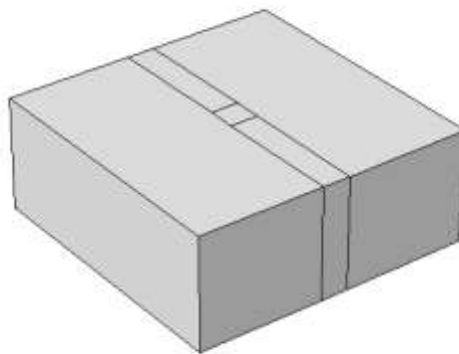


Fig3.1: Isometric view of the Geometry taken for calculation

### 3.3.4. MESHING:

Here the total modelling is done by the Finite Element Analysis software COMSOL. Mesh generation is the practice of generating a polygonal or polyhedral mesh that approximates a geometric domain. The term “grid generation” is often used interchangeably. Here the total material is divided into large number of small elements as shown in figure. In the middle portion of the material where the beam is falling, the material is meshed extremely fine.

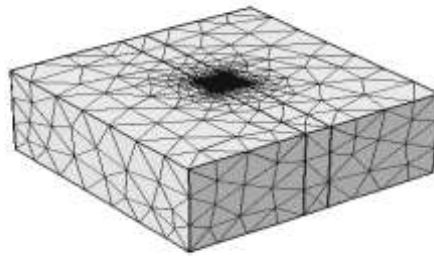


Fig3.2: Meshed Material

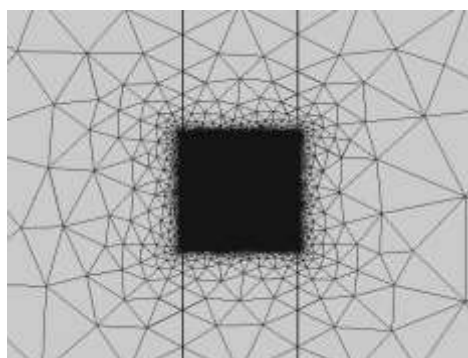


Fig3.3: The middle portion of extremely fine meshing

### 3.3.5. PARAMETER:

Here 18 sets of parameters have been taken. Parameters taken here are Gap Voltage, Gap Current and Pulse-on-time. The range of parameters have been collected from the previous journal papers.

Table.3.4. Parameter Setting

Serial No.	Gap Voltage	Gap Current	Pulse-on-time
1	40V	2A	40 $\mu$ s
			60 $\mu$ s
			80 $\mu$ s
2	40V	3A	40 $\mu$ s
			60 $\mu$ s
			80 $\mu$ s
3	40V	4A	40 $\mu$ s
			60 $\mu$ s
			80 $\mu$ s
4	45V	2A	40 $\mu$ s
			60 $\mu$ s
			80 $\mu$ s
5	45V	3A	40 $\mu$ s
			60 $\mu$ s
			80 $\mu$ s
6	45V	4A	40 $\mu$ s
			60 $\mu$ s
			80 $\mu$ s

### 3.4. HEAT FLUX:

The EDM plasma arc is falling on the middle of the top surface. So, the heat flux is given on the top surface. The heat flux induced by EDM is function of discharge time and also radial position. The heat flux obeys Gaussian distribution, is given as-

$$H(r,t) = [(C.U.I)/(3.14(R(t))^2)] \cdot \exp. [-m(r^2/R^2(t))] \text{ ----- 3.1}$$

Where,  $H(r,t)$ = Heat flux [ $W/m^2$ ],

$U$ = Gap Voltage[V],

$I$  = Gap Current [A],

$R(t)$ = Time dependent plasma arc radius [m],

$r$ = Radial distance from the plasma center (m)

$t$ = Discharge time (s)

$C$ = Fraction of plasmas energy to the workpiece

$m$ = Coefficient to tune the shape of Gaussian curve.

The fraction of plasmas energy to the workpiece is 0.18 based on the calibrated data by DiBitonto. The coefficient of Gaussian curve is  $m= 2$  since it only slight changes the slopes the curve. The time-dependent plasma radius can be determined by

$$R(t) = .0249 \cdot t^{.75} \text{ ----- 3.2}$$

[20]

## 4. RESULTS AND DISCUSSIONS:

### 4.1. ANALYSIS OF CHANGE OF TEMPERATURE DISTRIBUTION OVER SLICED PLANE:

After completing simulation in COMSOL MULTIPHYSICS the software has given the temperature distribution only on the outer surfaces of the material, it is not giving the temperature distribution along depth. Because of that to illustrate the temperature distribution along radial direction and along depth simultaneously, the sliced view through the plasma arc centre is taken.

#### A. $V_{\text{gap}}=40\text{V}$ , Gap Current (I)=2A:

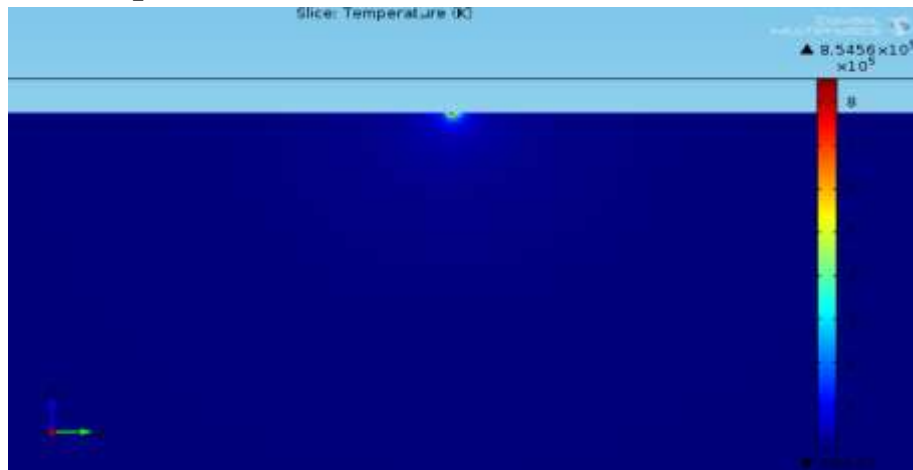


Fig4.1.Temp. Distribution over sliced plane 40V,2A, $T_{\text{on}}=40$ microsecond

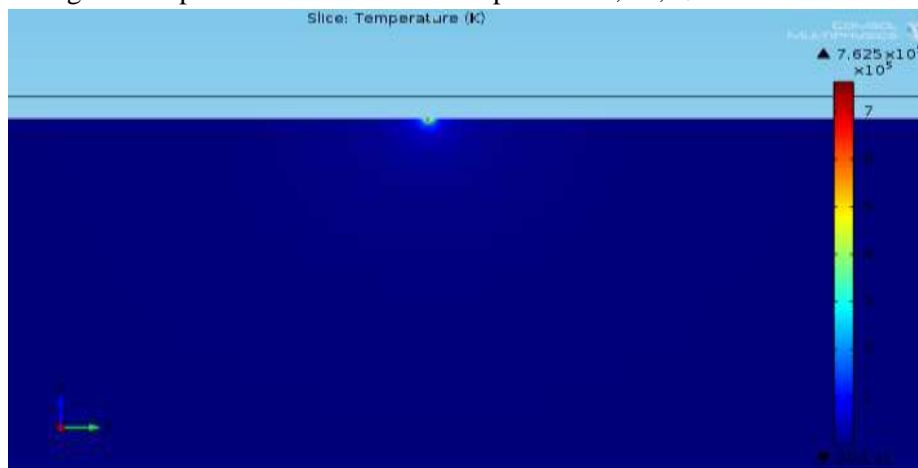


Fig4.2.Temp. Distribution over sliced plane 40V,2A, $T_{\text{on}}=60$ microsecond

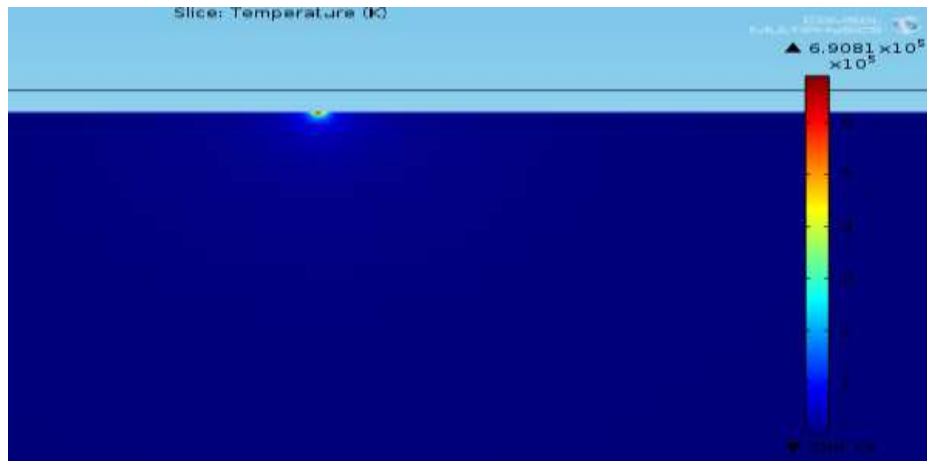


Fig4.3.Temp. Distribution over sliced plane 40V, 2A, $T_{on}=80$ microsecond

**B.  $V_{\text{gap}}=40\text{V}$ , Gap Current (I)=3A:**

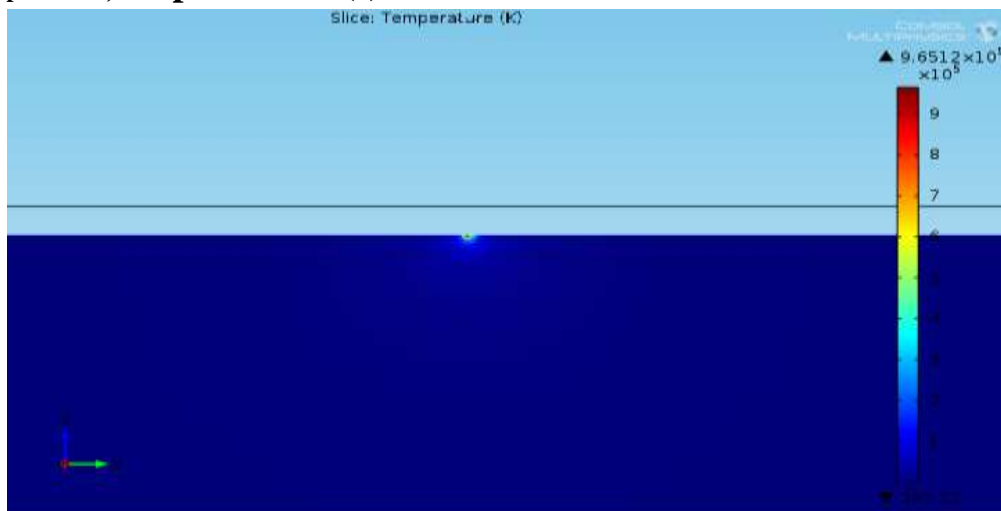


Fig4.4.Temp. Distribution over sliced plane 40V,3A, $T_{\text{on}}=40$ microsecond

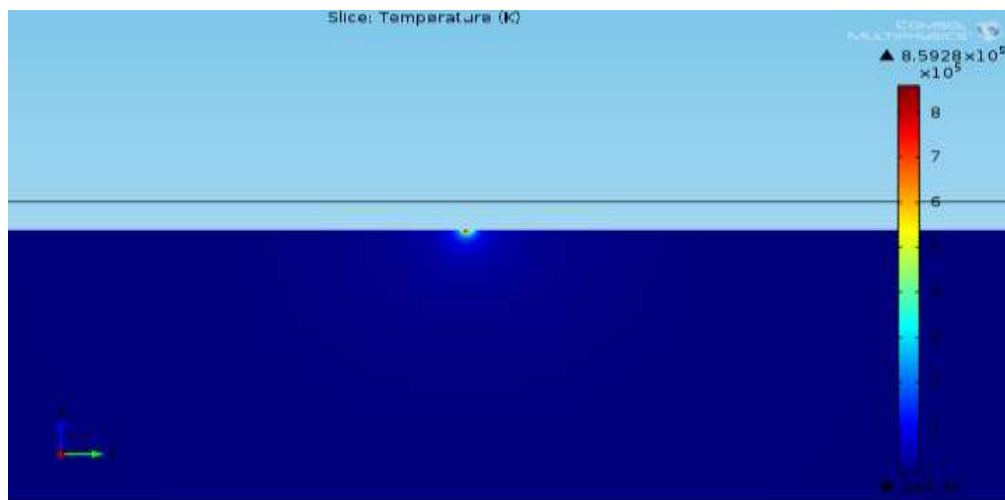


Fig4.5.Temp. Distribution over sliced plane 40V,3A, $T_{\text{on}}=60$ microsecond

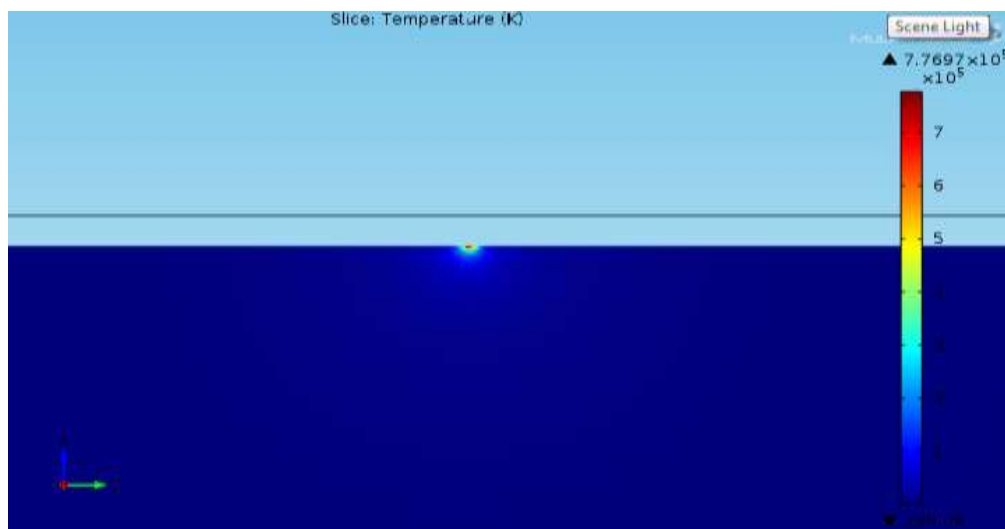


Fig4.6.Temp. Distribution over sliced plane 40V,3A, $T_{\text{on}}=80$ microsecond

**C.  $V_{\text{gap}}=40\text{V}$ , Gap Current (I)=4A:**

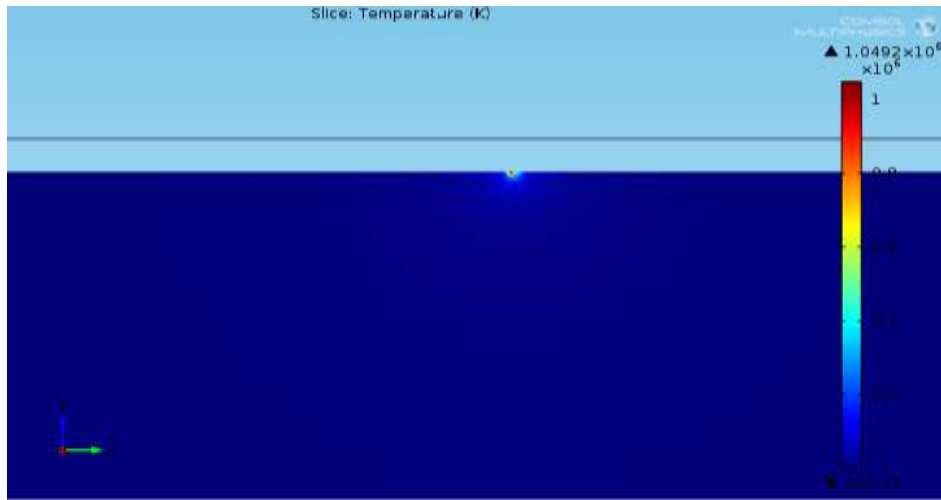


Fig4.7.Temp. Distribution over sliced plane 40V,4A, $T_{\text{on}}=40$ microsecond

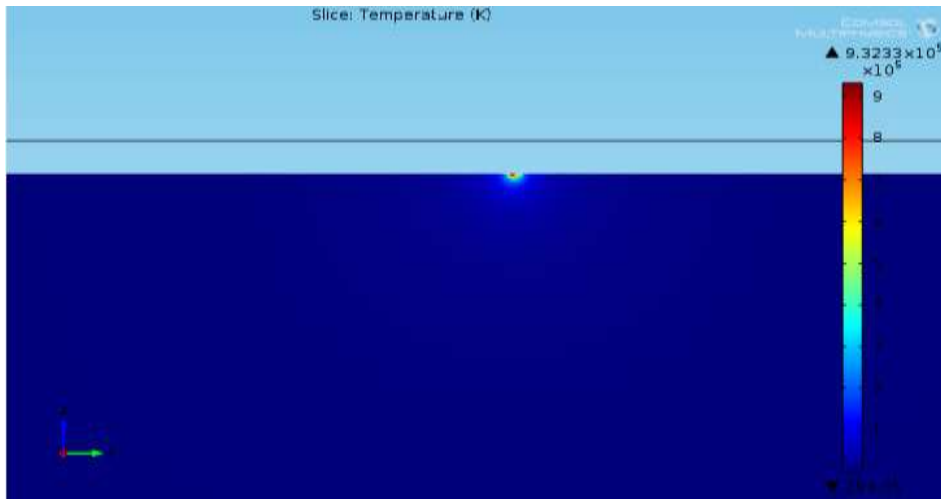


Fig4.8.Temp. Distribution over sliced plane 40V,4A, $T_{\text{on}}=60$ microsecond

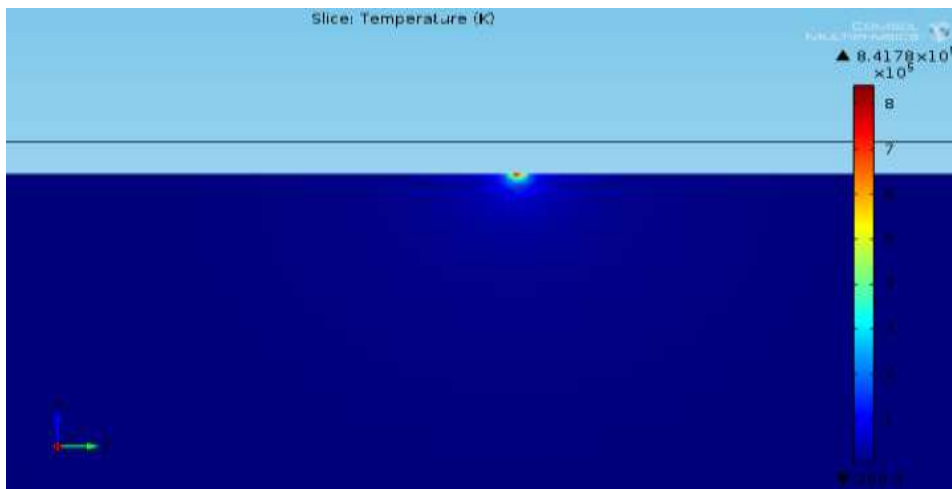


Fig4.9.Temp. Distribution over sliced plane 40V,4A, $T_{\text{on}}=80$ microsecond

**D.  $V_{\text{gap}}=45\text{V}$ , Gap Current (I)=2A:**

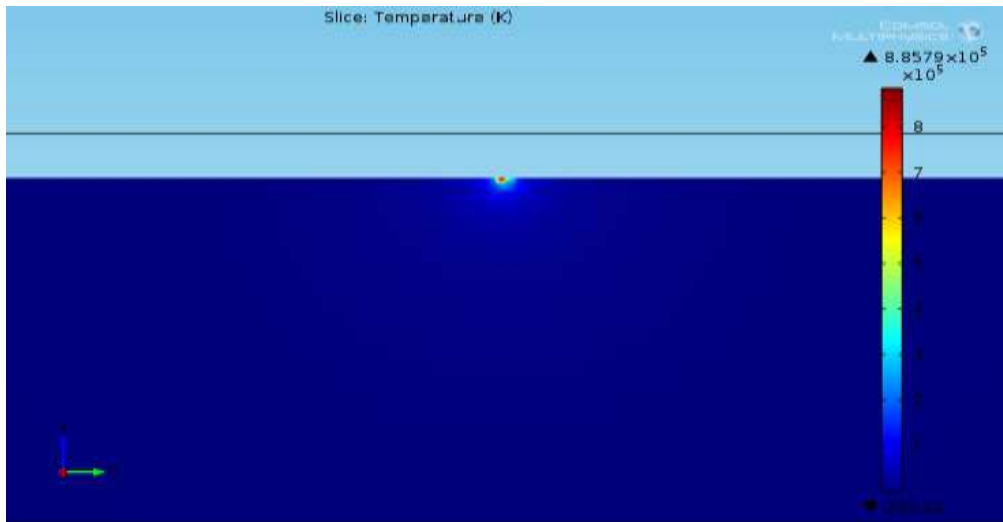


Fig4.10.Temp. Distribution over sliced plane 45V,2A, $T_{\text{on}}=40$ microsecond

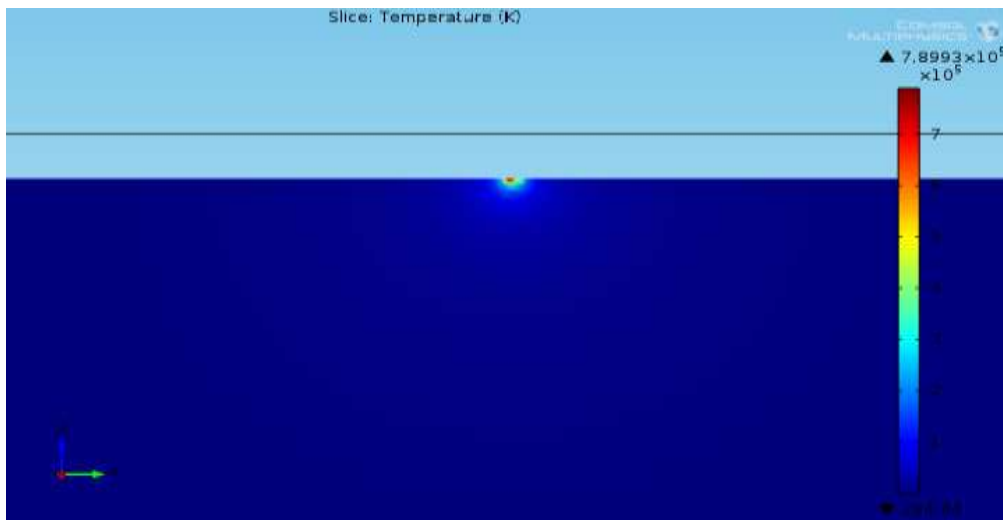


Fig4.11.Temp. Distribution over sliced plane 45V,2A, $T_{\text{on}}=60$ microsecond

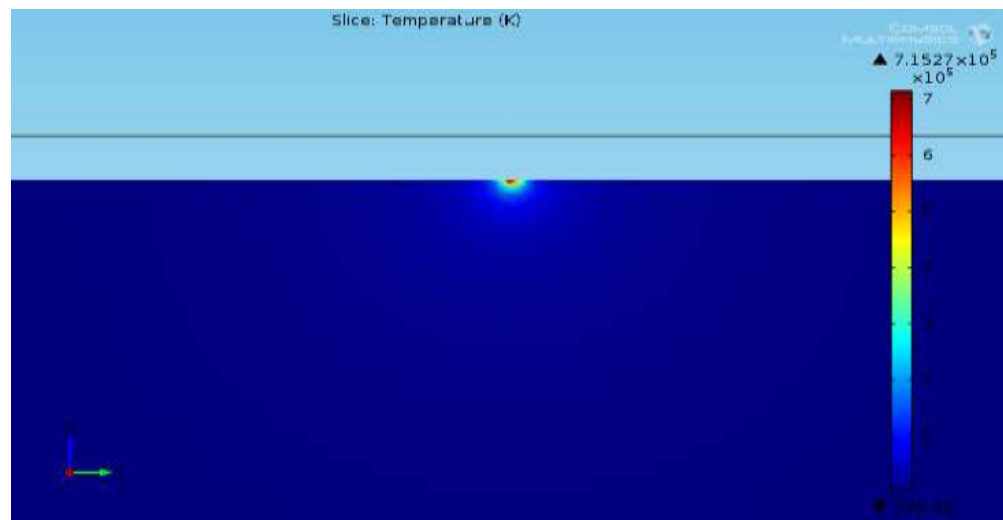


Fig4.12.Temp. Distribution over sliced plane 45V,2A, $T_{\text{on}}=80$ microsecond

**E.  $V_{\text{gap}}=45\text{V}$ , Gap Current (I)=3A:**

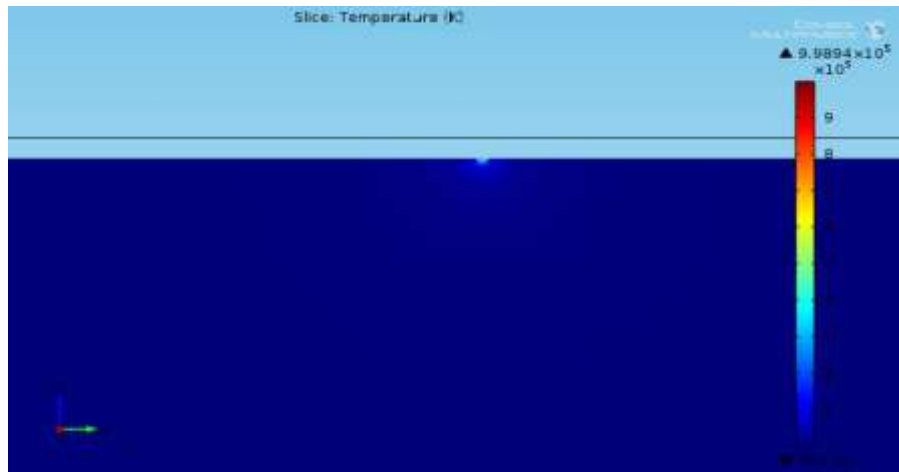


Fig4.13.Temp. Distribution over sliced plane 45V,3A, $T_{\text{on}}=40$ microsecond

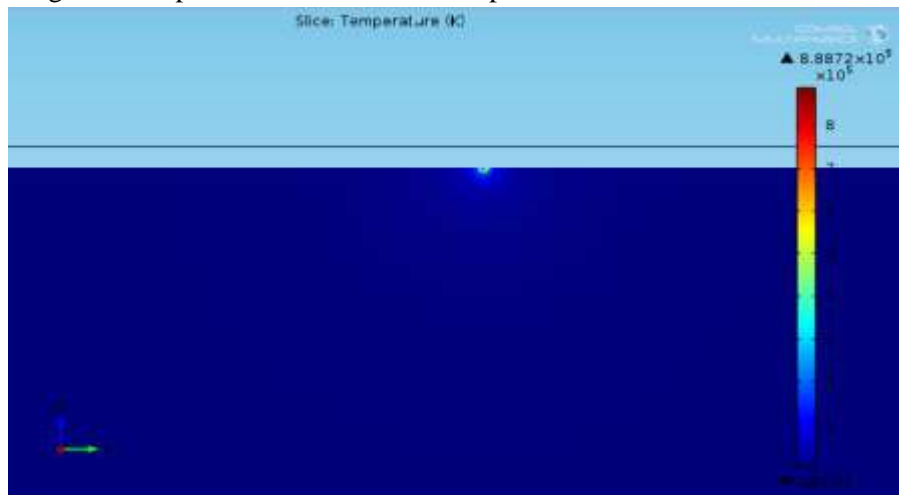


Fig4.14.Temp. Distribution over sliced plane 45V,3A, $T_{\text{on}}=60$ microsecond

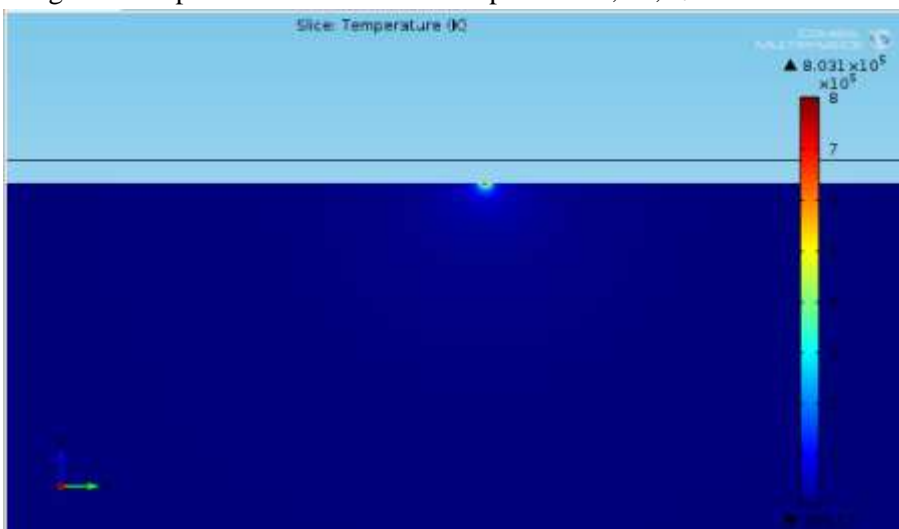


Fig4.15.Temp. Distribution over sliced plane 45V,3A, $T_{\text{on}}=80$ microsecond

**F.  $V_{\text{gap}}=45\text{V}$ , Gap Current (I)=4A:**

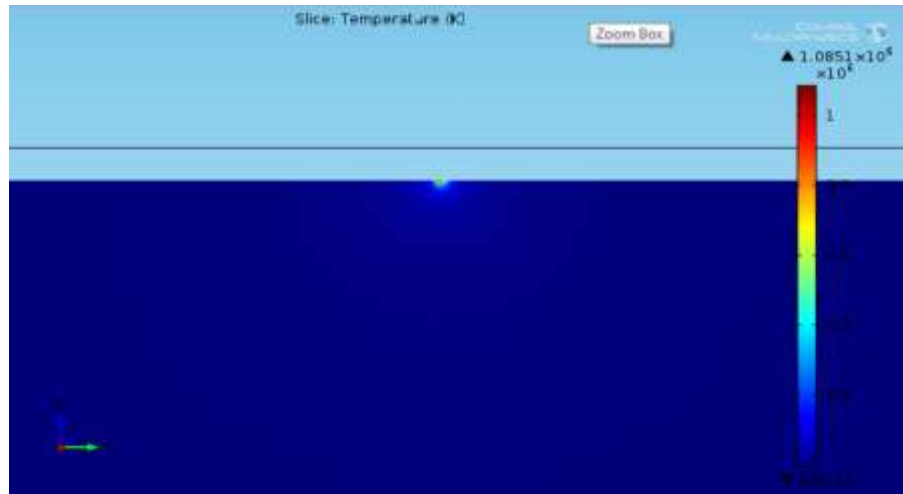


Fig4.16.Temp. Distribution over sliced plane 45V,4A, $T_{\text{on}}=40$ microsecond

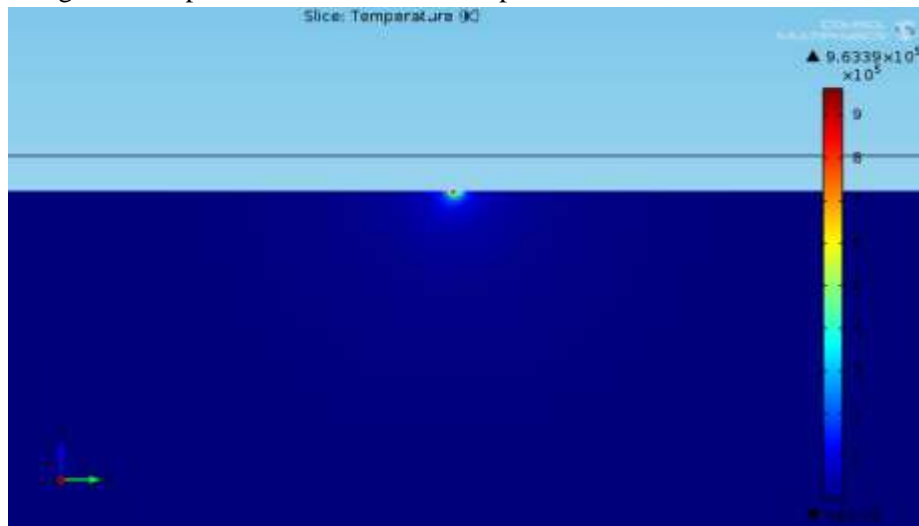


Fig4.17.Temp. Distribution over sliced plane 45V,4A, $T_{\text{on}}=60$ microsecond

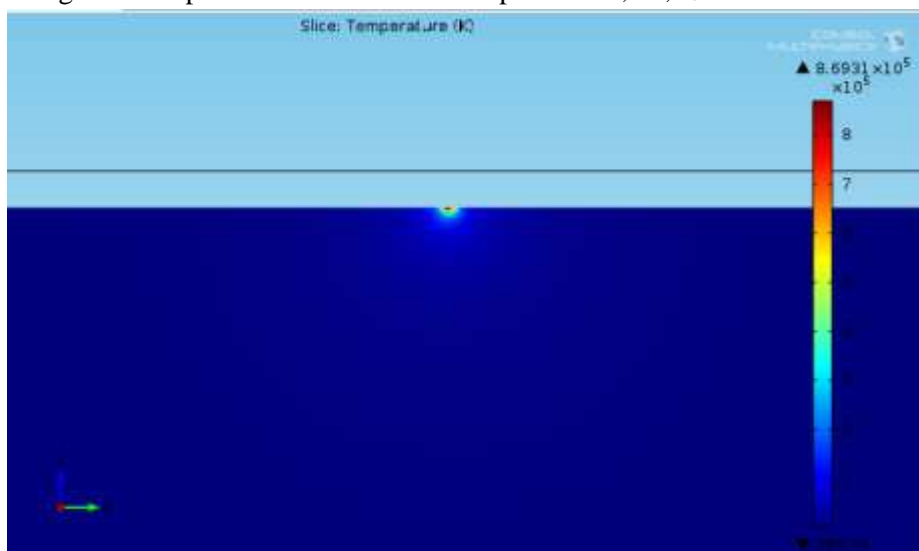


Fig4.18.Temp. Distribution over sliced plane 45V,4A, $T_{\text{on}}=80$ microsecond

The workpiece is sliced along Plasma Arc Centre here. Thus the temperature distribution over radial direction and along depth observed. As radius of the Plasma arc is very small and heat flux is following Gaussian distribution the temperature rise happens in a very small area at micron level. Also the difference between highest and lowest temperature is very high. Highest temperature is in the range of  $10^5$  K level where the lowest temperature is only 293.15K. Therefore to realize the temperature distributions properly the figures are zoomed and represented. From this figures it is hard to detect the zones with 2000K to 3000K temperature zone, although it comes under melting region. Because as the highest temperature is that much high, when the figure is showing zones in the 2000K to 3000K temperature region, it is apparently looking like the base material temperature region. To detect the melting region, Heat affected zone, unaffected zone perfectly, data generated by the software is referred.

## 4.2. ANALYSIS OF CHANGE OF TEMPERATURE AT THE PLASMA ARC CENTRE:

Temperature at the plasma arc centre, i.e., the point of application of heat flux, is recorded from the software. The temperature at the plasma arc centre through out the process has been recorded and later it is recorded in the table and plotted with respect to time.

Table.4.1. Temperature at Plasma Arc Centre

Gap Voltage $V_{\text{gap}}$ (V)	Gap Current $I$ (A)	Pulse-on-time $T_{\text{on}}$ (microsecond)	Temperature at the Plasma Arc Centre (K)
40	2	40	$8.5456 \times 10^5$
		60	$7.625 \times 10^5$
		80	$6.9081 \times 10^5$
	3	40	$9.6512 \times 10^5$
		60	$8.5928 \times 10^5$
		80	$7.7697 \times 10^5$
	4	40	$1.0492 \times 10^6$
		60	$9.3233 \times 10^5$
		80	$8.4178 \times 10^5$
45	2	40	$8.8579 \times 10^5$
		60	$7.8993 \times 10^5$
		80	$7.1527 \times 10^5$
	3	40	$9.9894 \times 10^5$
		60	$8.8872 \times 10^5$
		80	$8.031 \times 10^5$
	4	40	$1.0851 \times 10^6$
		60	$9.6339 \times 10^5$
		80	$8.6931 \times 10^5$

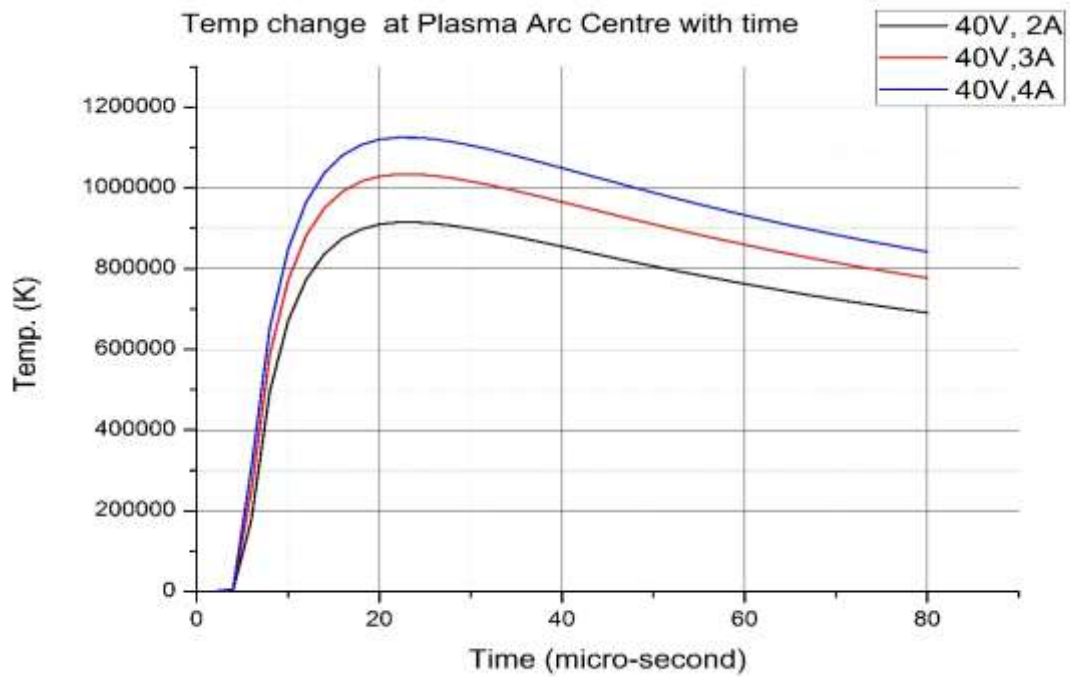


Fig.4.19. Change of Temperature at the Plasma Arc Centre  $V_{gap}=40V$

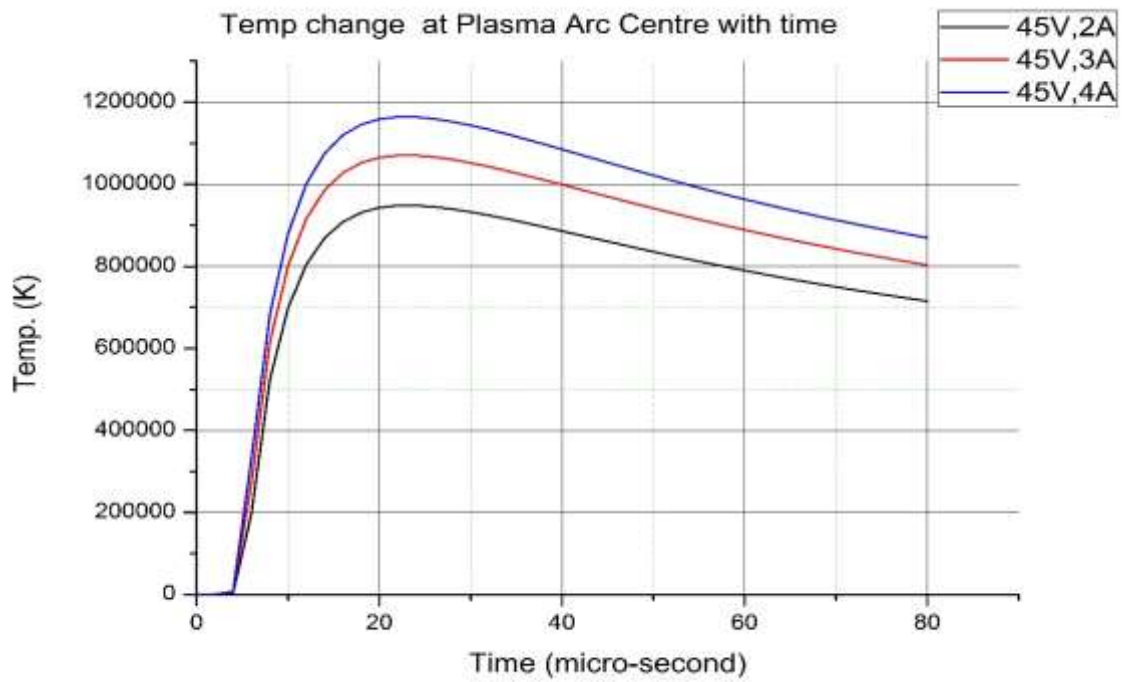


Fig.4.20. Change of Temperature at the Plasma Arc Centre  $V_{gap}=45V$

What is significant to see here in these figures is that the temperature at the plasma arc centre is increasing upto a time and the temperature is falling thereafter continuously. The cause of this temperature fall is

- i. As the time is going on the radius of the beam is increasing, so area under plasma arc is increasing, that's why heat flux is decreasing.
- ii. As the heat flux is following Gaussian Distribution, increasing plasma arc radius increasing the standard deviation term of the heat flux equation and as the standard deviation is increasing the heat flux is distributed over a larger area.
- iii. As the temperature is reaching in  $10^5$  range here instantly, the rate of conductive heat transfer ( $\propto \Delta T$ ) and radiative heat transfer ( $\propto (\Delta T)^4$ ) is increasing simultaneously. It is known from the basic heat transfer concept that,

$$\text{Heat flux Input} - (\text{Conductive Heat Transfer} + \text{Radiative Heat Transfer}) = m \cdot c_p \cdot \Delta T$$

Where  $c_p$  = specific heat

$m$  = mass

$\Delta T$  = change of temperature,

Because of that a point comes where

$$\text{Heat flux Input} - (\text{Conductive Heat Transfer} + \text{Radiative Heat Transfer}) = m \cdot c_p \cdot \Delta T = 0$$

This the point of maximum temperature rise, and then it becomes

$$\text{Heat flux Input} - (\text{Conductive Heat Transfer} + \text{Radiative Heat Transfer}) = m \cdot c_p \cdot \Delta T < 0$$

That means,  $m \cdot c_p \cdot \Delta T = -ve$ , so,  $\Delta T = -ve$ , or the temperature decreases.

It is observed from the figures that the maximum temperature is rising around 22 microsecond. The temperature may fall but the heat distribution spreads over a larger area as time increases. Increase of increasing Gap Voltage and gap current increases the maximum temperature rise.

### 4.3. STUDY OF TEMPERATURE DISTRIBUTION ALONG RADIAL DIRECTION AND DEPTH FROM PLASMA ARC CENTRE:

After slicing the material the temperature values along radial direction and along depth are collected from the software. These data have been plotted with respect to the distance from plasma arc centre. The effect of heat flux mainly distributed upto 30micrometer from plasma arc centre. That's why temperature distribution upto 30micrometer is plotted in the graph.

#### A. $V_{\text{gap}}=40\text{V}$ , Gap Current (I)=2A:

- i) Pulse-on-time( $T_{\text{on}}$ )=40 microsecond:

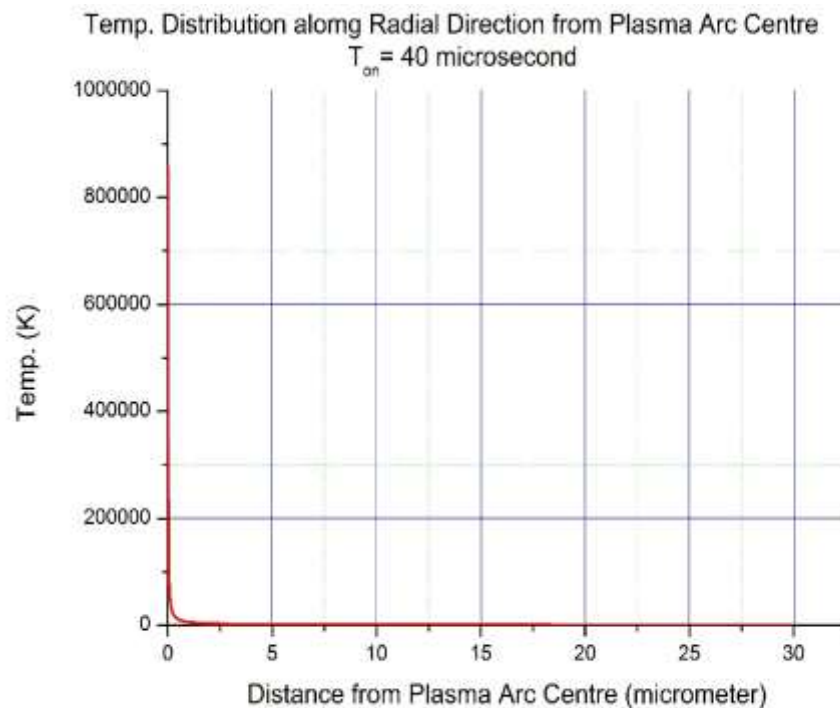


Fig4.21.:Temp. Distribution along radial direction 40V,2A, $T_{\text{on}}=40$ microsecond

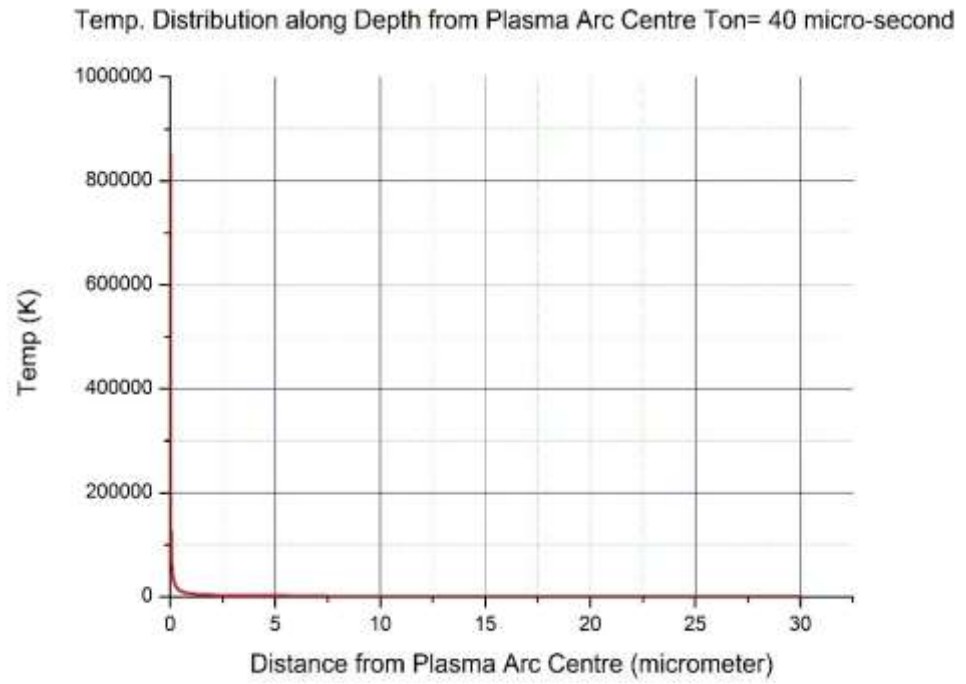


Fig 4.22.: Temp. Distribution along Depth 40V,2A, $T_{on}=40$ microsecond

ii) Pulse-on-time( $T_{on}$ )=60 microsecond:

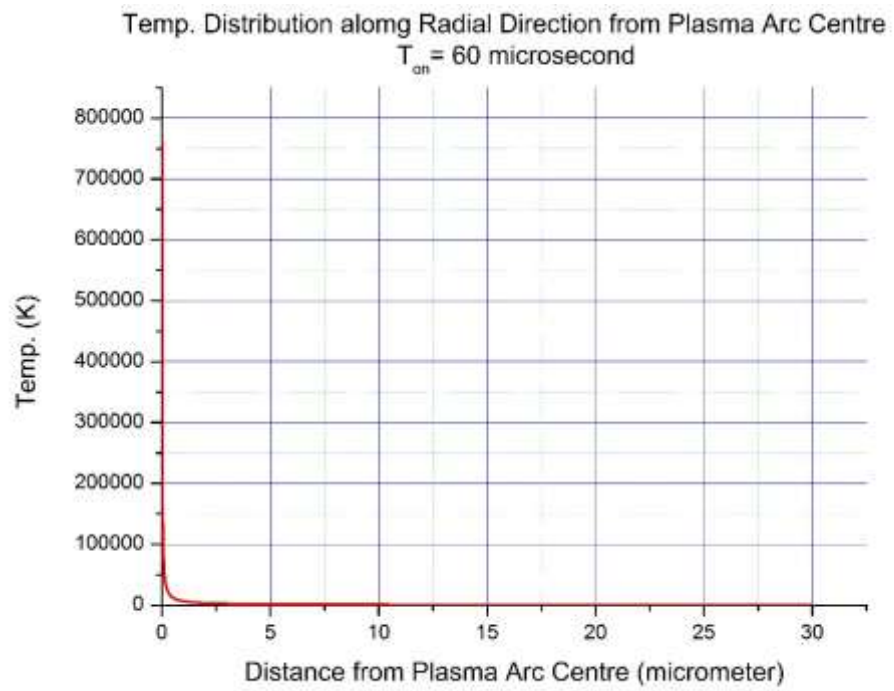


Fig4.23.:Temp. Distribution along radial direction 40V, 2A, $T_{on}$ =60microsecond

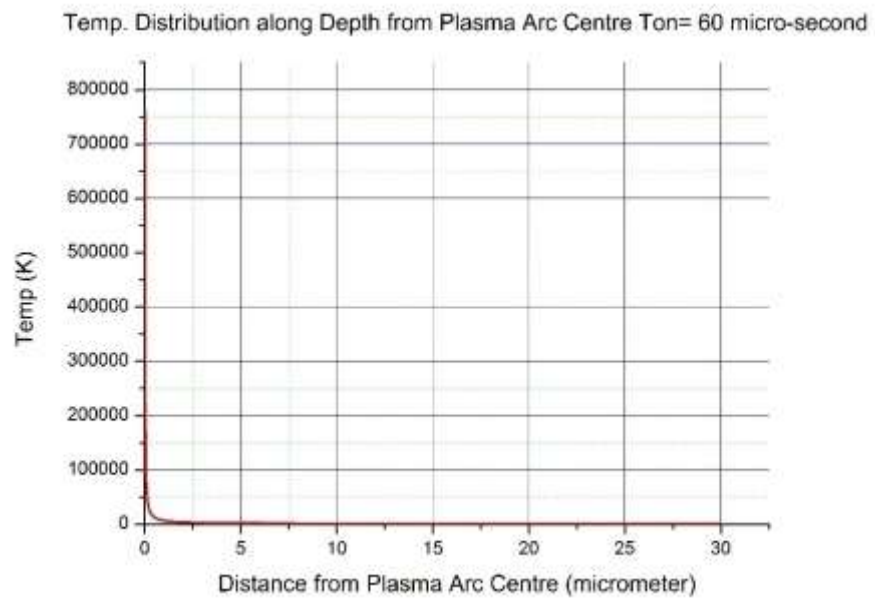


Fig4.24.:Temp. Distribution along Depth 40V, 2A,  $T_{on}$ =60microsecond

iii) Pulse-on-time( $T_{on}$ )=80 microsecond:

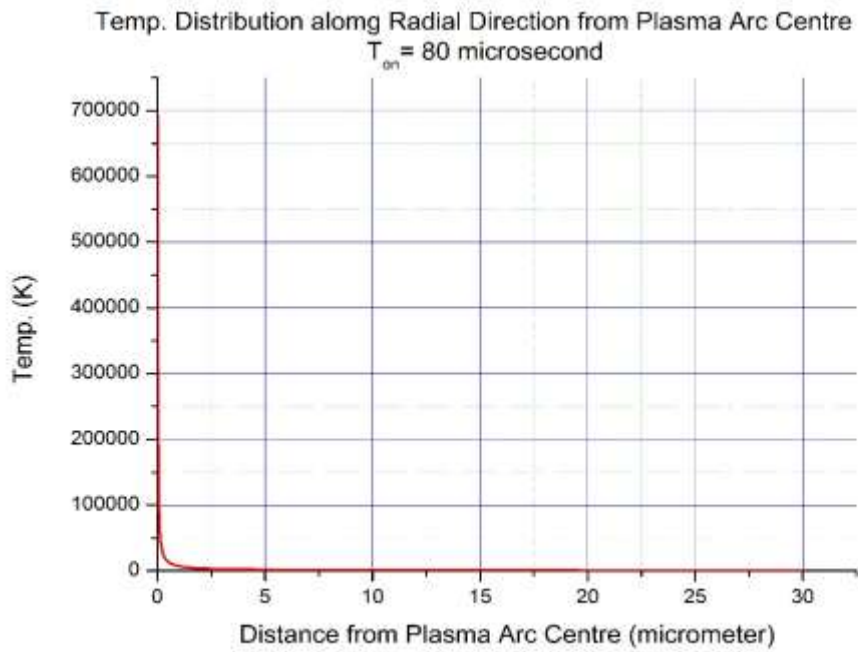


Fig4.25.:Temp. Distribution along radial direction 40V, 2A, $T_{on}$ =80microsecond

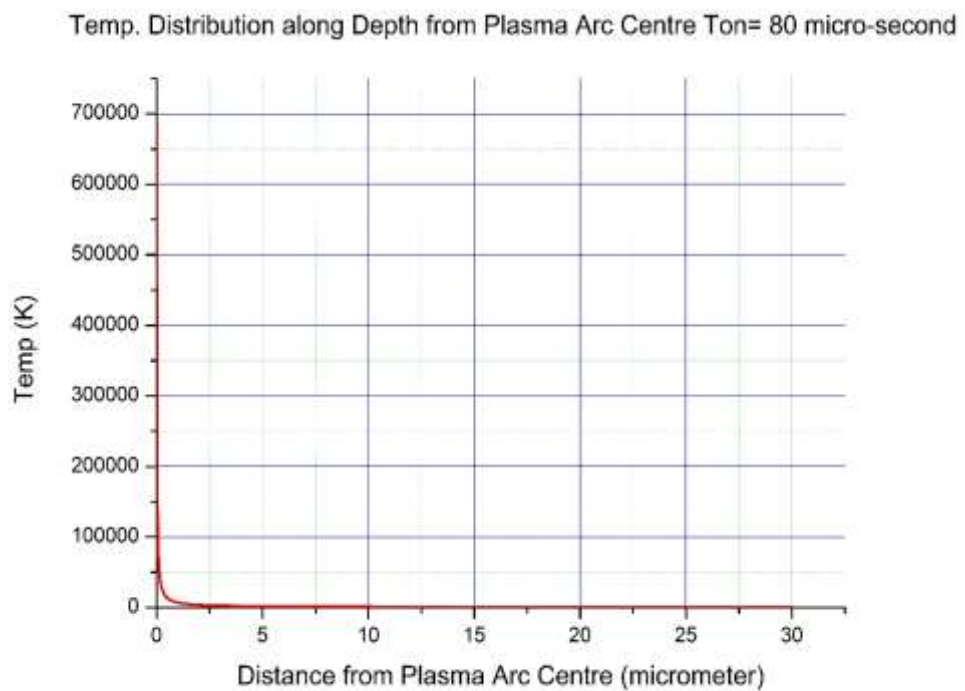


Fig4.26.:Temp. Distribution along Depth 40V, 2A,  $T_{on}$ =80microsecond

**B.  $V_{gap}=40V$ , Gap Current ( $I$ )=3A:**

- i. Pulse-on-time( $T_{on}$ )=40 microsecond:

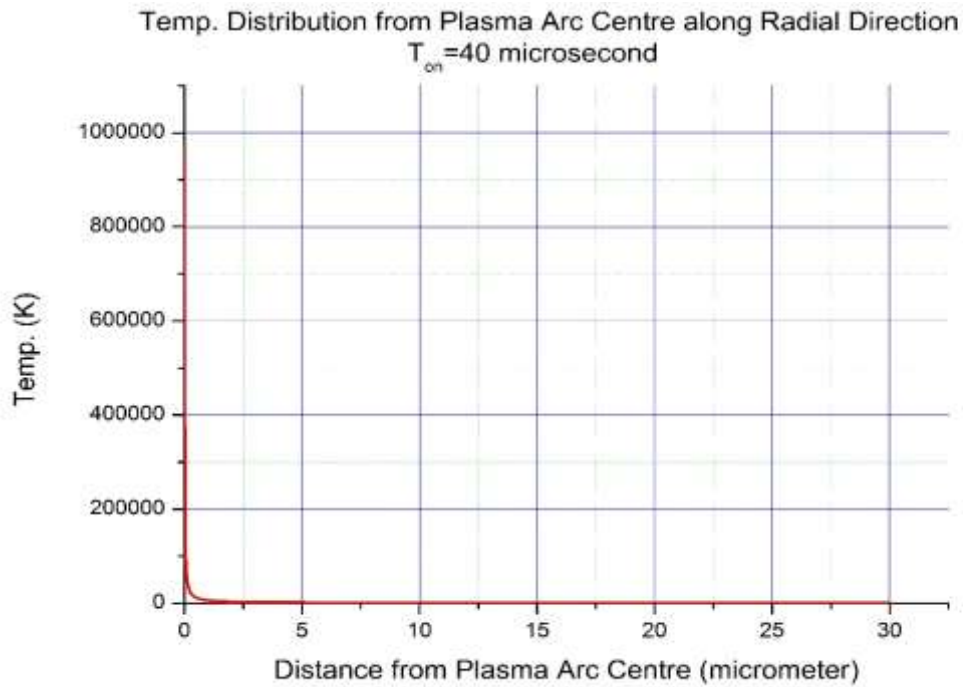


Fig4.27.:Temp. Distribution along radial direction 40V, 3A, $T_{on}$ =40microsecond

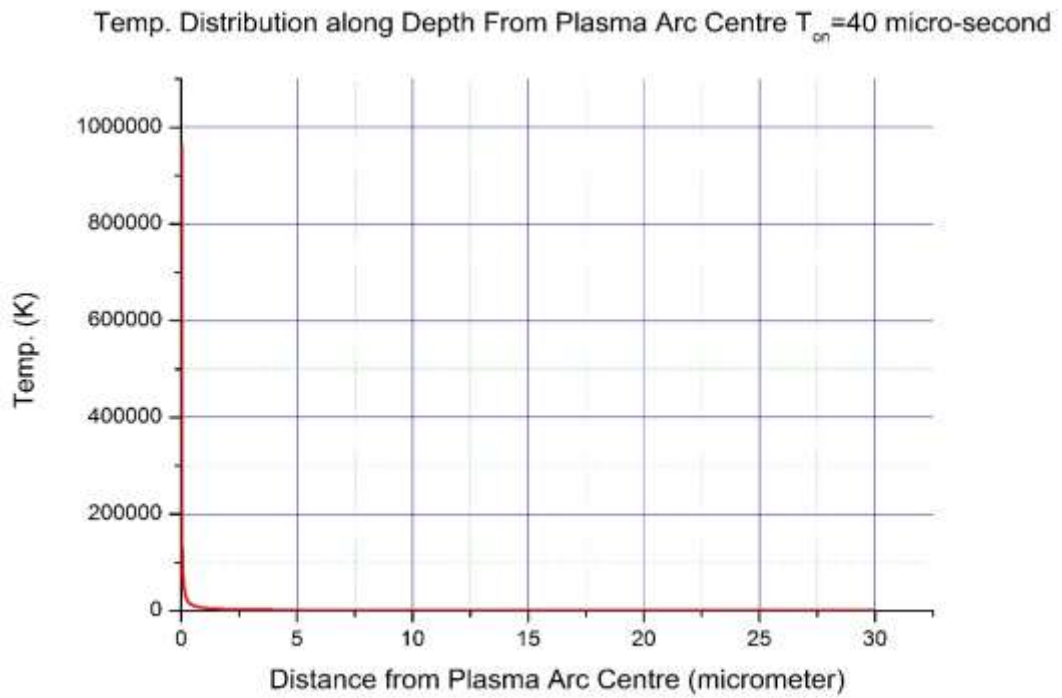


Fig4.28.:Temp. Distribution along Depth 40V, 3A,  $T_{on}$ =40microsecond

ii. Pulse-on-time( $T_{on}$ )=60 microsecond:

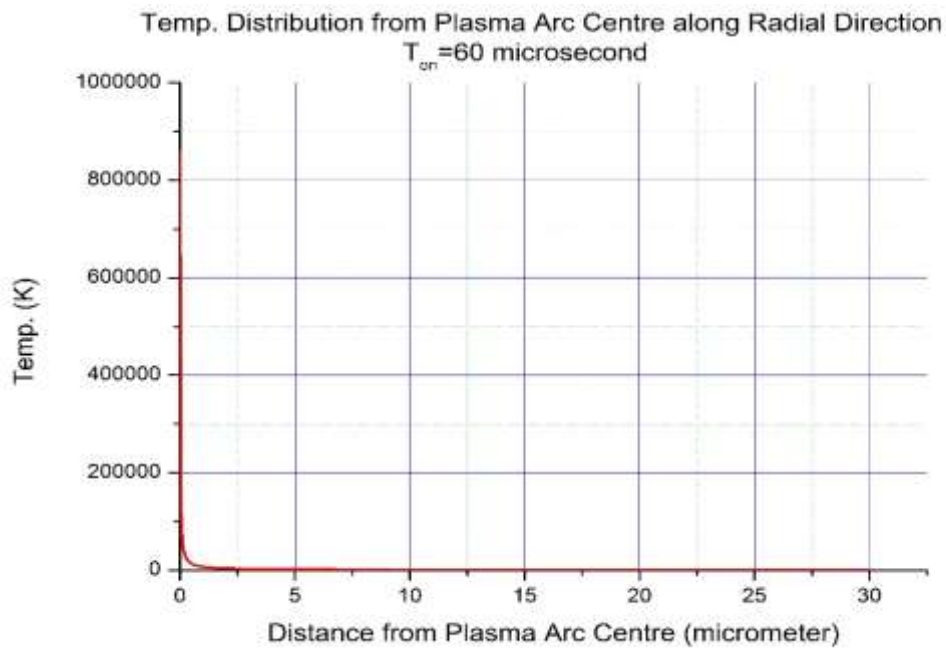


Fig4.29.:Temp. Distribution along radial direction 40V, 3A, $T_{on}$ =60microsecond

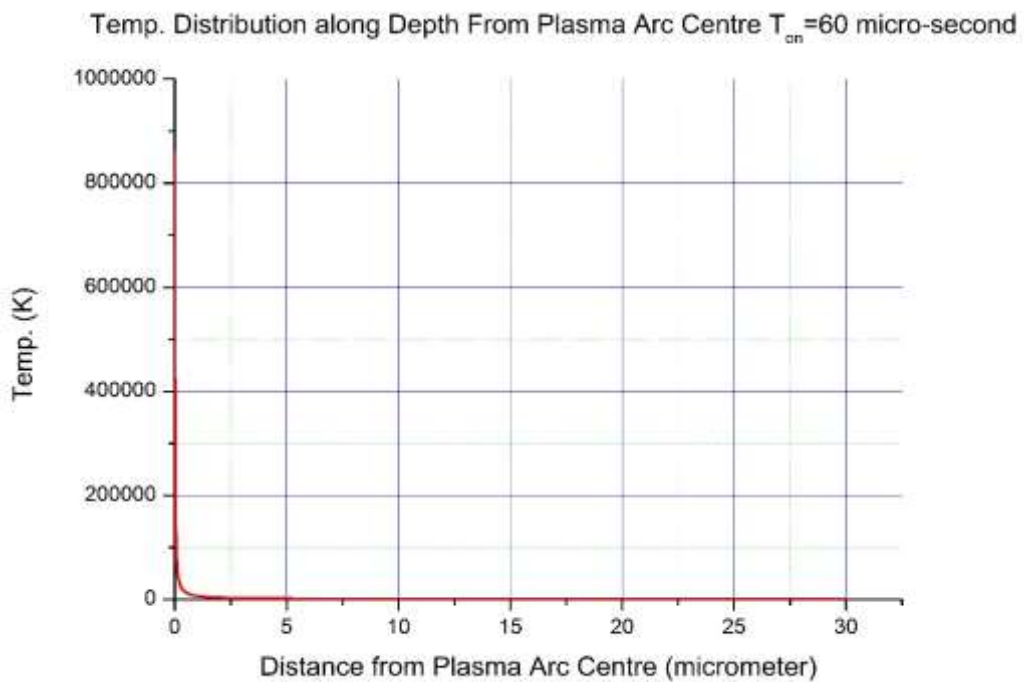


Fig4.30.:Temp. Distribution along Depth 40V, 3A,  $T_{on}$ =60microsecond

iii. Pulse-on-time( $T_{on}$ )=80 microsecond:

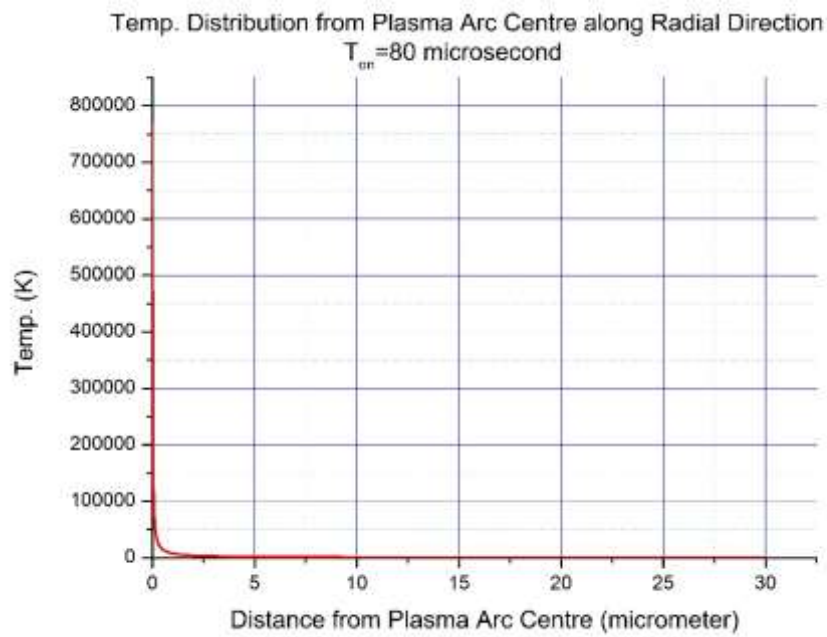


Fig4.31.:Temp. Distribution along radial direction 40V, 3A, $T_{on}$ =80microsecond

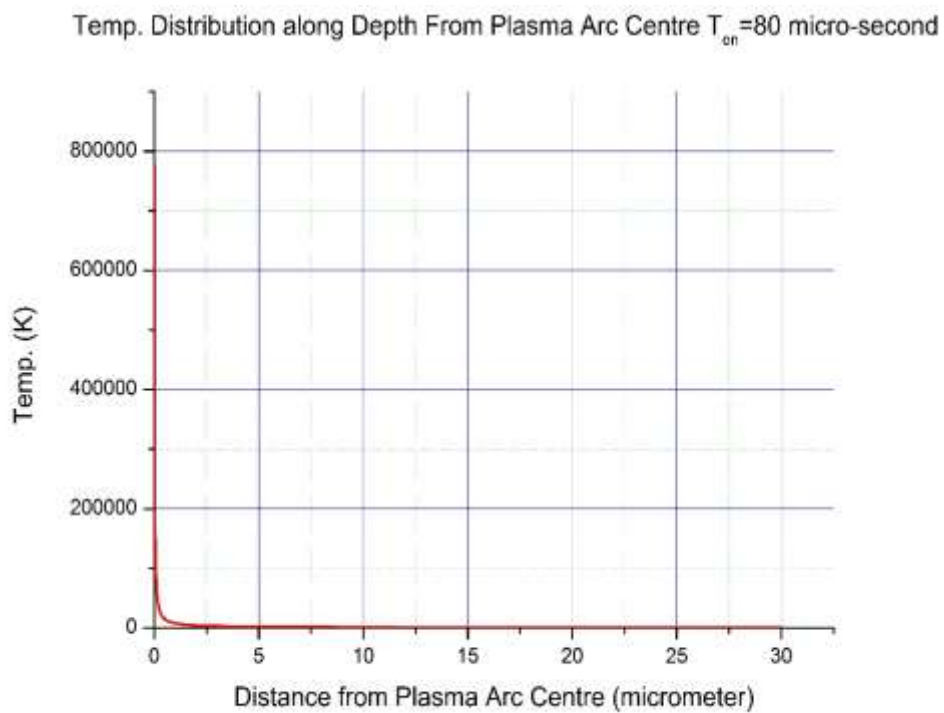


Fig4.32.:Temp. Distribution along Depth 40V, 3A,  $T_{on}$ =80microsecond

**C.  $V_{gap}=40V$ , Gap Current ( $I$ )=4A:**

- i. Pulse-on-time( $T_{on}$ )=40 microsecond:

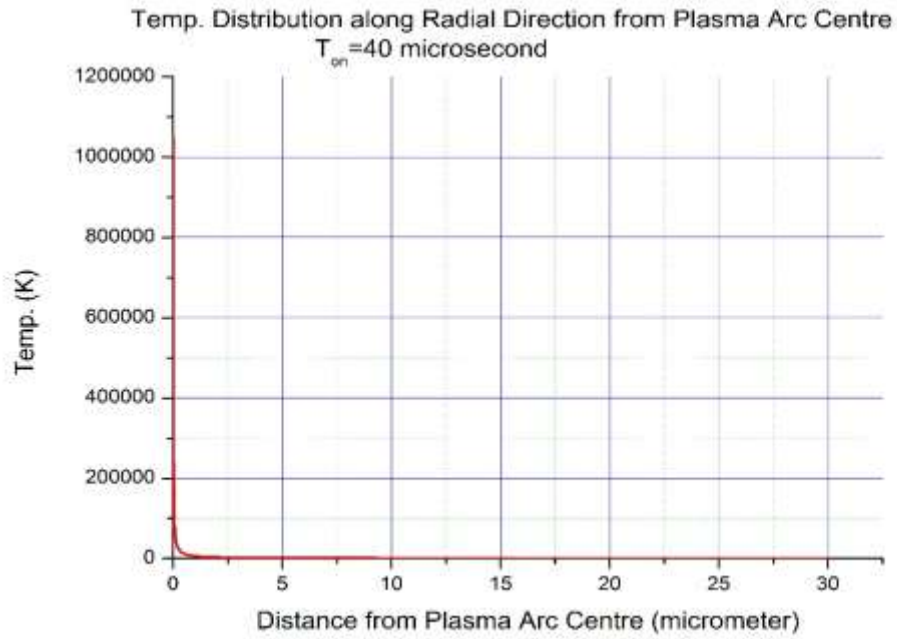


Fig4.33.: Temp. Distribution along radial direction 40V, 4A,  $T_{on}$ =40microsecond

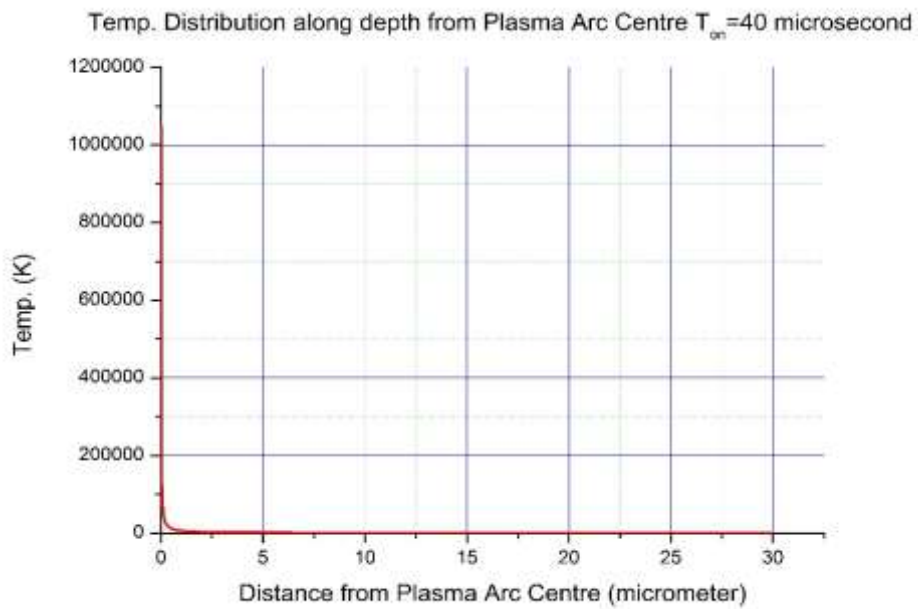


Fig4.34.:Temp. Distribution along Depth 40V, 4A,  $T_{on}$ =40microsecond

ii. Pulse-on-time( $T_{on}$ )=60 microsecond:

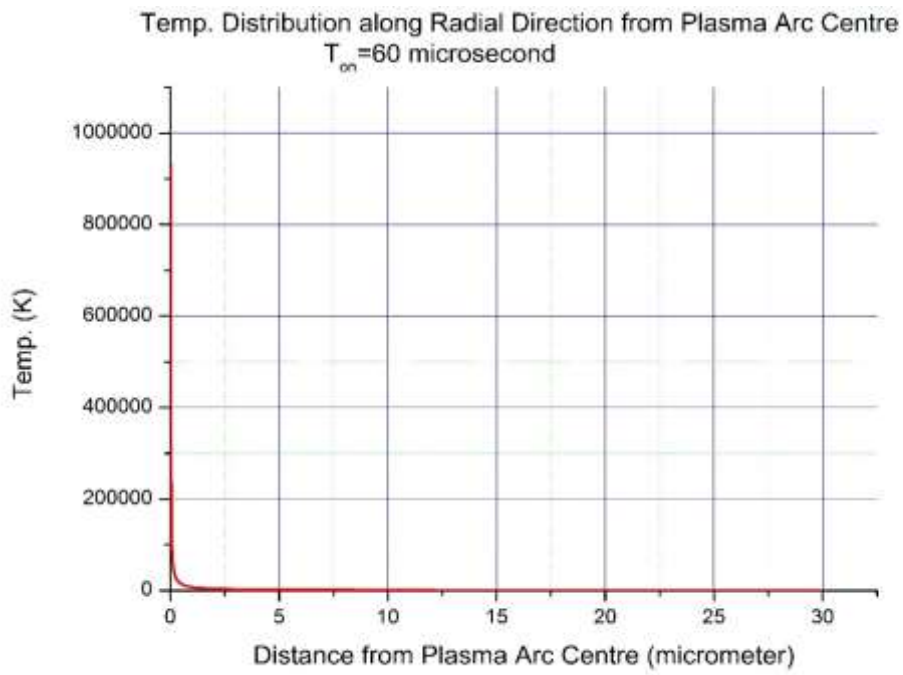


Fig4.35.: Temp. Distribution along radial direction 40V, 4A,  $T_{on}$ =60microsecond

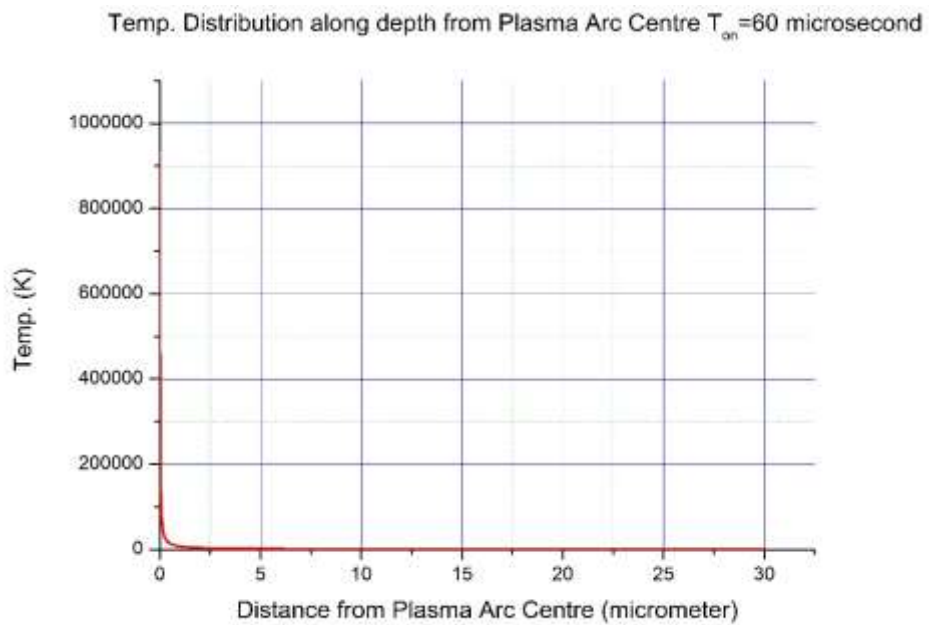


Fig4.36.:Temp. Distribution along Depth 40V, 4A,  $T_{on}$ =60microsecond

iii. Pulse-on-time( $T_{on}$ )=80 microsecond:

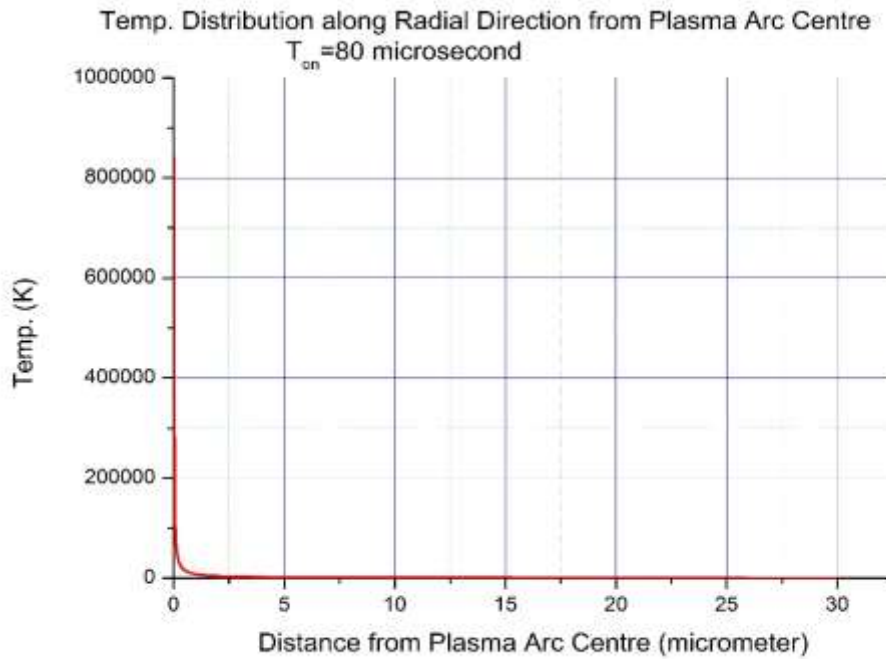


Fig.4.37.: Temp. Distribution along radial direction 40V, 4A,  $T_{on}$ =80microsecond

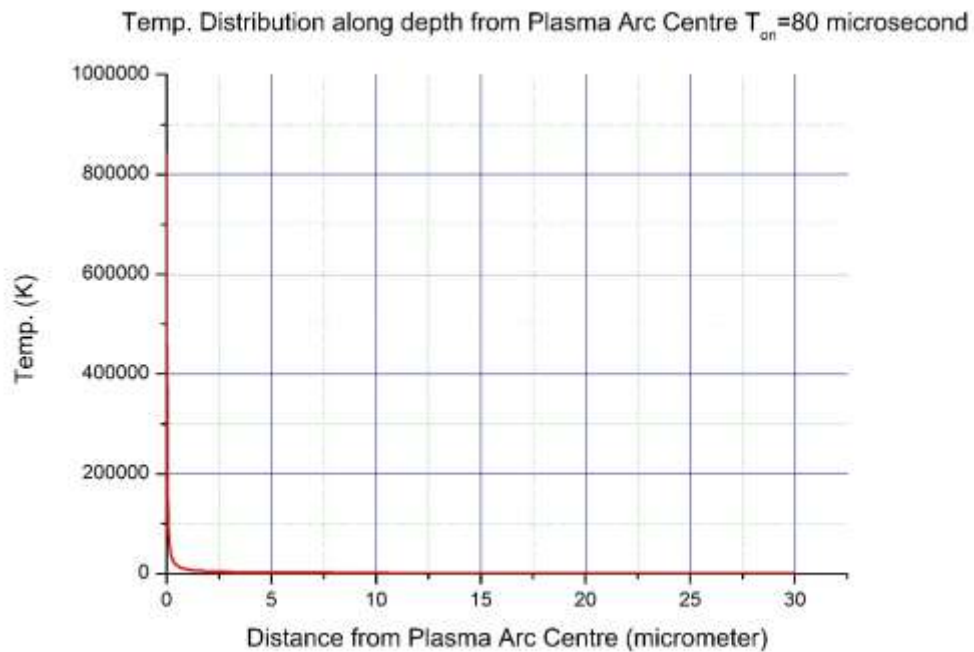


Fig4.38.:Temp. Distribution along Depth 40V, 4A,  $T_{on}$ =80microsecond

**D.  $V_{gap}=45V$ , Gap Current ( $I$ )=2A:**

- i. Pulse-on-time( $T_{on}$ )=40 microsecond:

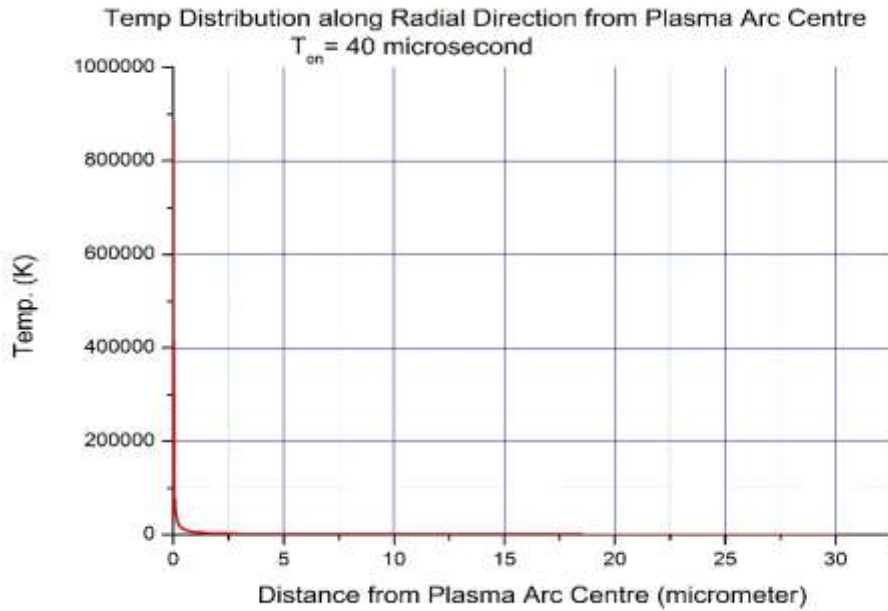


Fig.4.39.: Temp. Distribution along radial direction 45V, 2A,  $T_{on}$ =40microsecond

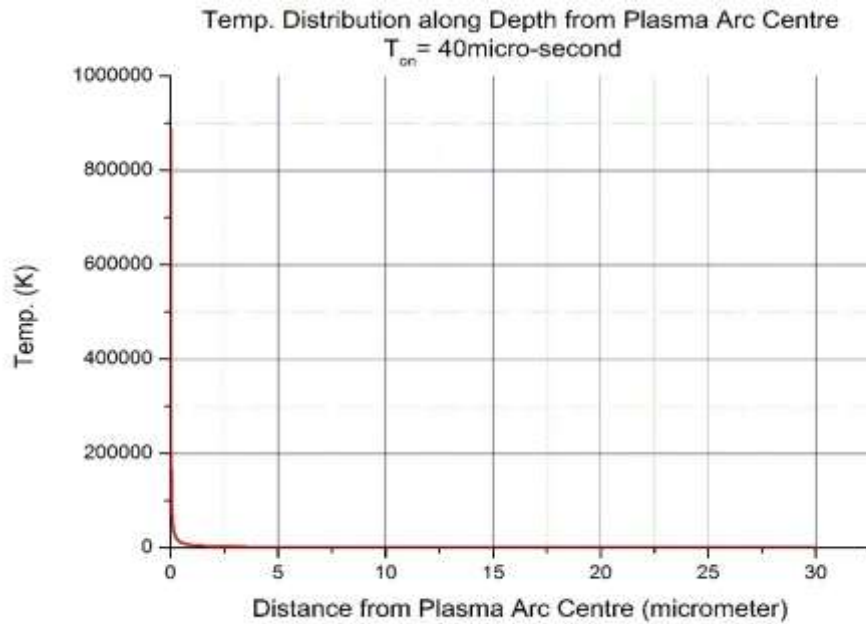


Fig4.40.:Temp. Distribution along Depth 45V, 2A,  $T_{on}$ =40microsecond

ii. Pulse-on-time( $T_{on}$ )=60 microsecond:

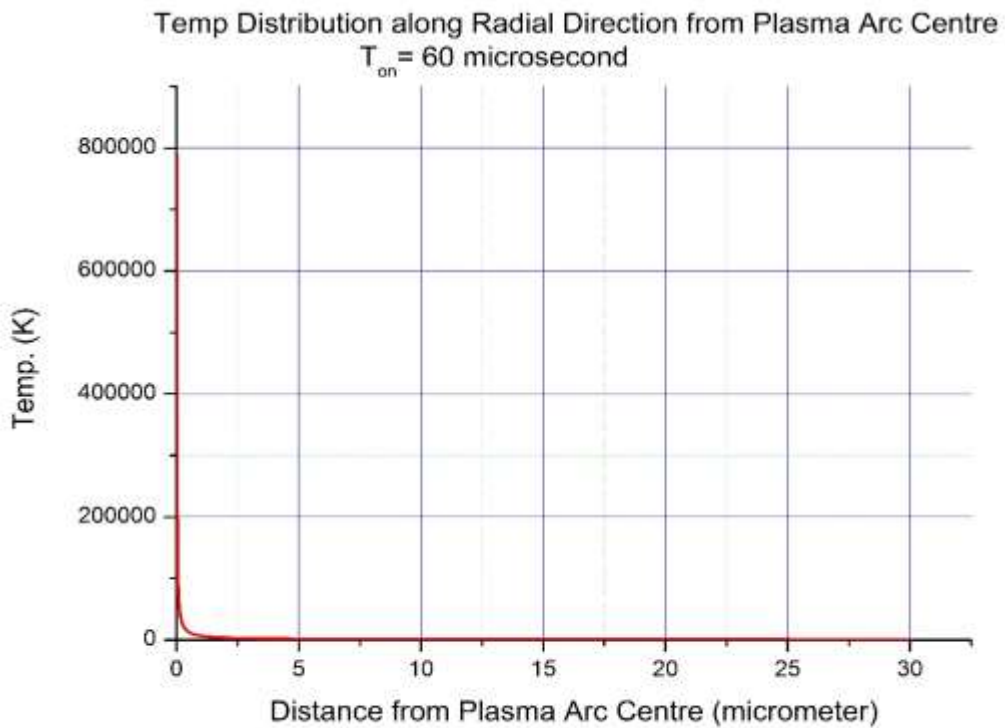


Fig.4.41.: Temp. Distribution along radial direction 45V, 2A,  $T_{on}$ =60microsecond

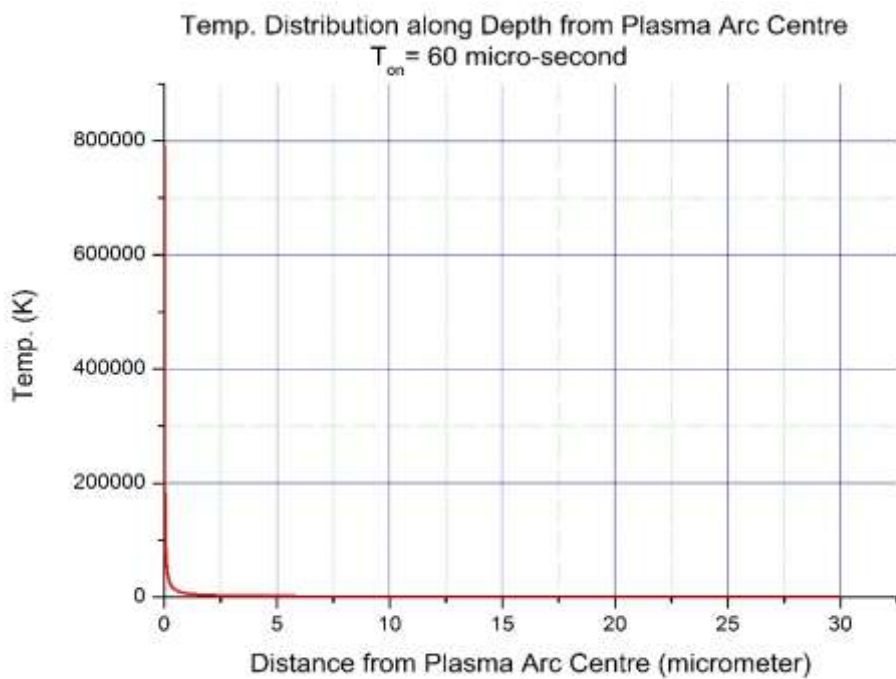


Fig4.42.:Temp. Distribution along Depth 45V, 2A,  $T_{on}$ =60microsecond

iii. Pulse-on-time( $T_{on}$ )=80 microsecond:

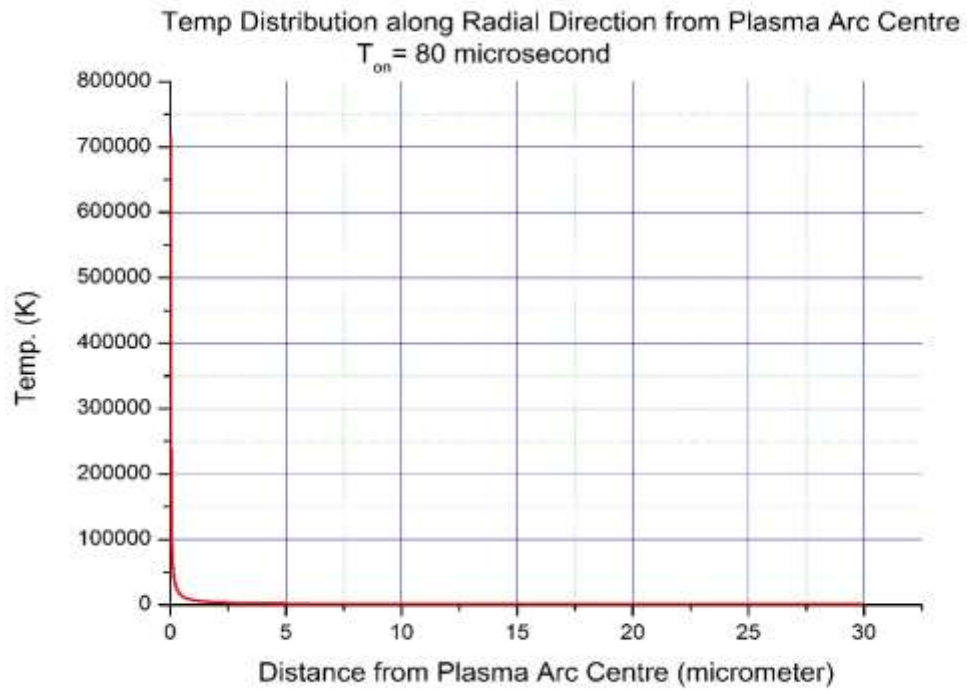


Fig.4.43.: Temp. Distribution along radial direction 45V, 2A,  $T_{on}$ =80microsecond

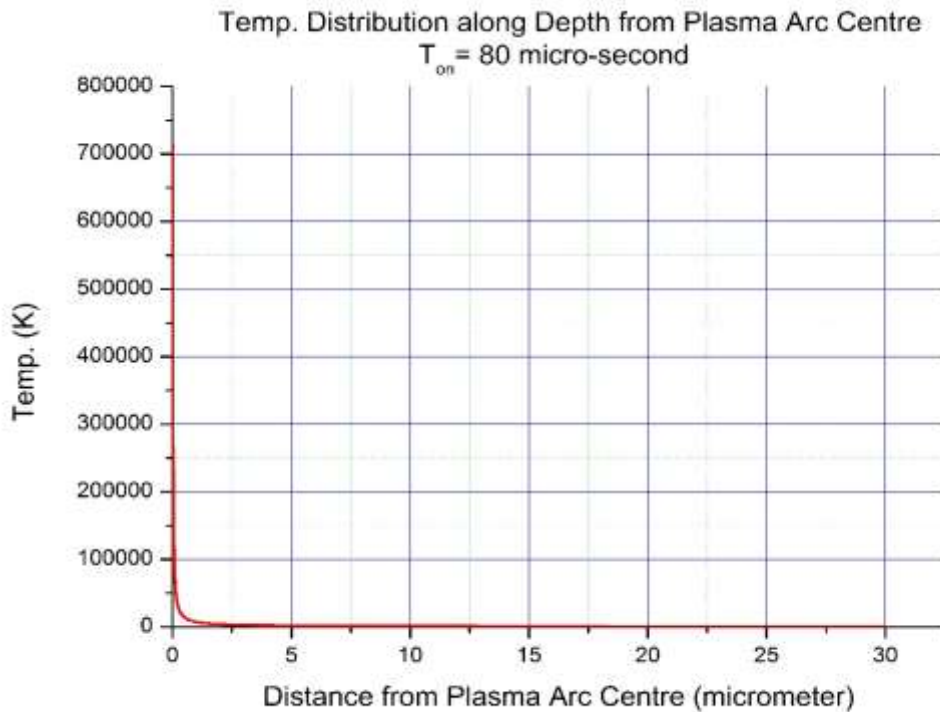


Fig4.44.:Temp. Distribution along Depth 45V, 2A,  $T_{on}$ =80microsecond

**E.  $V_{gap}=45V$ , Gap Current (I)=3A:**

- i. Pulse-on-time( $T_{on}$ )=40 microsecond:

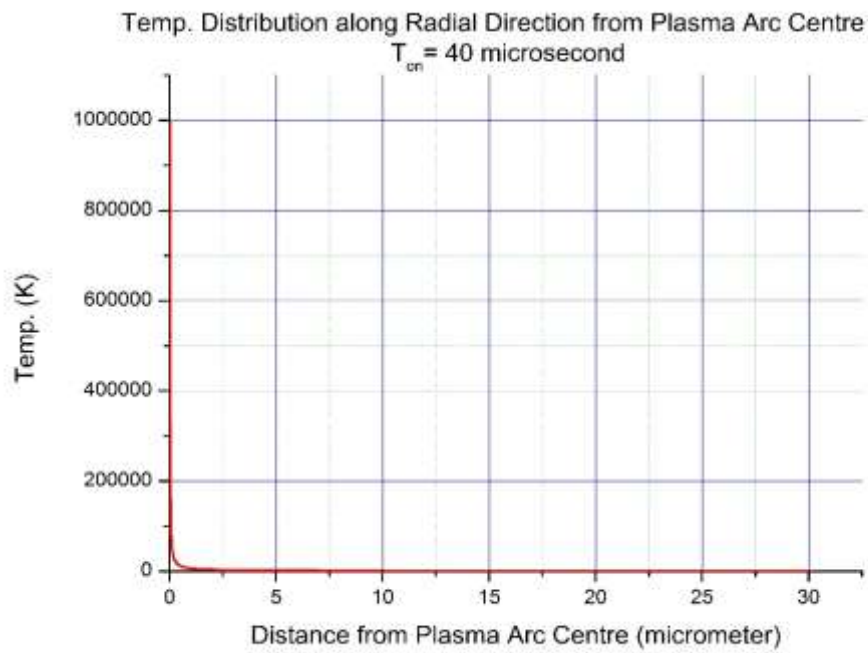


Fig.4.45.: Temp. Distribution along radial direction 45V, 3A,  $T_{on}=40$ microsecond

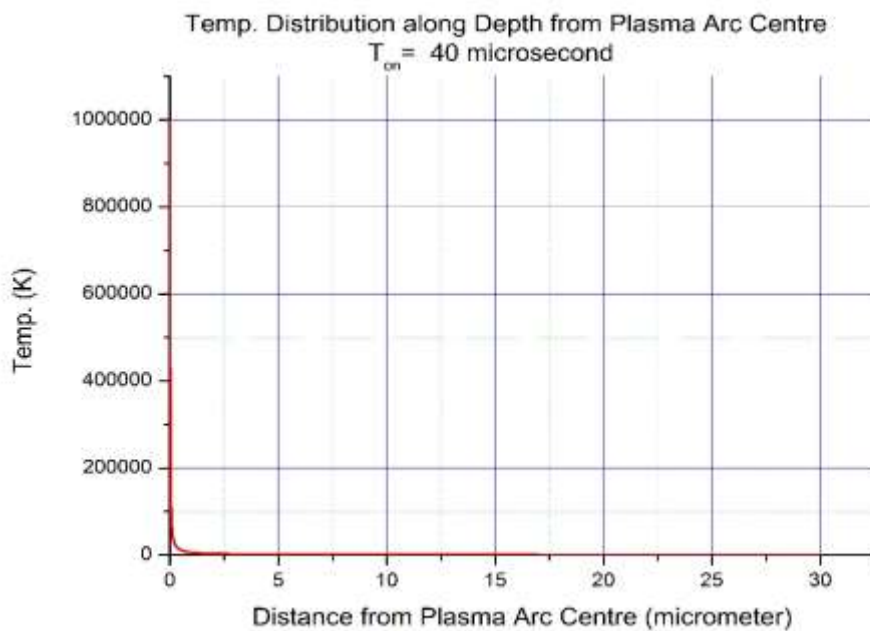


Fig4.46.:Temp. Distribution along Depth 45V, 3A,  $T_{on}=40$ microsecond

ii. Pulse-on-time( $T_{on}$ )=60 microsecond:

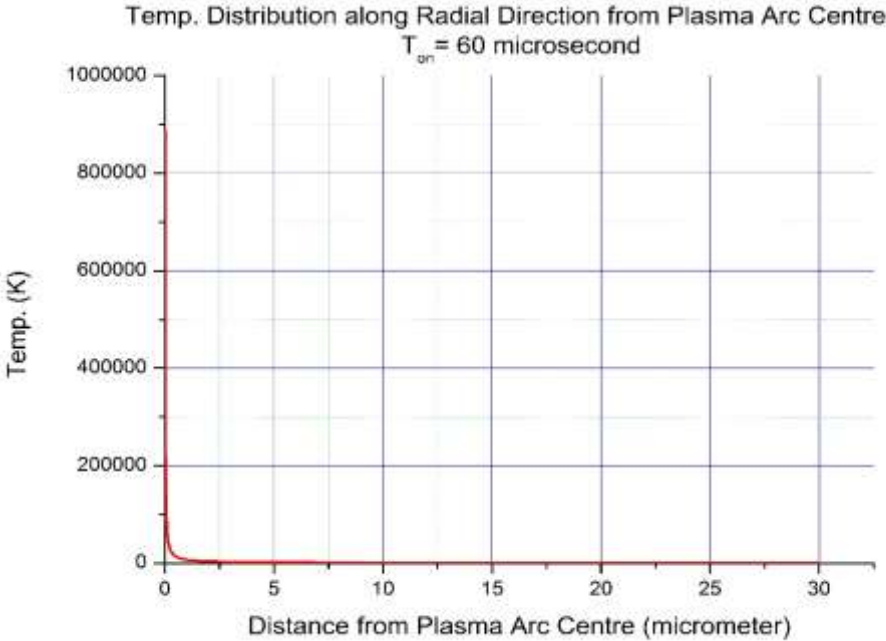


Fig.4.47: Temp. Distribution along radial direction 45V, 3A,  $T_{on}$ =60microsecond

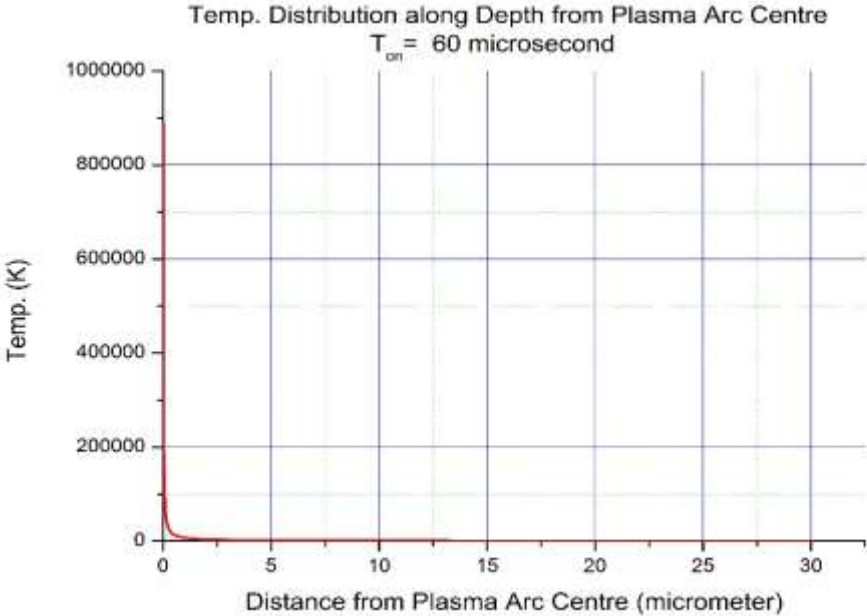


Fig4.48.:Temp. Distribution along Depth 45V, 3A,  $T_{on}$ =60microsecond

iii. Pulse-on-time( $T_{on}$ )=80 microsecond:

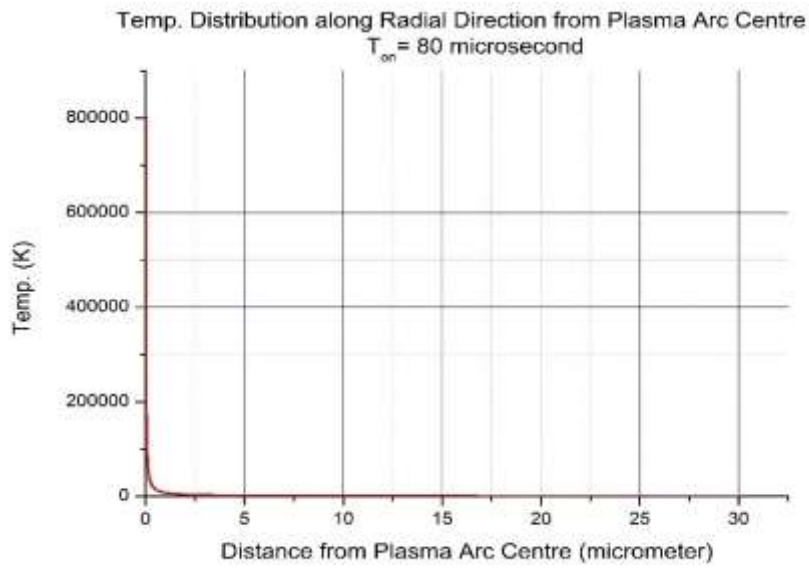


Fig.4.49: Temp. Distribution along radial direction 45V, 3A,  $T_{on}$ =80microsecond

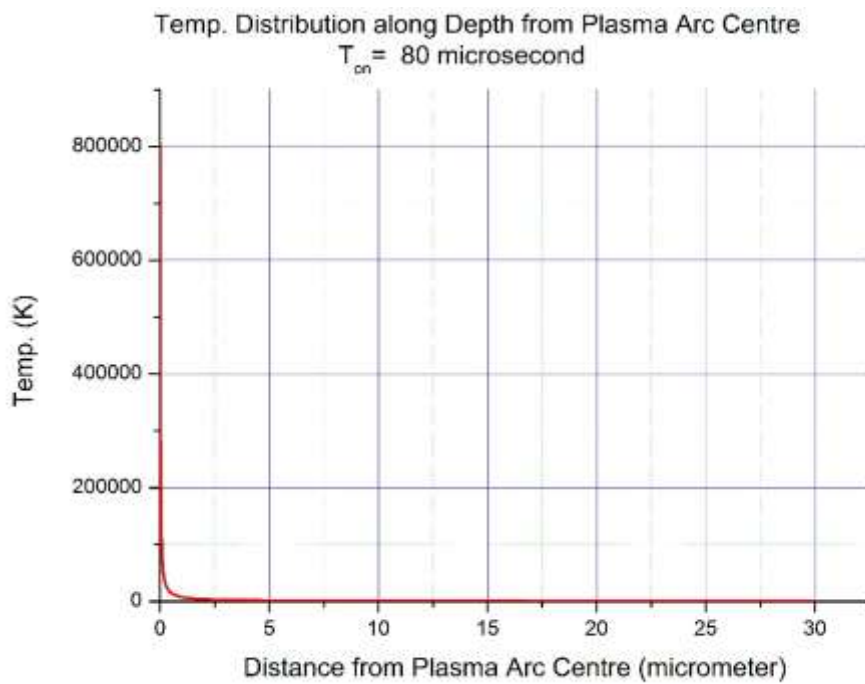


Fig4.50.: Temp. Distribution along Depth 45V, 3A,  $T_{on}$ =80microsecond

**F.  $V_{gap}=45V$ , Gap Current ( $I$ )=4A:**

- i. Pulse-on-time( $T_{on}$ )=40 microsecond:

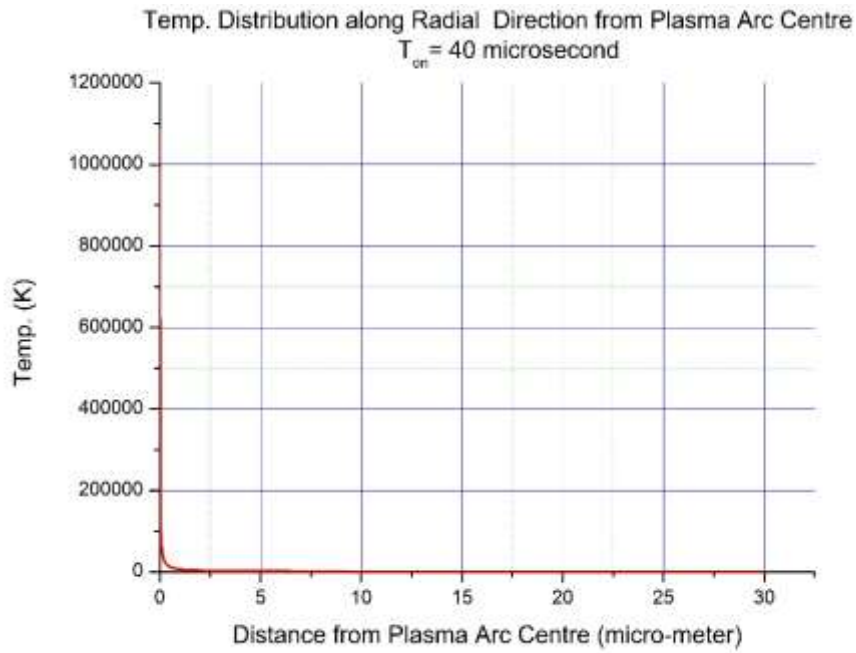


Fig.4.51: Temp. Distribution along radial direction 45V, 4A,  $T_{on}=40$ microsecond

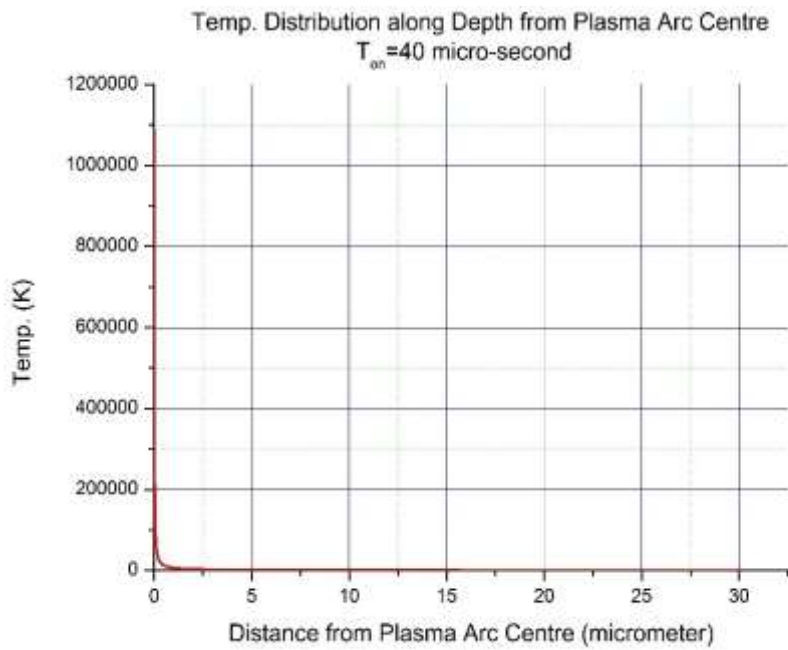


Fig4.52.: Temp. Distribution along Depth 45V, 4A,  $T_{on}=40$ microsecond

ii. Pulse-on-time( $T_{on}$ )=60 microsecond:

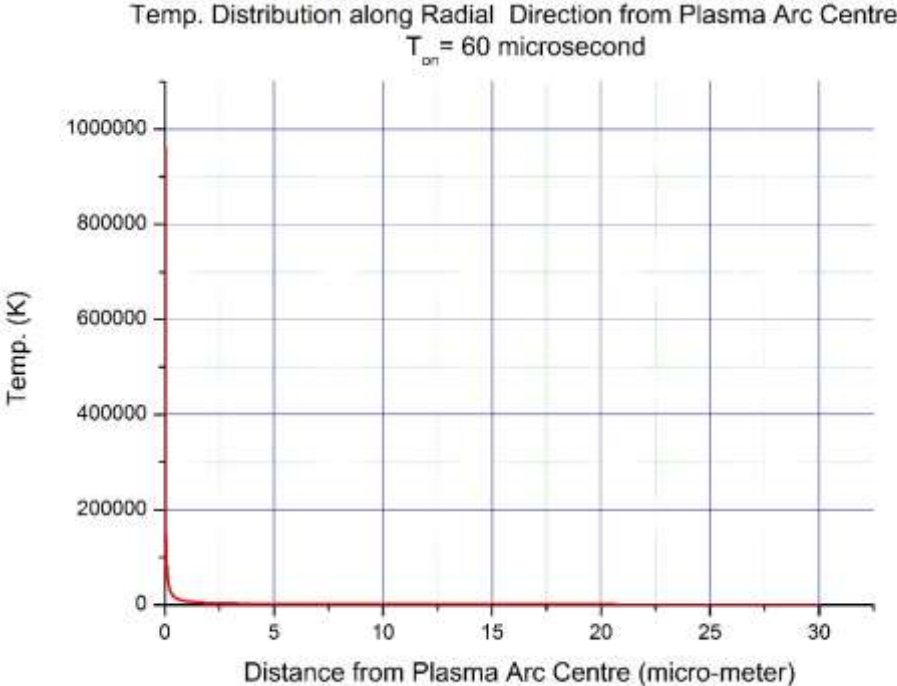


Fig.4.53: Temp. Distribution along radial direction 45V, 4A,  $T_{on}$ =60microsecond

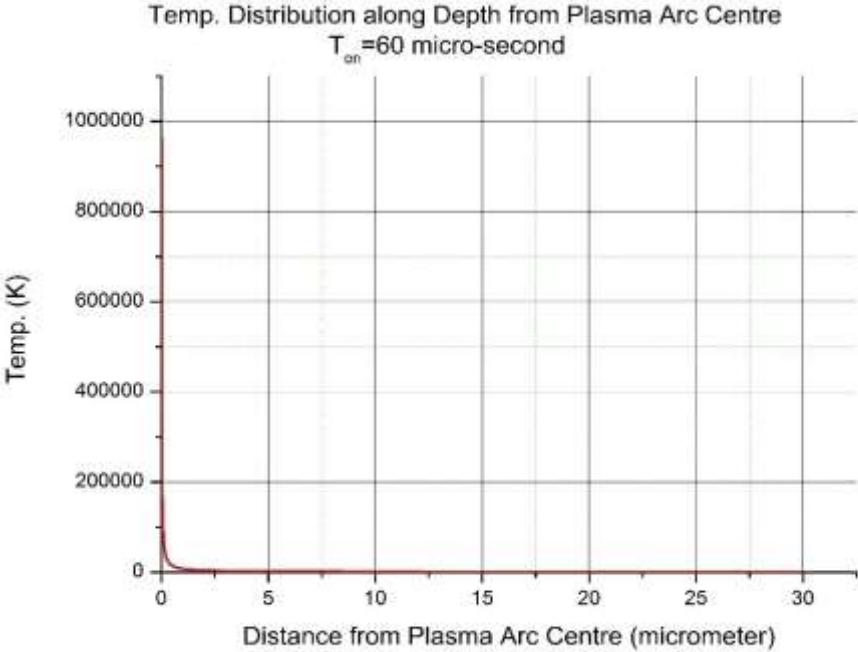


Fig4.54.: Temp. Distribution along Depth 45V, 4A,  $T_{on}$ =60microsecond

iii. Pulse-on-time( $T_{on}$ )=80 microsecond:

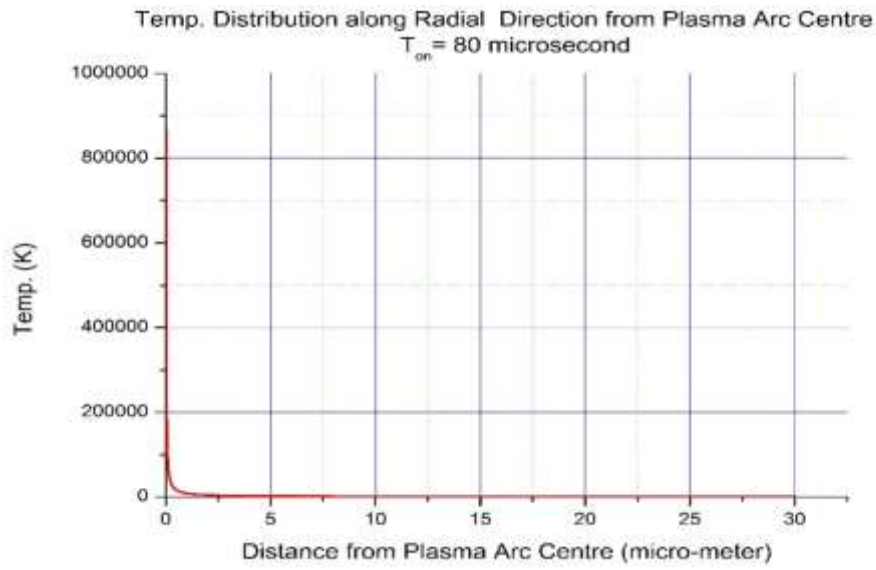


Fig.4.55: Temp. Distribution along radial direction 45V, 4A,  $T_{on}$ =80microsecond

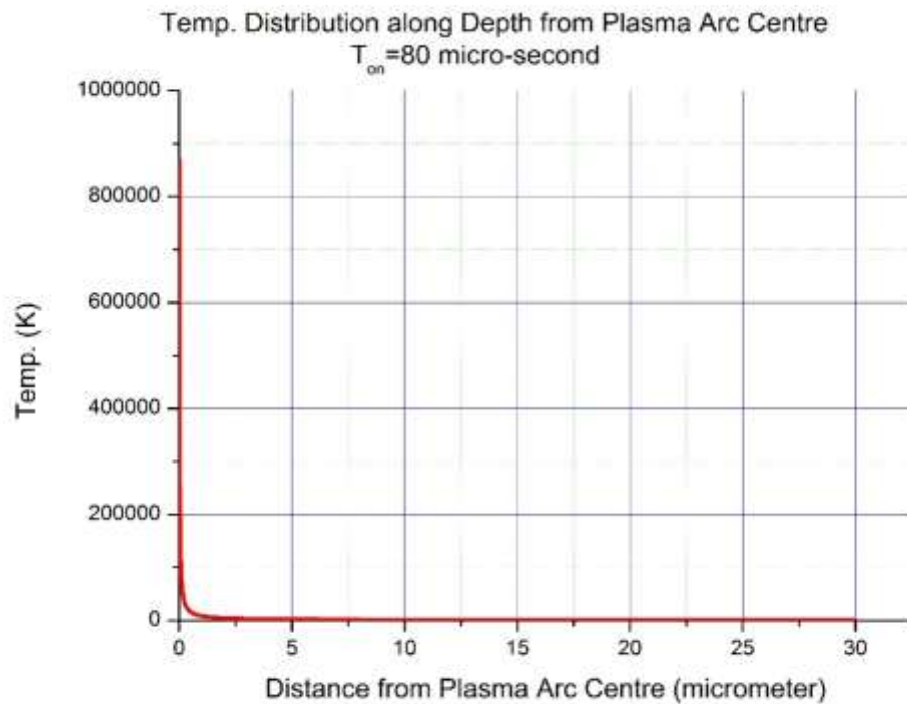


Fig4.56.: Temp. Distribution along Depth 45V, 4A,  $T_{on}$ =80microsecond

As the radius of the plasma arc is in nano-meter range, the temperature rise is happening in a very small area and rise of temperature is very high. Also the pulse-on-time is in micro-second range, so, there is not much time to heat flow into the material through conduction. Also as the temperature is very high at plasma arc centre a large amount of heat goes out through radiation. Because of this reasons temperature gradient around the plasma arc centre is very high. Whereas the after some distance from plasma arc centre the graph becomes almost flat. This figures are showing that temperature distribution is happening in a very small area which is favourable for any machining process. The graphs are showing almost same characteristics and temperature distribution along radial direction and along depth.

#### 4.4. ANALYSIS OF TEMPERATURE DISTRIBUTION IN THE HEAT AFFECTED ZONE:

As already mentioned the temperature gradient around plasma arc centre is that much high, previous graphs are not clearly showing temperature distribution in Heat Affected Zone. To analyse the HAZ the focus has been concentrated to the region just neighbour to the melted region.

**$V_{\text{gap}}=40\text{V}$ , Gap Current (**I**)=2A:**

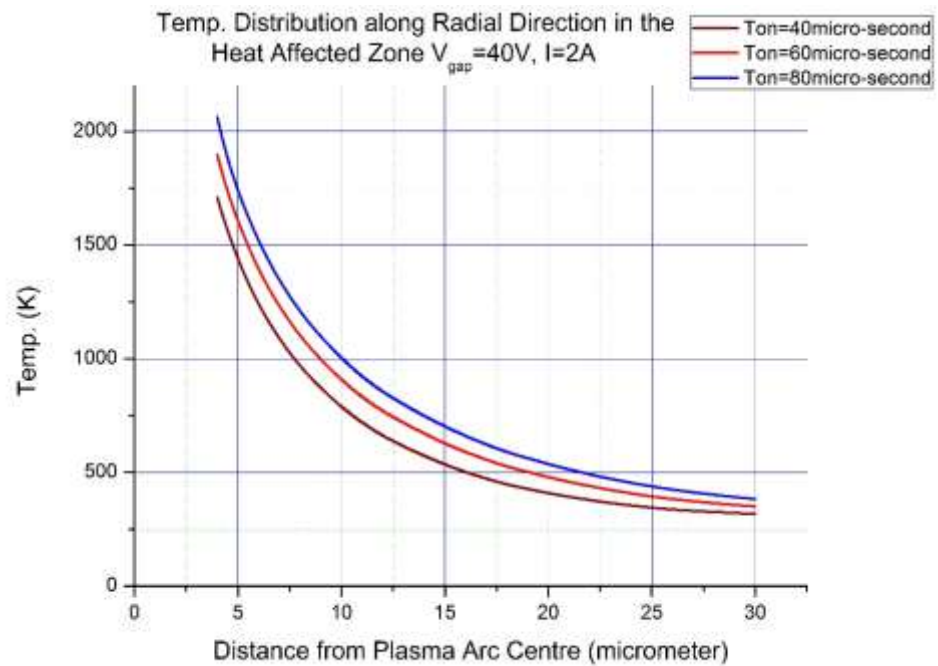


Fig.4.57.Temp. Distribution at the Heat Affected Zone along Radial Direction 40V, 2A

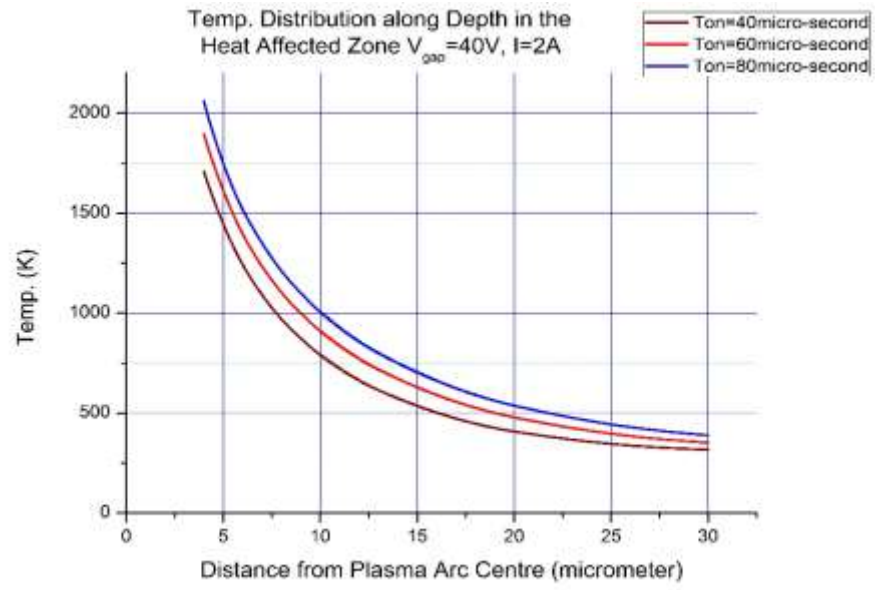


Fig.4.58.Temp. Distribution at the Heat Affected Zone along Depth 40V, 2A

**$V_{gap}=40V, \text{Gap Current (I)}=3A:$**

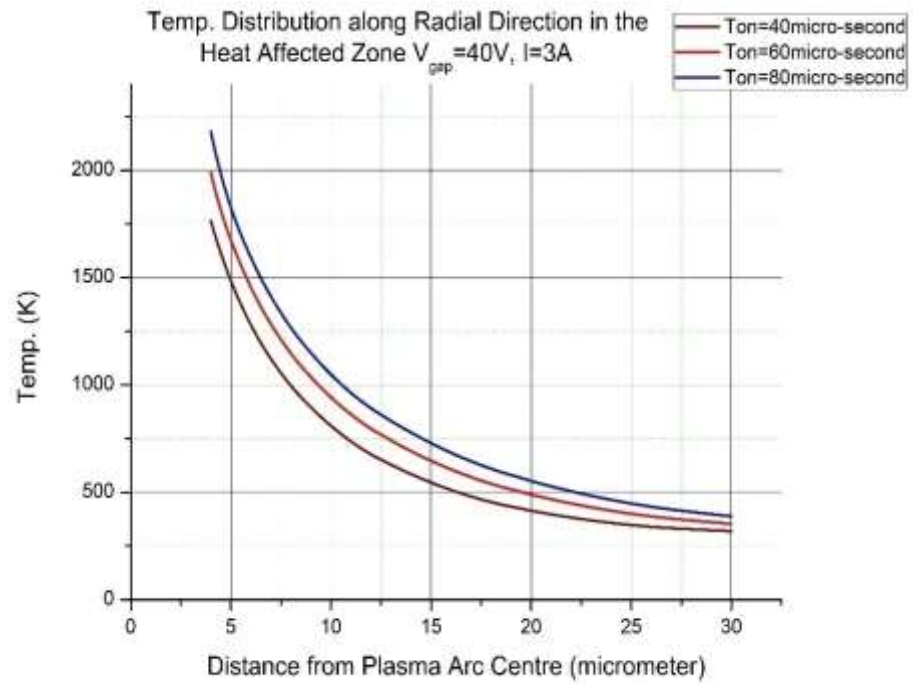


Fig.4.59.Temp. Distribution at the Heat Affected Zone along Radial Direction 40V, 3A

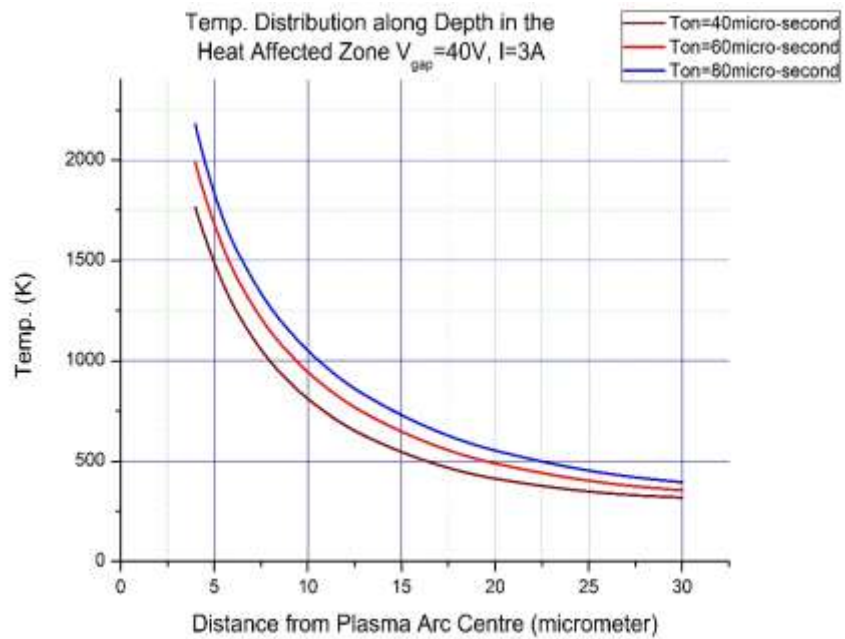


Fig.4. 60.Temp. Distribution at the Heat Affected Zone along Depth 40V, 3A

**$V_{gap}=40V$ , Gap Current ( $I$ )=4A:**

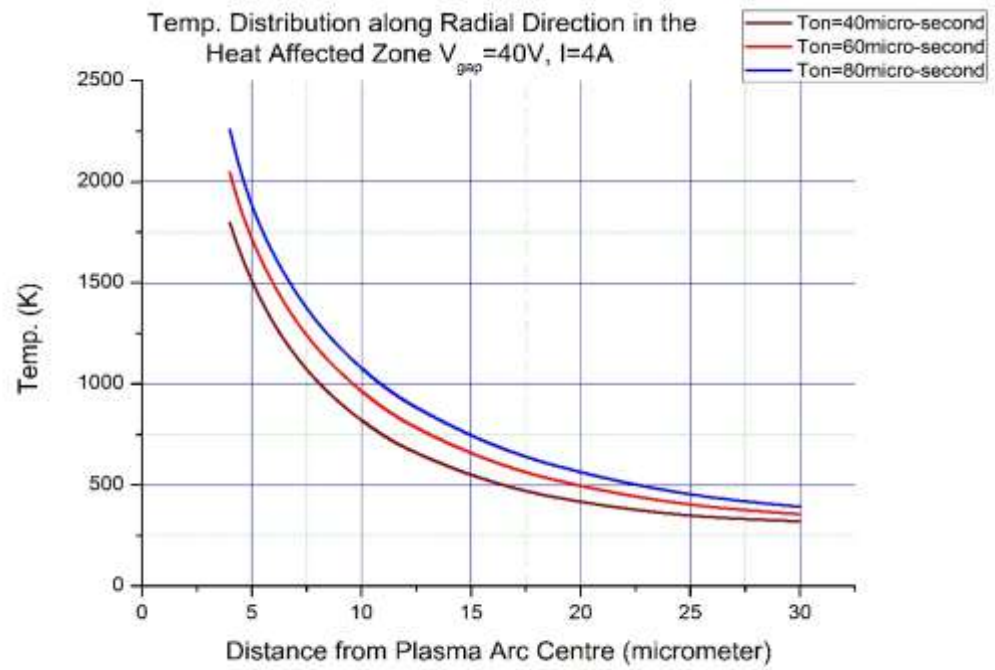


Fig.4.61.Temp. Distribution at the Heat Affected Zone along Radial Direction 40V, 4A

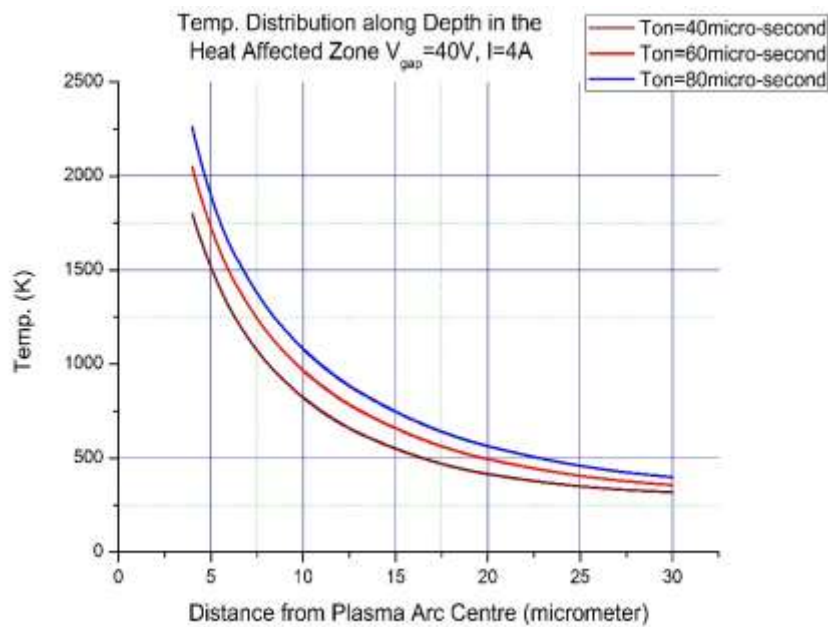


Fig.4.62.Temp. Distribution at the Heat Affected Zone along Depth 40V, 4A

**$V_{gap}=45V, \text{Gap Current (I)}=2A:$**

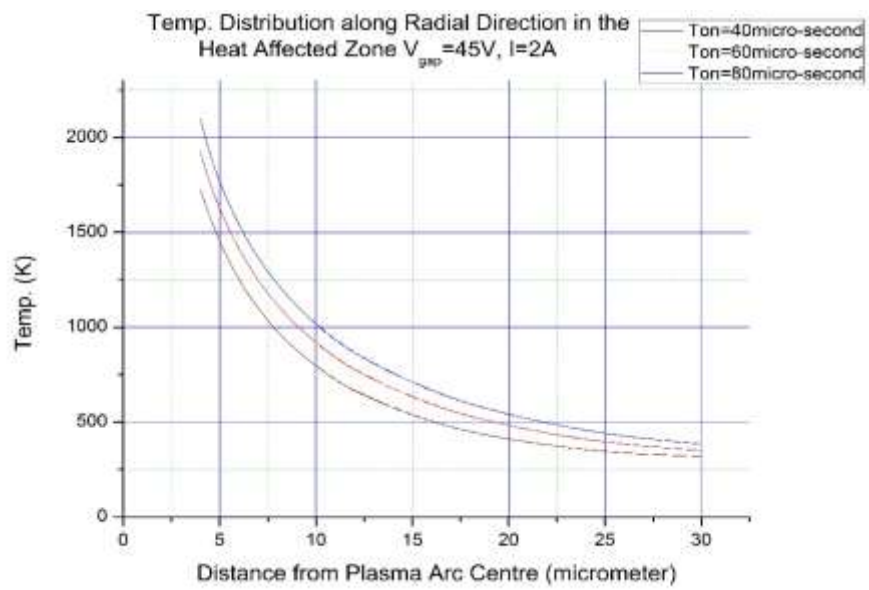


Fig.4.63.Temp. Distribution at the Heat Affected Zone along Radial Direction 45V, 2A

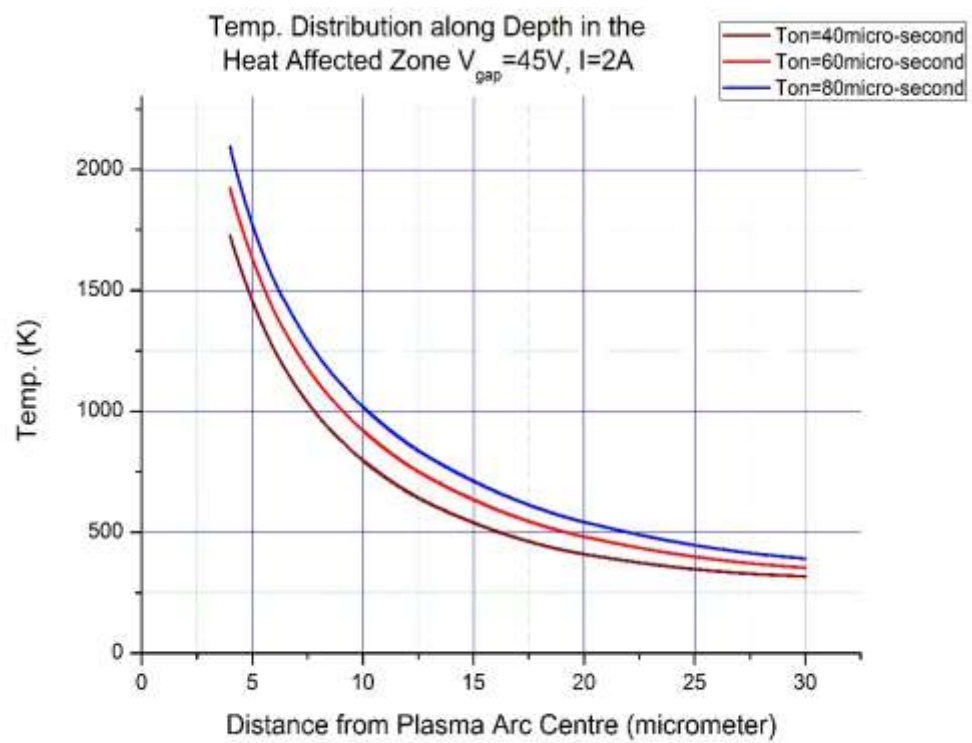


Fig.4.64.Temp. Distribution at the Heat Affected Zone along Depth 45V, 2A

$V_{gap}=45V, \text{Gap Current (I)}=3A:$

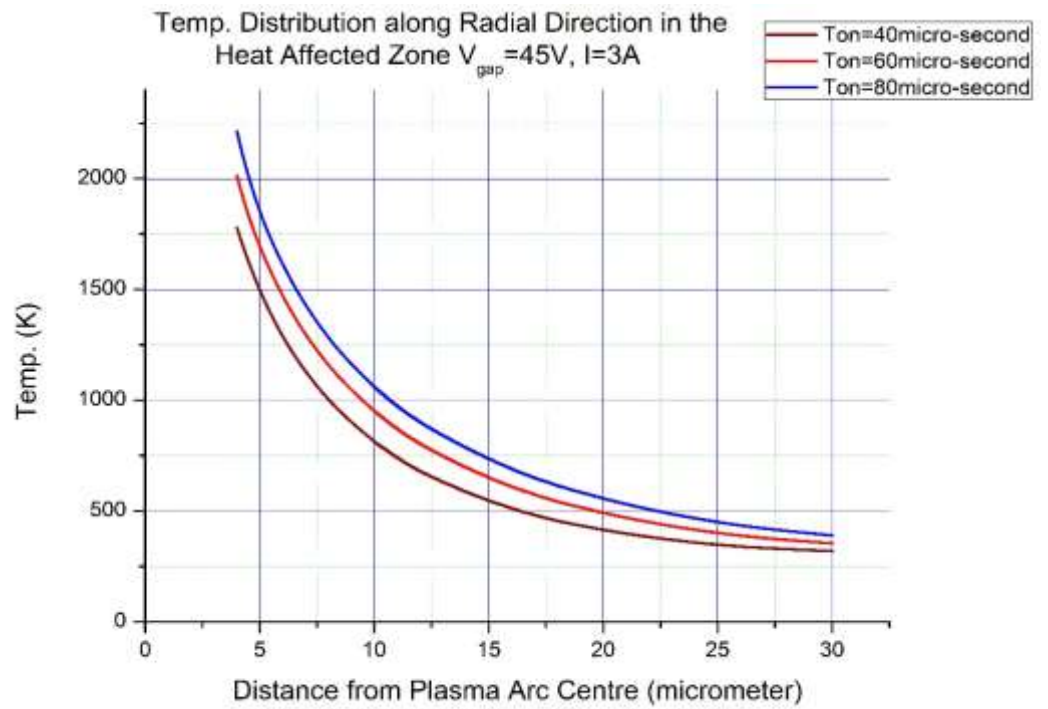


Fig.4.65.Temp. Distribution at the Heat Affected Zone along Radial Direction 45V, 3A

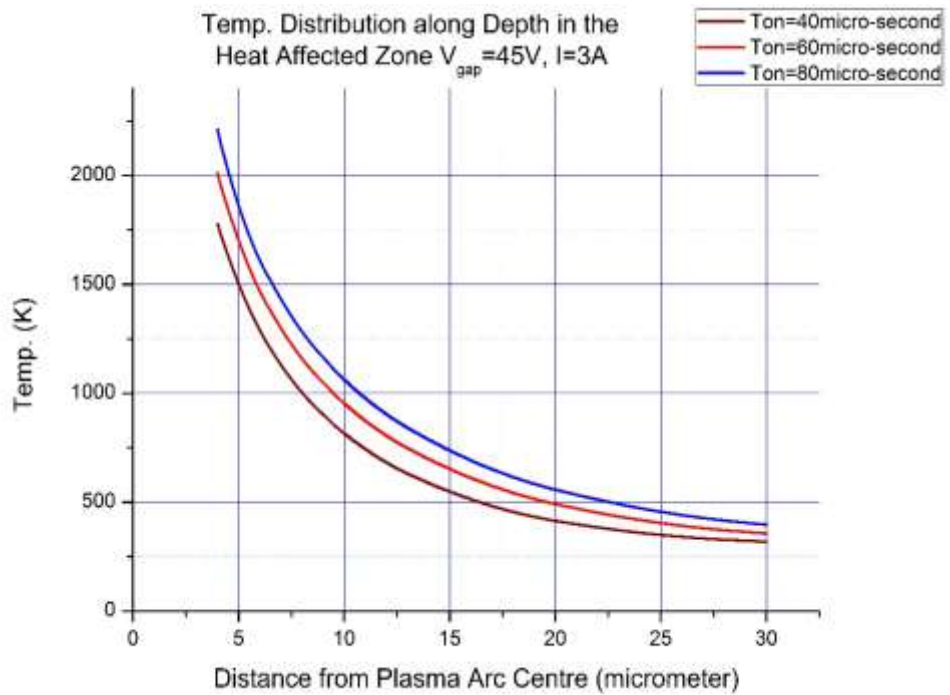


Fig.4.66.Temp. Distribution at the Heat Affected Zone along Depth 45V, 3A

$V_{gap}=45V, \text{Gap Current (I)}=4A:$

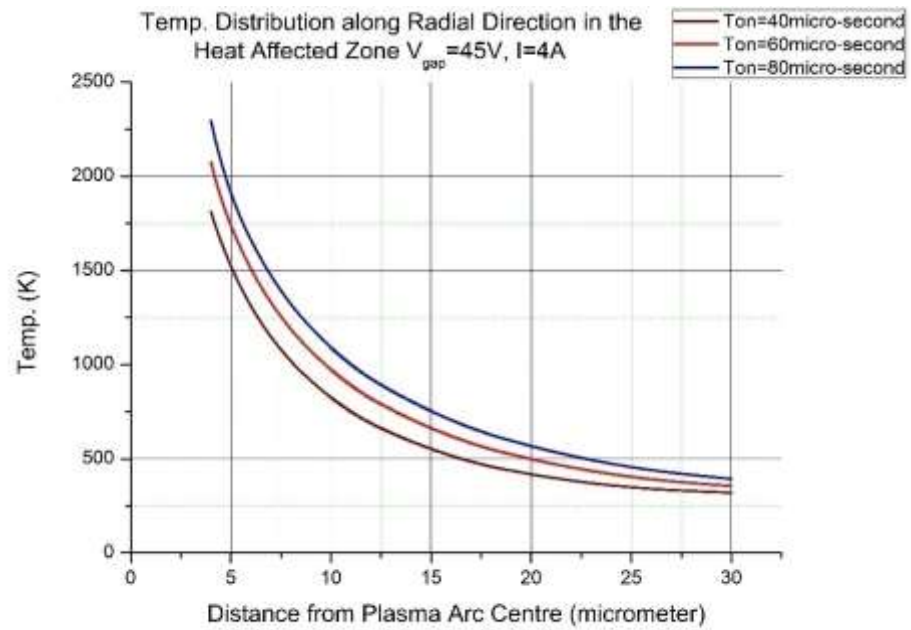


Fig.4.67.Temp. Distribution at the Heat Affected Zone along Radial Direction 45V, 4A

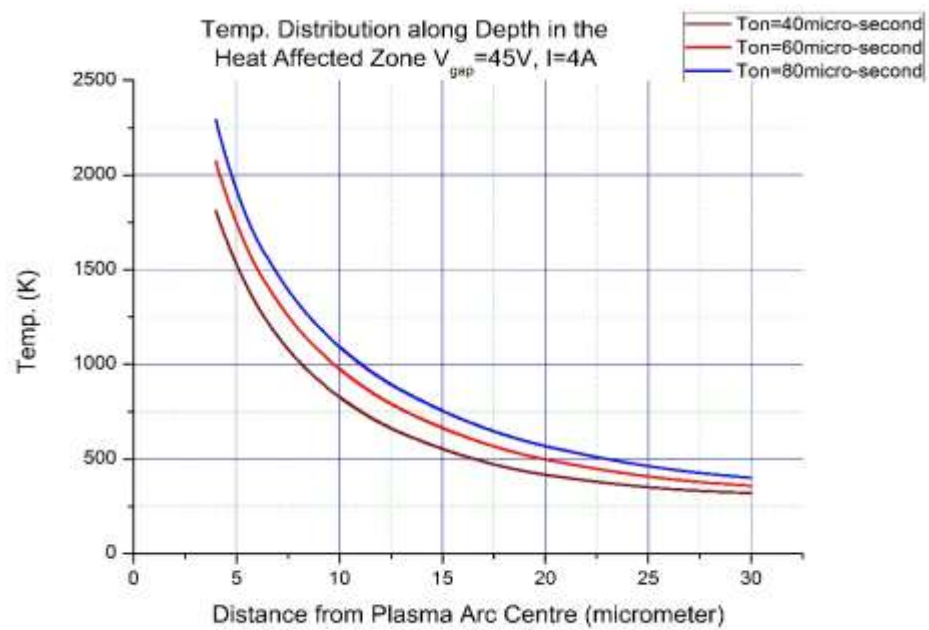


Fig.4.68.Temp. Distribution at the Heat Affected Zone along Depth 45V, 4A

The temperature distribution curve is showing a parabolic nature in the Heat Affected Zone. The temperature gradient is decreasing along the plasma arc centre from Plasma Arc Centre and finally the temperature gradient is becoming zero where the material is reaching initial temperature 293.15K. The figures are showing the HAZ is distributed mainly around 5 micro-meter to 30 micro-meter. The temperature distribution is almost same for the top surface and along depth.

#### 4.5. STUDY OF CRATER SIZE:

As discussed previously temperature value have been taken along radial direction and along depth from plasma arc centre for every simulation. The material taken here is AISI304 stainless steel, melting temperature of this material is 1673K. So, from the data set the portion of material above 1673K has been identified and it is taken as the crater.

Table.4.2. Crater Dimension

Gap Voltage $V_{\text{gap}}$ (V)	Gap Current I (A)	Pulse-on-time $T_{\text{on}}$ (microsecond)	Crater Dimension	
			Radius on the top surface (micro-meter)	Depth (micro-meter)
40	2	40	4.12	4.11
		60	4.73	4.76
		80	5.27	5.29
	3	40	4.29	4.30
		60	5.00	5.03
		80	5.62	5.63
	4	40	4.39	4.40
		60	5.18	5.20
		80	5.85	5.84
45	2	40	4.17	4.17
		60	4.82	4.84
		80	5.38	5.39
	3	40	4.34	4.35
		60	5.09	5.11
		80	5.72	5.72
	4	40	4.44	4.45
		60	5.26	5.27
		80	5.94	5.93

**4.5.1. INFLUENCE OF PULSE-ON TIME ON CRATER SIZE:**

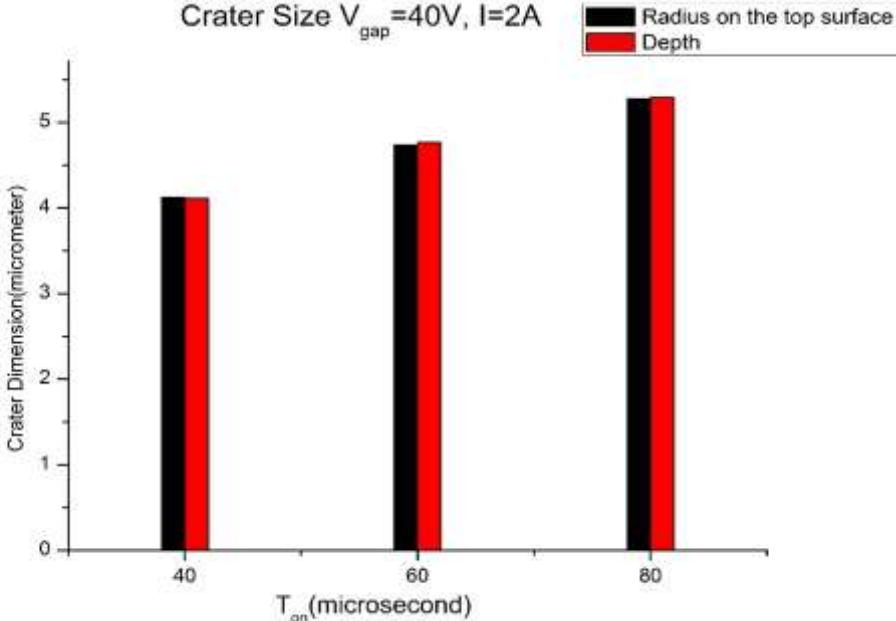


Fig.4.69. Crater Dimension.  $V_{gap}=40V, I=2A$

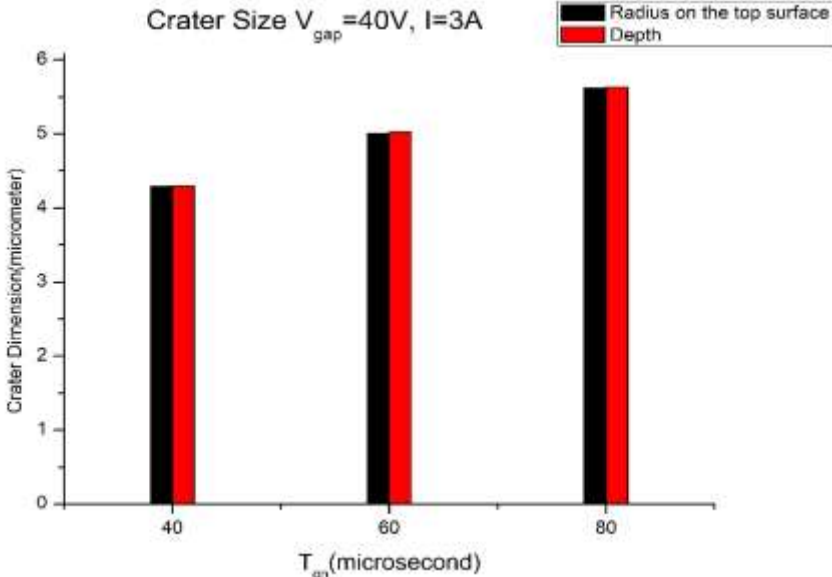


Fig.4.70. Crater Dimension.  $V_{gap}=40V, I=3A$

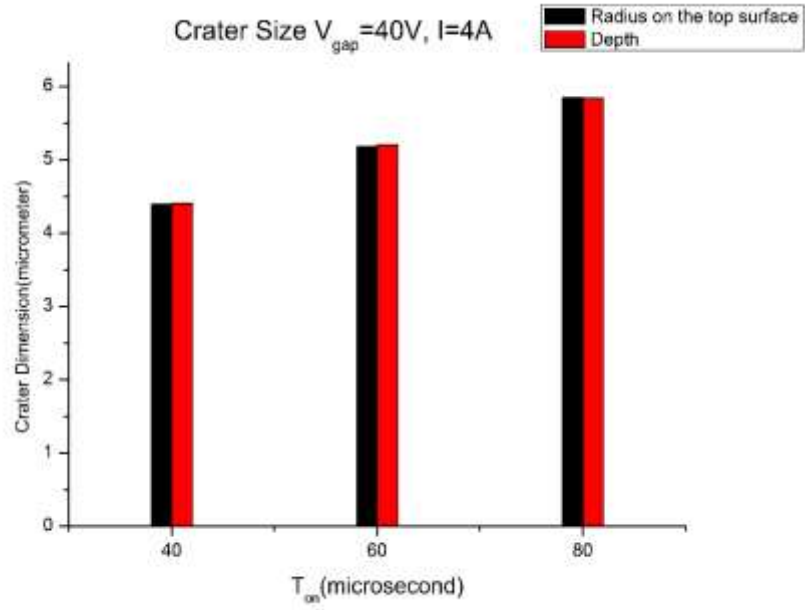


Fig.4.71. Crater Dimension.  $V_{gap} = 40V, I = 4A$

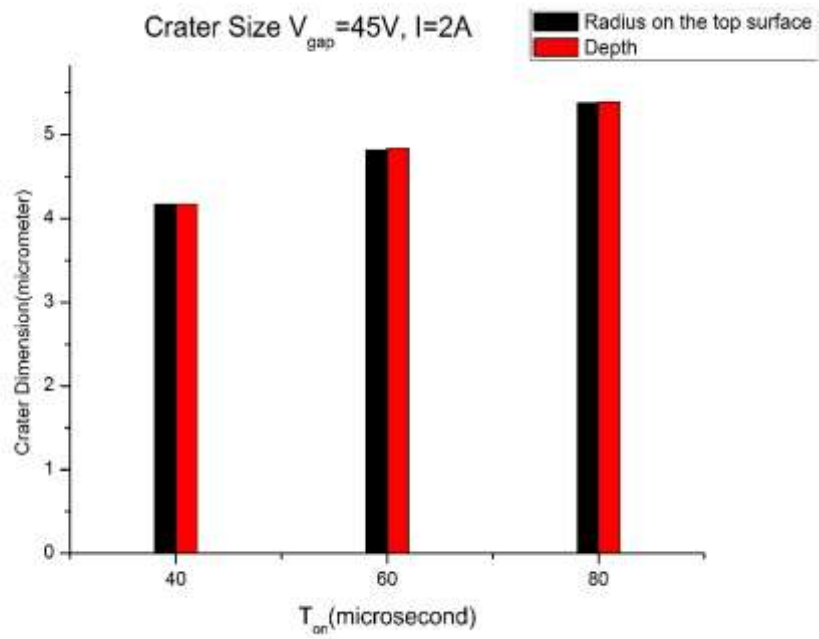


Fig.4.72. Crater Dimension.  $V_{gap} = 45V, I = 2A$

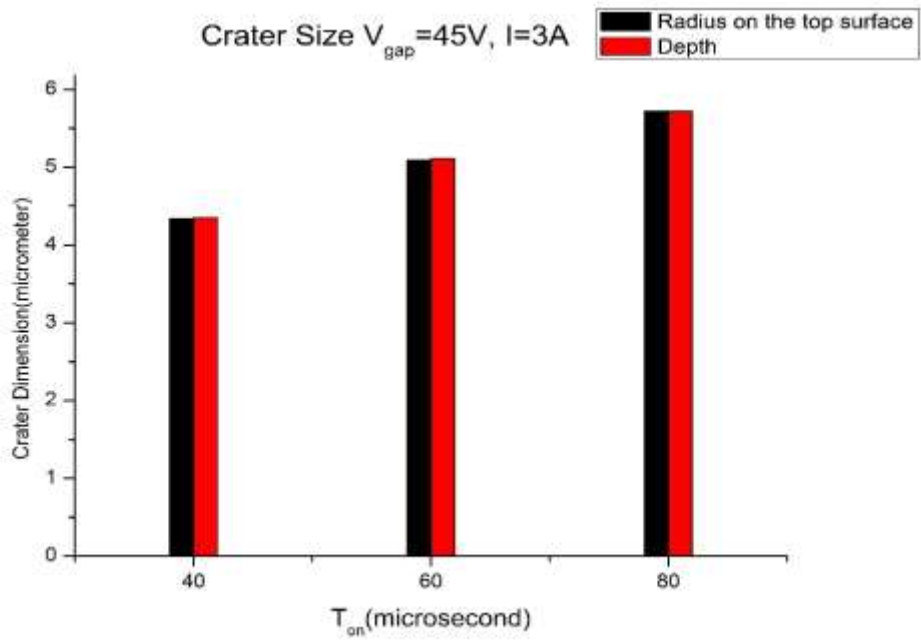


Fig.4.73. Crater Dimension.  $V_{gap}=45V, I=3A$

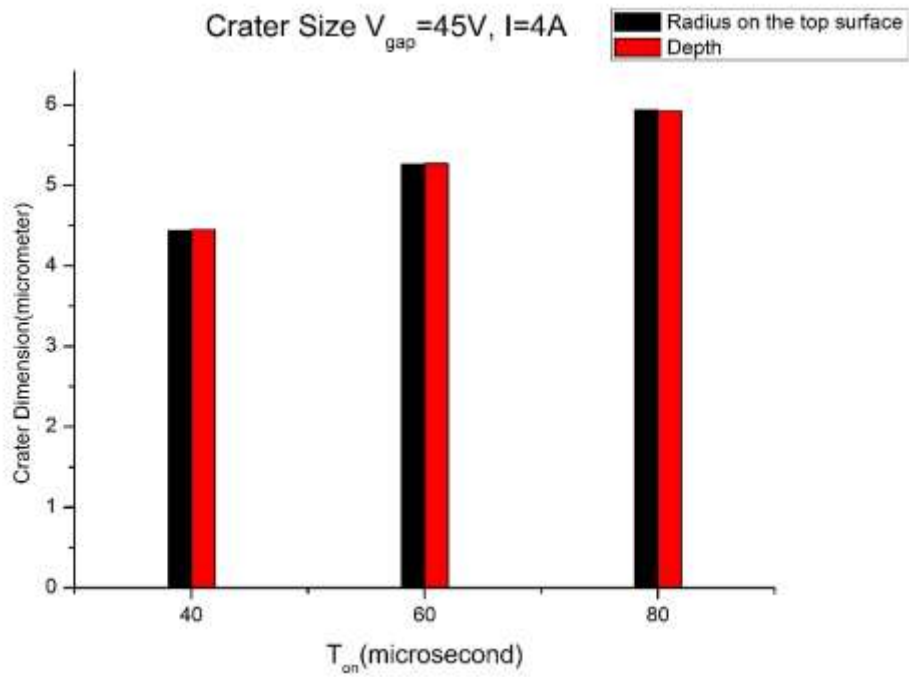


Fig.4.74. Crater Dimension.  $V_{gap}=45V, I=4A$

It is observed from the figure that as the pulse on time is increasing the crater size also increasing significantly, although temperature at plasma arc centre is decreasing. Which is supporting the discussion made at the 4.2 section. That means the heat is spreading continuously through conduction and increasing the crater size.

#### 4.5.2. INFLUENCE OF GAP CURRENT ON CRATER DIMENSION:

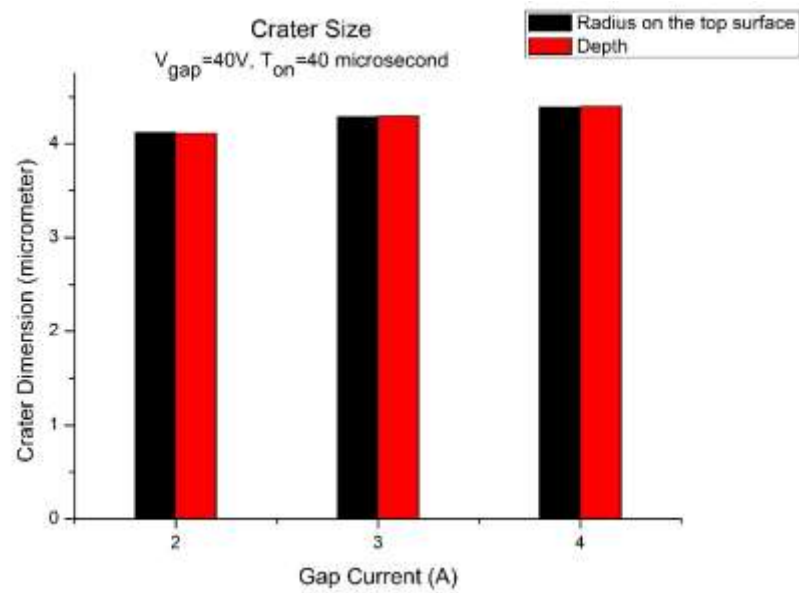


Fig.4.75. Crater Dimension.  $V_{gap}=40V$ ,  $T_{on}=40$ microsecond

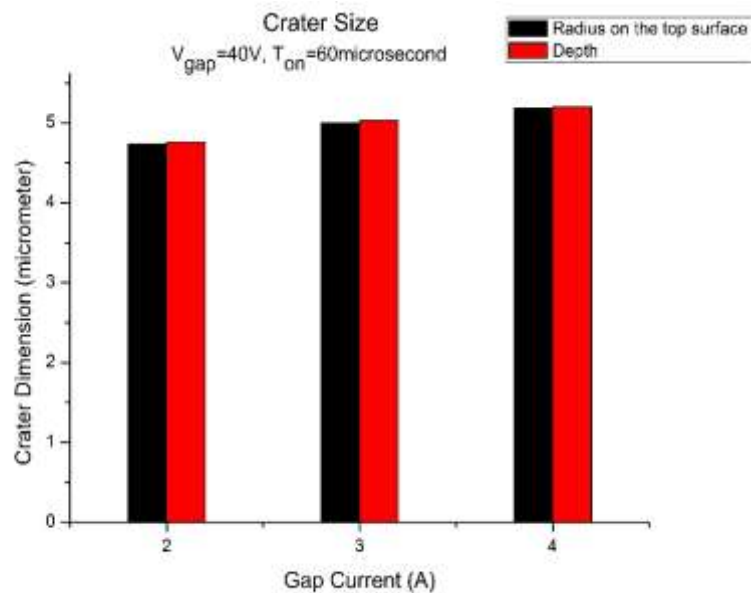


Fig.4.76. Crater Dimension.  $V_{gap}=40V$ ,  $T_{on}=60$ microsecond

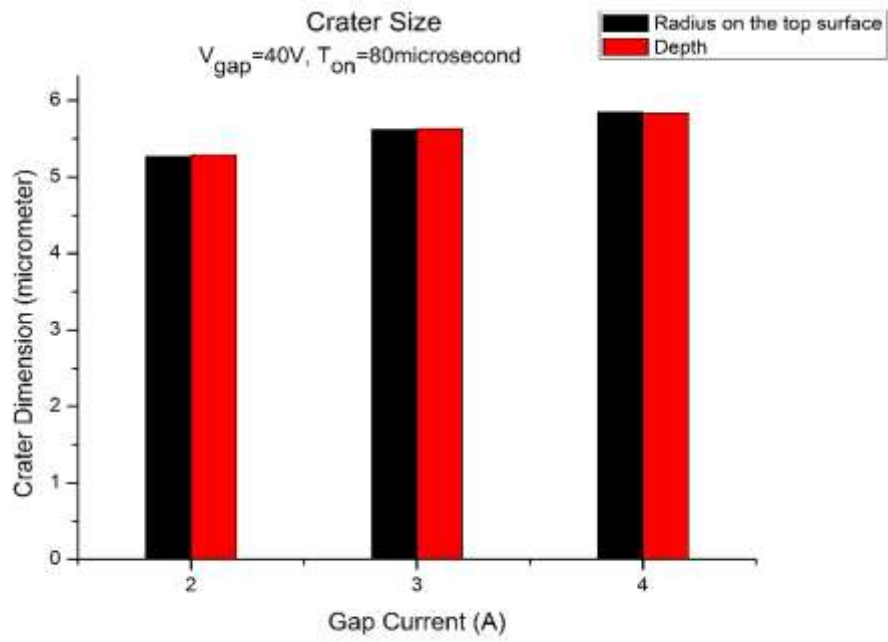


Fig.4.77. Crater Dimension.  $V_{gap}=40V, T_{on}=80\mu s$

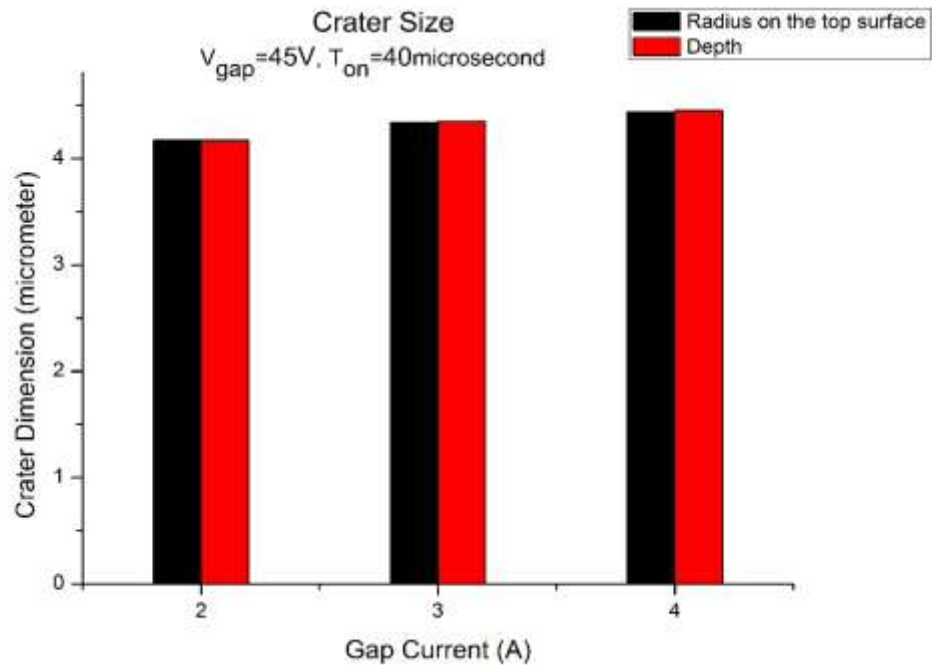


Fig.4.78. Crater Dimension.  $V_{gap}=45V, T_{on}=40\mu s$

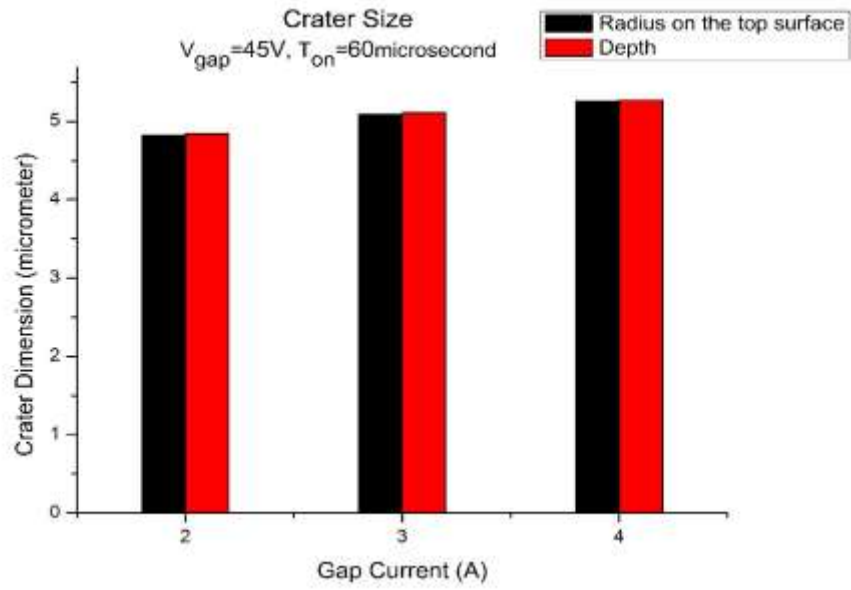


Fig.4.79. Crater Dimension.  $V_{gap}=45V, T_{on}=60$  microsecond

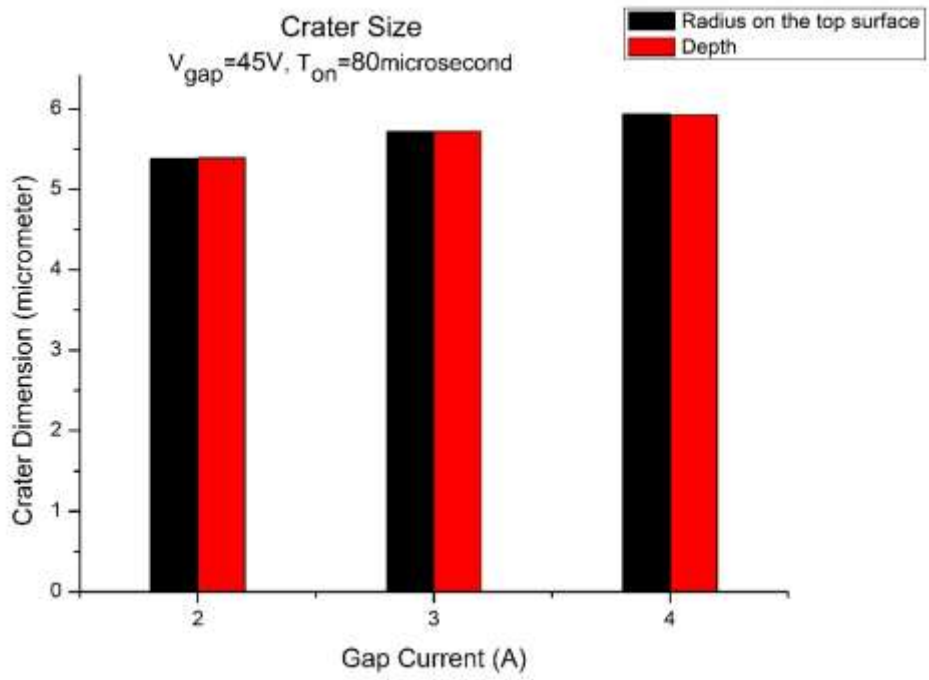


Fig.4.80. Crater Dimension.  $V_{gap}=45V, T_{on}=80$  microsecond

It is observed from the figure that as the current is increasing the crater size is also increasing. This is because as the gap current is increasing the heat flux application is also increasing. As the temperature is increasing the rate of conduction is also increasing (because heat flow through conduction is directly proportional to temperature difference). Because of that reason the crater size is increasing with time.

Y.B.Guo et al. [20] showed that the depth of crater is always lesser than the radius of crater along radial direction on the top surface. The ratio of depth to radius of crater on the top surface they proposed is 0.92 to 0.99. But in this thesis it is showing that the radius along radial direction and depth of crater is almost same. In maximum case the depth is slightly greater than the radius of crater on the top surface. This because in Y.B.Guo et al. they have not considered the heat loss by radiation from the outer surfaces. But in this thesis the radiative heat loss is considered and as the heat is being lost from the top surface radius of the crater on the top surface is becoming slightly lesser than the depth.

## **5. GENERAL CONCLUSION & FUTURE SCOPE OF WORK:**

### **5.1. GENERAL CONCLUSION:**

The gap phenomenon in the Electro Discharge Machining is very much complicated. So, it is hard to measure temperature distribution in the material by doing practical experiment during EDM. But by doing thermal modelling temperature distribution is studied here. Here a single spark of Gaussian distribution is considered. The heat source is applied on the top surface of the material and temperature distribution is studied with the help of Finite Element Analysis software COMSOL MULTIPHYSICS. By analysing the result the following conclusions can be drawn:

- i) The temperature at the plasma arc centre during the process rises with a high rate upto a time range (almost 22 micro-second) and there after the temperature falls continuously because of loss of heat due to conduction into the material and loss due to radiation.
- ii) Temperature distribution along radial direction and along depth follows almost a similar pattern.
- iii) Temperature gradient just around the plasma arc centre is very high. Temperature gradient decreases along the distance from the plasma arc centre and after almost 30 micro-meter distance the gradient becomes zero.
- iv) The size of crater size increases with pulse-on-time.
- v) The size of the crater also increases with increasing gap current, as the applied heat flux increases with time.

### **5.2. FUTURE SCOPE OF WORK:**

The future scopes of this work includes:

- i) Consideration of material killing after vaporization (just after it is reaching the vaporization temperature during the process).
- ii) A flow simulation can be made to check the portion of melted material is removing and the portion of material creating recrystallization zone.
- iii) The effect of plasma arc pressure can be considered.
- iv) The effect of debris and bubbles can be made in the machining zone.
- v) The work has been done only for single spark at single stage. Multi-spark at multi-stages can be considered by making a development of this work by detecting randomized spark locations and counting the sparks. Etc.

## 6. REFERENCE:

1. P.K.Mishra. Non-conventional machining.Narosa Publishing House. ISBN-978-81-7319-138-1.
2. Jain.V.K. “Advanced machining Processes”.NarosaPublishing House.
3. Yuan-Feng Chen, Yan-Cherng Lin. Surface modification of the Al-Zn-Mg alloy using combined EDM with ultrasonic machining and addition of TiC particles into the dielectric. Journal of materials processing technology 209(2009) 4343-4350.
4. M. P. Jahan&PegahKakavand& E. L. M. Kwang& M. Rahman & Y. S.Wong. An experimental investigation into the micro-electro-discharge machining behaviour of aluminium alloy (AA 2024). Int J AdvManufTechnol (2015) 78:1127–1139.
5. Balbir Singh, Jatinder Kumar, and Sudhir Kumar. Influences of Process Parameters on MRR Improvement in Simple and Powder - Mixed EDM of AA6061/10% SiCComposite.Materials and Manufacturing Processes, 30: 303–312, 2015.
6. G. D’Urso , C. Merla. Workpiece and electrode influence on micro-EDM drilling performance. Precision Engineering 38 (2014) 903–914.
7. Soraya Plaza, Jose A. Sanchez, Endika Perez, Ruben Gil, BorjaIzquierdo, Naiara Ortega, Inigo~ Pombo. Experimental study on micro EDM-drilling of Ti6Al4V using helical electrode.Precision Engineering 38 (2014) 821–827.
8. D. Gurguía, E. Vázquez, I. Ferrer. Influence of the Process Parameters to Manufacture Micro-cavities by Electro Discharge Machining (EDM). Procedia Engineering 63 ( 2013 ) 499 – 505.
9. Cheol-Soo Lee a, Eun-Young Heo b, Jong-Min Kim b, In-Hugh Choi c, Dong-Won Kim. Electrode wear estimation model for EDM drilling. Robotics and Computer-Integrated Manufacturing 36 (2015) 70–75.
- 10.Lin Li, C. Diver, J. Atkinson1, R. Giedl-Wagner, H. J. Helml. Sequential Laser and EDM Micro-drilling for Next Generation Fuel Injection Nozzle Manufacture.

11. M.P. Jahan , Y.S. Wong , M. Rahman. Evaluation of the effectiveness of low frequency workpiece vibration in deep-hole micro-EDM drilling of tungsten carbide. *Journal of Manufacturing Processes* 14 (2012) 343–359.
12. Hao Tong, Yong Li, Yang Wang. Experimental Research on vibration assisted EDM of micro structures with non circular cross section. *JOURNALS OF MATERIALS PROCESSING TECHNOLOGY*. 208(2008) 289-298.
13. Cheol-Soo Lee, Eun-Yong Heo, Jong Min Kim, In-Hung Choi, Dong-Won Kim. Electrode Wear Estimation mode for EDM drilling.
14. Prof.Dr. Ir. J.-P. Kruth, Ir. L. Stevens, Prof.Dr. Ir. L. Froyen, Dr. Ir. B. Lauwers , K. U. Leuven, Study of the White Layer of a Surface Machined by Die-Sinking Electro-Discharge Machining, Received on January 9, 1995.
15. Daryl D. DiBitonto. Theoretical models of the electrical discharge machining process. I. A simple cathode erosion model. *Journal of Applied Physics* 66, 4095 (1989); doi: 10.1063/1.343994.
16. Mukund R. Patel, Maria A. Barrufet. and Philip T. Eubank, Daryl D. DiBitonto. Theoretical models of the electrical discharge machining process. II. The anode erosion model. Received 20 February 1989; accepted for publication 11 July 1989. *Journal of Applied Physics* 66, 4104 (1989); doi: 10.1063/1.343995.
17. Philip T. Eubank, Mukund R. Patel, Maria A. Barrufet, and Bedri Bozkurt. Theoretical models of the electrical discharge machining process. III. The variable mass, cylindrical plasma model. *Journal of Applied Physics* 73, 7900 (1993); doi: 10.1063/1.353942.
18. S. Hinduja, M. Kunieda. Modelling of ECM and EDM processes. *CIRP Annals - Manufacturing Technology* 62 (2013) 775–797.
19. Fritz Klocke, Sebastian Schneider, Simon Harst, David Welling, Andreas Klink. Energy-based approaches for multi-scale modelling of material loadings during Electric Discharge Machining (EDM). *Procedia CIRP* 31 ( 2015 ) 191 – 196.

20. Y.B. Guo, A. Klink, F. Klocke, Y.B. Guo. Multiscale modeling of sinking-EDM with gaussian heat flux via user subroutine. *Procedia CIRP* 6 (2013) 438 – 443.
21. C. Mascaraque-Ramirez, P. Franco. Numerical modelling of surface quality in EDM processes. *Procedia Engineering* 132 (2015) 671 – 678.
22. J.F. Liu, Y.B. Guo. Modeling of White Layer Formation in Electric Discharge Machining (EDM) by Incorporating Massive Random Discharge Characteristics. *Procedia CIRP* 42 (2016) 697 – 702.
23. Jiajing Tang, Xiaodong Yang. A Thermo-hydraulic Modeling for the Formation Process of the Discharge Crater in EDM. *Procedia CIRP* 42 (2016) 685 – 690.
24. Y. Zhang, Y. Liu, Y. Shen, Z. Li, R. Ji, F. Wang. A new method of investigation the characteristic of the heat flux of EDM plasma. *Procedia CIRP* 6 (2013) 450 – 455.
25. <http://www.nptel.ac.in/courses/112105127/pdf/LM-39.pdf>.
26. Yunus, A.C., 2003. *Heat Transfer: a Practical Approach*, MacGraw-Hill.
27. [https://en.wikipedia.org/wiki/Electrical\\_discharge\\_machining](https://en.wikipedia.org/wiki/Electrical_discharge_machining)
28. [https://en.wikipedia.org/wiki/Surface\\_roughness](https://en.wikipedia.org/wiki/Surface_roughness)